Volume 67A
Number 3
May–June 1963

Physics and Chemistry

6

U.S. DEPARTMENT OF COMMERCE

SECTION A

JOURNAL OF RESEARCH

NATIONAL BUREAU OF STANDARDS

Journal of Research

of the

National Bureau of Standards

A. Physics and Chemistry

MAY–JUNE • 1963

VOLUME • 67A

NUMBER • 3

Editor: C. W. Beckett

Associate Editors: D. D. Wagman
I. M. Richardson

Publication dates:
Feb. 1, Apr. 1, June 1, Aug. 1, Oct. 1, Dec. 1, 1963.

JOURNAL OF RESEARCH

The National Bureau of Standards Journal of Research reports research and development in the fields of activity shown at right. Also included from time to time are survey articles on topics closely related to the Bureau's scientific and technical program.

The Journal is published in four separate sections as follows:

A. Physics and Chemistry

Contains papers of interest primarily to scientists working in these fields. Issued six times a year. Annual subscription: domestic, $4.00; foreign, $4.75.

B. Mathematics and Mathematical Physics

Presents studies and compilations designed mainly for the mathematician and the theoretical physicist. Issued quarterly. Annual subscription: domestic, $2.25; foreign, $2.75.

C. Engineering and Instrumentation

Reports research and development results of interest chiefly to the engineer and the applied scientist. Issued quarterly. Annual subscription: domestic, $2.25; foreign, $2.75.

D. Radio Propagation

Reports work in radio propagation, upper atmospheric physics, and communications. Issued six times a year. Annual subscription: domestic, $4.00; foreign, $4.75.

Functions and Activities

The functions of the National Bureau of Standards are set forth in the Act of Congress, March 3, 1901, as amended. These include the development and maintenance of the national standards of measurement and the provision of means and methods for making measurements consistent with these standards; the determination of physical constants and properties of materials; the development of methods and instruments for testing materials, devices, and structures; advisory services to government agencies on scientific and technical problems; invention and development of devices to serve special needs of the Government; and the development of standard practices, codes, and specifications. The work includes basic and applied research, development, engineering, instrumentation, testing, evaluation, calibration services, and various consultation and information services. The Bureau also serves as the Federal technical research center in a number of specialized fields. The scope of activities of the National Bureau of Standards is suggested in the following listing of the divisions and sections engaged in technical work.

Washington, D.C.

Electricity. Resistance and Reactance. Electrochemistry. Electrical Instruments. Magnetic Measurements. Dielectrics. High Voltage.
Metrology. Photometry and Colorimetry. Refractometry. Photographic Research. Length. Engineering Metrology. Mass and Scale. Volumetry and Densimetry.
Heat. Temperature Physics. Heat Measurements. Cryogenic Physics. Equation of State. Statistical Physics.
Radiation Physics. X-ray. Radioactivity. Radiation Theory. High Energy Radiation. Radiological Equipment. Nucleonic Instrumentation. Neutron Physics.
Analytical and Inorganic Chemistry. Pure Substances. Spectrochemistry. Solution Chemistry. Standard Reference Materials. Applied Analytical Research. Crystal Chemistry.
Mechanics. Sound. Pressure and Vacuum. Fluid Mechanics. Engineering Mechanics. Rheology. Combustion Controls.
Polymers. Macromolecules: Synthesis and Structure. Polymer Chemistry. Polymer Physics. Polymer Characterization. Polymer Evaluation and Testing. Applied Polymer Standards and Research. Dental Research.
Metallurgy. Engineering Metallurgy. Microscopy and Diffraction. Metal Reactions. Metal Physics. Electrolysis and Metal Deposition.
Inorganic Solids. Engineering Ceramics. Glass. Solid State Chemistry. Crystal Growth. Physical Properties. Crystallography.
Building Research. Structural Engineering. Fire Research. Mechanical Systems. Organic Building Materials. Heat Transfer. Inorganic Building Materials. Metallic Building Materials.
Applied Mathematics. Numerical Analysis. Computation. Statistical Engineering. Mathematical Physics. Operations Research.
Data Processing Systems. Components and Techniques. Computer Technology. Measurements Automation. Engineering Applications. Systems Analysis.
Atomic Physics. Spectroscopy. Infrared Spectroscopy. Solid State Physics. Electron Physics. Atomic Physics.
Instrumentation. Engineering Electronics. Electron Devices. Electronic Instrumentation. Mechanical Instruments. Basic Instrumentation.
Physical Chemistry. Thermochemistry. Surface Chemistry. Organic Chemistry. Molecular Spectroscopy. Molecular Kinetics. Mass Spectrometry.

Office of Weights and Measures
Boulder, Colo.

Cryogenic Engineering. Laboratory. Cryogenic Equipment. Cryogenic Processes. Properties of Materials. Cryogenic Technical Services.

Central Radio Propagation Laboratory

Ionosphere Research and Propagation. Low Frequency and Very Low Frequency Research. Ionosphere Research. Prediction Services. Sun-Earth Relationships. Field Engineering. Radio Warning Services. Vertical Soundings Research.
Radio Propagation Engineering. Data Reduction Instrumentation. Radio Noise. Tropospheric Measurements. Tropospheric Analysis. Propagation-Terrain Effects. Radio-Meteorology. Lower Atmosphere Physics.
Radio Systems. Applied Electromagnetic Theory. High Frequency and Very High Frequency Research. Modulation Research. Antenna Research. Navigation Systems.
Upper Atmosphere and Space Physics. Upper Atmosphere and Plasma Physics. Ionosphere and Exosphere Scatter. Airglow and Aurora. Ionospheric Radio Astronomy.

Radio Standards Laboratory

Radio Physics. Radio Broadcast Service. Radio and Microwave Materials. Atomic Frequency and Time-Interval Standards. Millimeter-Wave Research.
Circuit Standards. High Frequency Electrical Standards. Microwave Circuit Standards. Electronic Calibration Center.

U.S. DEPARTMENT OF COMMERCE
Luther H. Hodges, Secretary

NATIONAL BUREAU OF STANDARDS
A. V. Astin, Director

Order all publications from the Superintendent of Documents
U.S. Government Printing Office, Washington 25, D.C.

Use of funds for printing this publication approved by the Director of the Bureau of the Budget (June 19, 1961).

JOURNAL OF RESEARCH of the National Bureau of Standards—A. Physics and Chemistry
Vol. 67A, No. 3, May-June 1963

An Absolute Calibration of the National Bureau of Standards Thermal Neutron Flux

E. J. Axton[1]

(February 12, 1963)

The NBS Thermal Neutron Flux has been calibrated in terms of the gold thermal neutron capture cross section. The effective thermal neutron (below cadmium cutoff energy) flux density is estimated to be 4307 ± 2 percent n/cm^2 sec in September 1961. This figure is in agreement with a recent value quoted by the NBS.

1. Introduction

The NBS Standard Thermal Neutron Flux has been calibrated in terms of the $B(n,\alpha)$ cross section [De Juren and Rosenwasser, 1954] and of the gold thermal neutron capture cross section [Mosburg and Murphey, 1961]. The present calibration, based on absolute counting of ^{198}Au activity by the $4\pi\beta-\gamma$ coincidence method, represents part of a program of international comparisons of thermal neutron flux density measurement.

2. Method and Procedure

The method is similar to that used for the absolute calibration of the neutron flux in the AERE reactor GLEEP [Axton, 1963]. This calibration was based on absolute counting of ^{56}Mn and of ^{198}Au by the $4\pi\beta-\gamma$ coincidence method, and some of the same gold foils and the same counting equipment are used in the present experiment, so that the various correction factors associated with the foils and equipment have already been evaluated and, where appropriate, are reproduced in table 1.

TABLE 1

Foil	Mass mg	Nominal thickness mg/cm²	Foil data					
			N_β/N	$1/F$	F_{Cd}	$f_{(\alpha)}$	G_t	$g\sigma_0$
G_1	23.19	30	0.6841	1.028	1.01	0.991	0.441	99.32
G_2	23.48	30	.6924					
G_3	23.44	30	.6896					
G_4	22.97	30	.6961					

A pair of foils (G_1, G_2) 30 mg/cm² in thickness and 1 cm diam were irradiated in the flux for one week. A similar pair (G_3, G_4), encased in cadmium 0.1 cm thick, were irradiated for 11 days.

The foils were counted in the $4\pi\beta$ counter of the coincidence equipment previously described [Axton, 1963]. For G_1, G_2, the total counting rate was approximately 11 c/s against a background of 0.9 c/s. For G_3, G_4, the counting rate was approximately 2.2 c/s, against a background counting rate of 0.9 c/s. In view of the low counting rate it was not possible to make coincidence measurements on these foils. However, the ratio between N_β, the net counting rate in the $4\pi\beta$ counter, and N, the absolute disintegration rate has been measured for these foils a number of times both before and after this irradiation in the course of the GLEEP flux measurement.

The reaction rate D_0 per milligram of foil is obtained from the equation

$$D_0=\frac{D\exp[\lambda(t_3-t_2)]\lambda(t_4-t_3)}{\{1-\exp[-\lambda(t_2-t_1)]\}\{1-\exp[-\lambda(t_4-t_3)]\}} \tag{1}$$

where λ is the decay constant of ^{198}Au and D is the average disintegration rate per mg from time t_3 to time t_4 of a foil irradiated from time t_1 to time t_2.

The thermal neutron flux density, defined as $n_{th}v_0$, where n_{th} is the neutron density below the cadmium cutoff energy, and $v_0=2200$ m/sec, is given by

$$n_{th}v_0=\frac{(1/F)(D_0-D_{0\,Cd}F_{Cd})A}{0.001N_0g\sigma_0} \tag{2}$$

where

$D_{0\,Cd}$ is the reaction rate per mg obtained with the foil under cadmium.
F_{Cd} is a correction factor for the attenuation of resonance neutrons in the cadmium.
$1/F$ is a correction factor for thermal neutron flux density depression and self shielding.
$g\sigma_0$ is the effective absorption cross section for neutrons with a Maxwellian distribution of velocities at 20 °C.
σ_0 =98.8b (Hughes and Schwartz, 1958).
g =1.0053 (Westcott, 1960).
A =Atomic Weight.
N_0 =Avogradro's Number.

The values of both F and g are dependent upon the temperature T associated with the most probable velocity in the Maxwellian distribution. The temperature is assumed here to be T_0 to conform to the value of g quoted by Mosburg and Murphey [1961]. $T_0=293.6$ °K and kT_0 is the energy corresponding to the neutron velocity $v_0=2200$ m/sec at which thermal cross sections are normally tabulated.

[1] National Physical Laboratory, Dept. of Scientific and Industrial Research, Teddington, Middlesex, England. (An invited paper.)

$$1/F = X/[\tfrac{1}{2} - E_3(X)] \text{ where } X = \sum_{eff} t = \frac{N_0 t}{A}$$

$$\times 1.08 g\sigma_0 \ (T_0/T)^{1/2}$$

and

$$E_3(X) = \int_1^\infty u^{-3} \exp(-uX) du$$

t is the foil thickness in g/cm^2.

3. Results

The results are presented in table 2 from which it can be deduced that the effective thermal neutron (below cadmium cutoff energy) flux density is given by

$$n_{th} v_0 = 4307 \ n/cm^2 \text{ sec.}$$

TABLE 2. *Results*

Foil	N_β c/s corrected for decay	D_0 dps/mg	D_0 Cd dps/mg	R_{Cd}	r	$n_{th} v_0$ September 1961
G_1	19.961	1.507	------	----	------	------
G^2	20.209	1.489	------	----	------	------
G_3	3.4257	------	0.2260	----	------	------
G_4	3.2981	------	.2200	----	------	------
Mean	----------	1.498	.2230	6.72	0.0212	4307

For comparison purposes the values of $n_{th} v_0$ obtained at NBS are presented in table 3, column 1, and corrected to September 1961 in column 2.

However, the procedure used to calculate the neutron flux differs from that of Mosburg and Murphey [1961] in three respects.

Firstly, the value 1.048 calculated by Mosburg and Murphey, and used by them for the correction factor F_{Cd} is believed to be too large. The calculation of this factor is difficult, since it involves an effective cross section for cadmium. To obtain such an effective cross section it is not sufficient to calculate the absorption of the resonance neutrons in the cadmium; nor is it sufficient to measure the reduction of the activity produced by a further equal thickness of cadmium. This follows because the activity of the cadmium covered foil is not produced wholly by the resonance-energy neutrons. Mosburg and Murphey used the cadmium total cross section at the gold resonance energy in their calculation of F_{Cd}. However, to satisfy the experimentally derived value for F_{Cd} quoted in table 1, it is necessary to use only the capture cross section plus a fraction of the scatter cross section. This fraction is expected to vary with foil thickness as will the relative contribution of the resonance-energy neutrons to the activity of the cadmium covered foil. However, there are insufficient data available at the present time to establish variations of F_{Cd} with foil thickness. Thus, the experimentally determined value for these particular foils and cadmium covers (table 1) is preferred. If the results of Mosburg and Murphey, who used similar thicknesses, are recalculated using this value of F_{Cd}, the flux value is raised by about 0.6 percent.

TABLE 3. *Comparison of NBS and NPL measurements*

	$n_{th} v_0$		
	Published value	Corrected for polonium growth September 1961	Corrected for change in F_{Cd} and in effective cross sections September 1961
	n/cm^2 sec	n/cm^2 sec	n/cm^2 sec
NBS (Gold) Mosburg-Murphey, [1961]	4167±1.5%	4188±1.5%	4195
NBS (Boron) De Juren and Rosenwasser, [1954]	4276±2%	4297±2%	4297
Weighted mean [a]	4203±1.5%	4224±1.5%	4229±1.5%
Ratio NPL measurement/NBS weighted mean	----------	1.020	1.018

[a] The means given here are those quoted by Mosburg and Murphey (1961), who give arbitrary weights of 2 and 1 to the gold and boron measurements, respectively.

Secondly, the effective cross section $g\sigma_0$ is used instead of σ_0 to derive the neutron flux from the foil activity. This results in a reduction of about 0.5 percent and almost cancels out the first change.

Thirdly, the effective cross section 1.08 $g\sigma_0$ is used instead of σ_0 to derive the foil self-absorption correction.

The results of Mosburg and Murphey [1961] have been recalculated with these changes to produce the revised value for the neutron flux density shown in column 3.

Thus the ratio $\dfrac{\text{NPL flux density measurement}}{\text{NBS flux density measurement}}$ is 1.020,

which reduces to 1.018 if the adjustments to F_{Cd} and to the cross sections are made in the calculation of the NBS gold value.

It is sometimes of interest to specify the neutron flux density in terms of the total neutron density n, or of the density in some specific component of the flux. In order to do this with detectors whose cross section does not follow the $1/v$ law, it is necessary to assume a spectrum shape, which, in the case of well-moderated reactors, usually comprises a Maxwellian distribution of velocities at temperature T °K and a dE/E component terminated at an effective lower limit μkT. With the present system of point sources, it is unlikely that the spectrum follows the $1/E$ law very closely. Nevertheless, in the absence of specific information, the dE/E assumption has been made for the purposes of the following calculations, and the results therefore should be treated with reserve.

The relative intensity of the dE/E component is derived from cadmium ratio measurements. The cadmium ratio R_{Cd} (ratio of activity obtained with bare foil to that obtained with cadmium covered foil) is given by the equation

$$R_{Cd} = \frac{F(r\sqrt{T/T_0})^{-1} + G_t s_0/g}{1/K + f(\delta) G_t (s_0/g - W)} \qquad (3)$$

which is based on the equation of Walker et al. [1960] with (a) the addition of the self-shielding factor F, and (b) the assumption of zero penetration of thermal neutrons through the cadmium.

s_0 is a function of the resonance integral $s_0=17.3$ [Westcott 1960] (s_0 is the $T=T_0$ value of Westcott's s_4).

W is a function of the resonance integral below the cadmium cutoff energy. $W=0.027$. [Walker et al. 1960].

K is a function of the cadmium cutoff energy. For 0.1 cm Cd, $K=2.2931$ [Westcott et al. 1958].

r is a measure of the relative intensity of the dE/E component. The fraction of the neutron density in the dE/E component of flux is $4r(\pi\mu)^{-\frac{1}{2}}$.

g 1.0053.

G_t accounts for the self-screening of the resonance-energy neutrons in the foil.

$f(\delta)$ accounts for the attenuation of the resonance-energy neutrons in the cadmium cover.

G_t and $f(\delta)$ are reproduced in table 1 from a previous paper [Axton, 1963].

For a full discussion on the meanings of these terms the reader is referred to the literature.

Thus, with the experimentally determined value for R_{Cd} the value of r can be calculated from eq (3). The value so obtained is $r=0.0212$. The total flux density nv_0 is then given by

$$nv_0=n_{th}v_0(R/R-1)=n_{th}v_0(1-r/K)^{-1}$$
$$=n_{th}v_0/0.9908=4347 \text{ m/cm}^2 \text{ sec}$$

where R is the cadmium ratio which would be obtained with a thin $1/v$ detector. $R=K/r$ from eq (3) with $F=1$, $T=T_0$, $s_0=W=0$. It appears that changes as high as 20 percent in the value of r have very little effect on the value obtained for the total neutron flux density.

The Maxwellian flux density n_mv_0 (where n_m is the neutron density in the Maxwellian component of the flux) is given by

$$n_mv_0=nv_0\left(1-\frac{4r}{(\pi\mu)^{\frac{1}{2}}}\right)=0.9751\ nv_0=4239 \text{ m/cm}^2 \text{ sec}.$$

The value of μ, which is determined by the effective lower energy limit of the dE/E component of the flux, is a matter for some discussion. The value used here (3.681) is that for which s_0 was computed.

4. Accuracy of Results

Table 4 shows the various errors α associated with the calculation of the thermal neutron flux density, together with the weights ω with which they influence the result.

The sum $[\Sigma(\omega\alpha)^2]^{1/2}$ is less than ± 1 percent. In addition, there may be a systematic error not exceeding ± 1 percent associated with the absolute measurement of the radioactivity. The combined error is thus ± 2 percent.

It is concluded that NBS and NPL measurements of thermal neutron flux density are in agreement within the limits of experimental error.

The author is grateful for the cooperation of the National Bureau of Standards in this work, which has been carried out as part of the general research program of the National Physical Laboratory, and this paper is published with the permission of the Director.

TABLE 4. *Errors associated with flux density measurement*

Error	Weight ω	Error α
Counting statistics:		%
(Bare foil and background)	0.832	0.4
(Foil in Cd and background)	.124	1.4
N_β/N (Bare foil)	.832	.75
N_β/N (Foil in Cd)	.124	.75
Mass (Bare foil)	.832	.1
Mass (Foil in Cd)	.124	.1
F	1	.3
F_{Cd}	.175	.5
$g\sigma_0$	1	.4

5. References

Axton, E. J., J. Nucl. Energy, Part A Reactor Science **17**, No. 5 (May 1963).
De Juren, J. and Rosenwasser, H., J. Research, NBS **52**, 93 (1954).
Hughes, D. J. and Schwartz, R. B., BNL 325 2d Ed (1958).
Mosburg, E. R. and Murphey, W. M., J. Nucl. Energy **14**, 25 (1961).
Westcott, C. H., CRRP, 960 (1960).
Westcott, C. H., Walker, W. H., and Alexander, T. K., A./Conf. 15/P/202.
Walker, W. H., Westcott, C. H., and Alexander, T. K., Can. J. Phys. **38**, 57 (1960).

(Paper 67A3–206)

JOURNAL OF RESEARCH of the National Bureau of Standards—A. Physics and Chemistry
Vol. 67A, No. 3, May–June 1963

Absorption Bands of Carbon Dioxide* From 5.3 to 4.6 Microns

Arthur G. Maki, Earle K. Plyler, and Robert J. Thibault

(February 12, 1963)

Measurements have been made of the frequencies of the infrared absorption lines of CO_2 in the region from 1850 cm^{-1} to 2150 cm^{-1}. Observations were made at various pressures and pathlengths up to a maximum of 72 meter-atmospheres. Vibration-rotation constants were obtained characterizing the transitions $11^{1c}0$–000, $11^{1d}0$–000, $03^{1c}0$–000, $03^{1d}0$–000, 200–$01^{1c}0$, $12^{2c}0$–$01^{1c}0$, $12^{2d}0$–$01^{1d}0$ for $C^{12}O_2$. The $11^{1c}0$–000 band due to the $C^{13}O_2$ molecule was also measured.

1. Introduction

The infrared spectrum of CO_2 has been exhaustively studied by Courtoy who has compiled a critical survey of the energy levels and vibration-rotation constants for the various isotopic species of that molecule [1, 2].[1]

The five micron region contains two weak absorption bands due to the transitions $03^{1}0$–000 and $11^{1}0$–000. These two bands form a Fermi resonant diad and are rather important for determining the best potential constants for CO_2. Migeotte, Neven, Swenson, and Benedict have reported previous measurements on this region [3], but the resolution and wavelength accuracy available at that time was not quite as good as that now available in this laboratory. Because of slight disagreements between calculated and observed values, it was felt that those measurements should be repeated. In addition we have been able to resolve and analyze two Q branches for which the constants seem not to have been previously reported. The intensities of these bands are of great interest and of particular interest is the intensity anomaly which causes the P branch to be strong while the R branch is weak. Since this anomaly has already been discussed by Benedict in quantitative terms [4], it will not be further discussed here.

2. Experimental Procedure

The spectra were measured on the NBS high resolution infrared spectrometer described elsewhere [5]. Measurements were made using one of two gratings and a liquid nitrogen cooled PbSe detector. The highest resolution was obtained by using a 1,860 lines/in. grating double passed in third order. With this grating measurements were interpolated from a wavelength scale provided by measurements on a 7,500 lines/in. grating. Only lines that were not resolved with the finer grating were measured with the 1,860 lines/in. grating. Most of the measurements reported here were obtained directly from measurements with a 7,500 lines/in. grating used in the first order and double passed. Calibration with this grating was carried out by means of accurately measured rare gas spectra with a Fabry-Perot interferometer fringe system superimposed on the spectra for interpolation as described in reference 6.

The majority of the measurements were made with a pathlength of 24 m and pressures up to 1 atm. Pressures up to 3 atm were used in trying to observe lines due to the weaker transitions, but the increased pressure broadening of the lines usually resulted in a reduced sensitivity to the weaker lines. To achieve the highest resolution of the strong Q branches a 4 m path was used thus decreasing reflection losses in the absorption cell.

*This research was supported in part by the U.S. Air Force Geophysics Research Directorate, Bedford, Mass.

[1] Figures in brackets indicate the literature references at the end of this paper.

3. Analysis and Results

3.1. Analysis

Except for the Q branches the spectra were all analyzed using a least squares computer program to fit the observed frequencies to the power series

$$\nu_{obs}=\nu_0+(B'+B'')m+(B'-B'')m^2 -2(D'+D'')m^3-(D'-D'')m^4$$

where the symbols have their usual meaning. The Q branch lines were fitted to the equation

$$\nu_{obs}=\nu_0+(B'-B'')J(J+1)-(D'-D'')J^2(J+1)^2.$$

The calculated and observed constants are tabulated in table 1. Where no observed constants are given, the data were insufficient to obtain those constants and the calculated values were used in the band analysis. Since it was felt that Courtoy's values for B'' and D'' were more accurate than values obtainable from these measurements, Courtoy's values, as given in reference 2, were used to determine the other constants for all the bands reported here.

The calculated values of B' are those given by Courtoy [2] with the incorporation of a correction term due to the Coriolis interaction discovered by Courtoy and explained by Andrade e Silva and Amat [7]. The correction to the B' terms was made in the manner described by Courtoy and Triaille [8]. This correction was quite small for these energy levels, the largest correction being about -1.4×10^{-5} cm^{-1} for B_{12^20}.

The equations given by Nielsen, Amat, and Goldsmith [9, 10] were used to determine the approximate l-type resonance and Fermi resonance corrections necessary for the centrifugal distortion terms (D_v). No attempt was made to include the effect of an additional $J(J+1)$ dependence in the Fermi resonance matrix element which has recently been predicted by Maes [11]. Since the calculated values of ΔD are probably as good as the measured values, the calculated values of ΔD were used in determining the final values of ΔB. In those cases where a value of ΔD was experimentally determinable, both observed and calculated ΔD's gave nearly the same ΔB's.

In table 1 the standard deviations are given for the various constants. These deviations were determined solely by the scatter of the data and do *not reflect possible absolute errors.*

Table 2 and 3 list the observed and calculated frequencies (wavenumbers) for the absorption lines in the various bands. Where comparison is possible, the observed wavenumbers given in table 2 and 3 generally agree with those listed in reference 3 to within a tenth of a wavenumber (cm^{-1}). For the least squares computations line measurements to three decimal places were used. Because of the doubtful significance of the third decimal place, the wavenumbers given in tables 2 and 3 have been rounded off to two decimal places.

TABLE 1. *Band constants for CO_2 absorption bands between 1900 and 2150 cm^{-1}*

All values are given in wavenumbers (cm^{-1}). The error limits given are standard deviations and do not reflect possible consistent errors which will affect the absolute values. Calculated values were obtained from constants given in reference 2

Assignment	$C^{13}O_2$ 11^10^0-000	20^00^1-0^00^0	12^20^0-01^10	12^40^0-01^10	03^10-000	03^30-000	11^10-000	11^30-000
ν_0 obs	2037.093±0.006	2129.769±0.005	2093.359±0.004		1932.477±0.004		2076.890±0.003	
ν_0 calc	2037.12	2129.63	2093.29		1932.46		2076.85	
B'' calc	0.39025	0.39062	0.39062	0.39123	0.39021	0.39021	0.39021	0.39021
B' obs	.39004	.39058$_7$	.39151$_2$	.39151$_2$	.39072$_3$	.39167$_7$	.39037$_7$	.39131$_1$
B' calc	.39011$_1$	.39059$_7$	.39153$_6$	.39153$_6$	.39070$_2$	.39165$_5$	.39045$_5$	.39134
D'' obs×10^5					13.3±1.3		13.6±1.1	
D'' calc×10^5	13.7	13.5	13.5	13.5	13.5	13.5	13.5	13.5
D' obs×10^5	12.3				14.6		12.8	
D' calc×10^5	12.8	9.8	10.5	12.4	14.7	15.2	12.4	11.9
ΔB obs	−0.00021±0.00002	−0.000038±0.000005	0.000892±0.000009	0.000282±0.000009	0.000513±0.000002	0.001467±0.000004	0.000167±0.000002	0.001101±0.000003
ΔD obs×10^5	1.4±0.7				1.1±0.2		−0.7±0.1	

TABLE 2. *Wavenumbers (cm^{-1}) of weak absorption bands due to $C^{13}O_2$ and $C^{12}O_2$ in 5 micron wavelength region*

J	$C^{13}O_2$ $11^{1c}0$–000		$C^{12}O_2$ 12^20–$01^{1c}0$				$C^{13}O_2$ 12^20–01^10				$C^{12}O_2$ 200–$01^{1c}0$			
	P		P		R		P		R		P		R	
	Obs	Calc	Obs	Calc	Obs	Calc	Obs	Calc	Obs	Calc	Obs	Calc	Obs	Calc
1					2094.93	.92								
2									2095.71	.71				
3					96.51	.50					2127.42	.42	2132.91	.89
4									97.31	.28				
5					98.07	.08					25.86	.86	34.49	.45
6									2098.85	.85				
7			2087.91	.93	2099.66	.67					24.28	.30		
8									2100.42	.42				
9			86.37	.39	2101.25	.27					22.71	.74	37.56	.58
10	2029.29	.27							02.01	.00				
11			84.86	.86							21.17	.17		
12	27.69	.70							03.59	.58				
13			83.34	.34							19.63	.61	2140.72	.70
14	26.13	.13							05.16	.16				
15			81.85	.83							18.04	.05		
16	24.54	.56							2106.77	.74				
17			80.31	.32							16.47	.48		
18	23.00	.98												
19														
20	21.40	.41												
21											13.36	.36		
22	19.83	.83					2076.28	.28						
23			75.84	.85							11.79	.80		
24							74.74	.74						
25											10.24	.24		
26							73.21	.21						
27			72.90	.91							08.68	.68		
28	15.09	.10					71.68	.68						
29			71.46	.46							07.16	.12		
30	13.51	.52					2070.17	.15						

3.2. $C^{13}O_2$ Band at 2037 cm^{-1}

The band due to the $11^{1c}0$–000 transition of $C^{13}O_2$ was measured at 2037.09 cm^{-1}. This band is part of a Fermi doublet of which the other band lies at about 1896.54 cm^{-1}. The other band was not detected in this work even at the highest pressures and pathlengths used. It is expected to be considerably weaker than the 11^10–000 band due in part to the diminished Fermi resonance in $C^{13}O_2$. Consequently, it will probably be necessary to use isotopicly enriched samples before this 03^10–000 transition will be measurable. The Q branch for the 11^10 band of $C^{13}O_2$ was not resolved in this work. This is understandable since the ΔB term, which governs the Q branch line spacing, is predicted to be rather small and relatively large pressures were necessary to observe this weak band. Furthermore, this Q branch is overlapped by the P branch of the much stronger $C^{12}O_2$ band.

Table 1 gives a comparison of the calculated and observed values of the various vibration-rotation constants necessary to describe this band. The discrepancies in ν_0 and B' are believed to be greater than the experimental error and are consequently indicative of either a very small error in Courtoy's constants or the neglect of some terms in the potential expansion. Such errors are not unexpected for $C^{13}O_2$ as Courtoy did not have a surfeit of data from which to derive his constants. Table 2 lists the lines measured and the values calculated using the constants given in table 1.

3.3. CO_2 Bands Between 1900 and 2150 cm^{-1}

The strongest CO_2 absorption bands in the 5μ region are those due to the Fermi doublet 03^10–000 and 11^10–000. For these transitions a rather large number of lines have been measured in the P and R branches and the Q branches were sufficiently well resolved to yield good values for ΔB.

Two more bands due to the transitions 200–01^10 and 12^20–01^10 have been measured in this region. The latter band is split into c and d components. When treated individually the two components yield values B_{12^20} which should be equal and in fact are found to be the same to within 5×10^{-6} cm^{-1}. Such agreement indicates that the standard deviations quoted are realistic. The values reported in table 1 for the 12^20—01^10 bands were obtained by assuming that the c and d components of the upper vibrational level had the same vibrational energy (band center) and B_v values.

Similarly the analysis of the c and d components of each of the two Fermi doublet bands $3\nu_2^1$ and $\nu_1+\nu_2^1$ was carried out simultaneously so as to yield the the same values for the band centers of the c and d components.

The important constants ν_0 and ΔB for the Fermi doublet are in slight disagreement with the values predicted by Courtoy's constants. At least in the case of $\nu_1+\nu_2$ this discrepancy is greater than experimental error. The band centers for the other bands in this region are in even greater disagreement with the calculated values.

TABLE 3. *Strongest CO_2 absorption bands between 4.6 and 5.3 microns*

Line measurements are given in units of wavenumbers (cm^{-1})

J.	$03^{1}0$–000				$03^{1}0$–000		$11^{1}0$–000				$11^{1}0$–000	
	P		R		Q		P		R		Q	
	Obs	Calc	Obs	Calc	Obs	Calc	Obs	Calc	Obs	Calc	Obs	Calc
0												
1												
2			1934.83	.82			2075.30	.33				
3												
4	1929.36	.36	36.39	.39			73.75	.77	2080.81	.80		
5												
6	27.82	.81	37.98	.97			72.19	.21	82.37	.36		
7												
8	26.26	.26	39.55	.55			70.64	.66	83.94	.93		
9												
10	24.72	.72					69.08	.10	85.51	.50		
11												
12							67.54	.55	87.07	.07		
13												
14	21.65	.65							88.62	.64		
15												
16	20.12	.11					64.43	.45				
17												
18					1932.97	.98			91.73	.78		
19												
20	17.07	.07					61.35	.35				
21												
22	15.56	.55	50.73	.70			59.80	.81	94.93	.93		
23												
24	14.04	.03	52.29	.31	33.32	.35	58.26	.26	97.50	.51	2077.56	.56
25												
26	12.53	.52	53.91	.92	33.49	.50	56.71	.72	98.07	.08	77.68	.67
27												
28	11.03	.02	55.52	.53	33.65	.66	55.17	.18	2099.66	.66	77.82	.79
29												
30	09.53	.52	57.13	.15	33.83	.83	53.64	.64	2101.25	.24	77.94	.93
31												
32			58.75	.77	34.00	.01	52.11	.11	02.83	.83	78.08	.07
33												
34	06.54	.52	60.37	.40	34.19	.20	50.58	.58	04.42	.41	78.24	.22
35												
36	05.05	.03	62.01	.02	34.40	.40	49.05	.05	06.00	.99	78.41	.39
37												
38	03.57	.55	63.64	.65	34.61	.61	47.52	.52	07.58	.58		
39												
40	02.08	.07	65.28	.29	34.83	.84	46.01	.99	09.18	.17	78.76	.74
41												
42	1900.61	.59			35.07	.07	44.47	.47	10.77	.76	78.94	.93
43												
44	1899.13	.11	68.54	.56	35.31	.31	42.96	.95	12.38	.35		
45												
46	97.66	.64	70.19	.20	35.57	.57			13.94	.95		
47												
48	96.19	.17	71.82	.84			39.94	.92	15.57	.54	79.54	.57
49												
50	94.73	.71	73.46	.49	1936.13	.11	38.41	.41	17.16	.14	79.78	.80
51												
52	93.27	.25	75.12	.13			36.91	.90	18.75	.74	2080.05	.05
53												
54	91.82	.79	76.74	.78			35.40	.40	20.38	.34		
55												
56	90.32	.34	1978.41	.43			33.91	.90	21.96	.95		
57												
58	88.93	.89					32.40	.40				
59												
60	87.45	.44					30.90	.91	25.16	.16		
61												
62	1885.99	.99					29.41	.42	2126.76	.77		
63												
64							27.91	.93				
65												
66												
67												
68							24.95	.98				
69												
70												
71												
72							22.04	.04				
73												
74							2020.54	.58				

No attempt has been made to reevaluate the various vibration-rotation constants in order to obtain a better fit with the data presented here. Such a task would be a major undertaking and Courtoy has indicated [8] that such work is in progress elsewhere. The fact that both c and d components of the two resonating diads have been resolved does allow one to make a direct evaluation of some combinations of constants.

For a resonance diad the sum of the l doubling terms (q_v) for the two resonating energy levels is constant and independent of the degree of resonance. From table 1 one finds $q_{11^10}+q_{03^10}=188.8\times10^{-5}$ cm^{-1}. Correcting for the interaction between the c levels and ν_3 this becomes 187.9×10^{-5} cm^{-1}.

Since $$q_v=\tfrac{1}{2}(v_2+1)\ [q_0-q_1v_1-q_2v_2-q_3v_3]$$

and $$q_{01^10}=61\times10^{-5}=q_0-q_2$$

then $$q_{11^10}+q_{03^10}=183\times10^{-5}-4q_2-q_1.$$

This gives $4q_2+q_1=-4.9\times10^{-5}$ cm^{-1}. Similarly the sum of ΔB_{11^10-000} and ΔB_{03^10-000} yields $-\alpha_1-4\alpha_2+\gamma_{11}+10\gamma_{22}+\gamma_{12}+2\gamma_{11}=162.9\times10^{-5}$ cm^{-1} when the Coriolis resonance correction is made. This compares very favorably with the value of 164.5×10^{-5} cm^{-1} calculated using the constants given on page 128 of reference 2. It is difficult to tell whether the difference of 1.6×10^{-5} cm^{-1} is significant.

The rather large deviations from the predicted positions of some of the band centers which has been found in this work and that of Plyler, Tidwell, and Benedict [12] may be due, at least in part, to the neglect of the constants x_{11l}, x_{21l}, and x_{3ll} in the vibrational energy expansion. These constants are necessary for N_2O [13] and have recently been found to be important for the vibrational analysis of HCN [14] and DCN.

The authors acknowledge the assistance of Joseph Hilsenrath in using the least squares computer program, and to Dr. W. S. Benedict for his suggestions concerning these measurements.

4. References

[1] C. P. Courtoy, Can. J. Phys. **35,** 608 (1957).
[2] C. P. Courtoy, Ann. Soc. Sci. Bruxelles, Ser. I, **73,** 5 (1959).
[3] M. Migeotte, L. Neven, J. Swensson, and W. S. Benedict, Mem. Soc. Roy. Sci. Liege, Special Vol. 2 (1957).
[4] W. S. Benedict, APCRC–TR–56–275 (1956).
[5] E. K. Plyler and L. R. Blaine, J. Research NBS **62,** 7 (1959) RP2922.
[6] E. K. Plyler, L. R. Blaine, and E. D. Tidwell, J. Research NBS **55,** 279 (1955) RP2630.
[7] Andrade e Silva and G. Amat, J. Mol. Spect. **9,** 354 (1962).
[8] C. P. Courtoy and E. A. Triaille, J. Mol. Spect. **9,** 339 (1962).
[9] G. Amat, M. Goldsmith, and H. H. Nielsen, J. Chem. Phys. **24,** 44 (1956).
[10] H. H. Nielsen, G. Amat, and M. Goldsmith, J. Chem. Phys. **26,** 1060 (1957).
[11] S. Maes, J. Mol. Spect. **9,** 204 (1962).
[12] E. K. Plyler, E. D. Tidwell, and W. S. Benedict, J. Opt. Soc. Am. **52,** 1017 (1962).
[13] E. D. Tidwell, E. K. Plyler, and W. S. Benedict, J. Opt. Soc. Am. **50,** 1243 (1960).
[14] A. G. Maki and L. R. Blaine, J. Mol. Spect. (in press).

(Paper 67A3–207)

JOURNAL OF RESEARCH of the National Bureau of Standards—A. Physics and Chemistry
Vol. 67A, No. 3, May–June 1963

Infrared Spectrum of the $\nu_2+\nu_6$ Band of $C^{13}C^{12}H_6$*

Walter J. Lafferty and Earle K. Plyler

(February 12, 1963)

The infrared spectrum of the $\nu_2+\nu_6$ band of $C^{13}C^{12}H_6$ has been analyzed and a value of $B_0=0.64865\pm0.00005$ cm^{-1} determined. When this value is combined with that found in recent work on isotopically normal ethane, a "r_s" value of 1.527 ± 0.004 A for the carbon-carbon bond distance is obtained. (Uncertainties are probable errors.)

1. Introduction

From recent infrared studies of ethane and ethane-d_6, a ground state carbon-carbon bond distance of 1.536 with probable error 0.002 A has been obtained [1, 2].[1] This bond distance is considerably higher than the C—C bond lengths, 1.526 with limits of error ±0.002 A, obtained for the saturated hydrocarbons propane and isobutane by the "r_s" or "substitution" method in the microwave studies of Lide [3, 4]. Since the two methods of determining bond distances are only approximately equivalent due to rotation-vibration effects, this difference is not surprising.

The purpose of this work was to examine the spectrum of $C^{13}C^{12}H_6$ in an attempt to obtain a "r_s" value for the C—C bond distance of ethane for comparison with these bond lengths reported for the more complex molecules. In addition other rotational constants would be obtained which would be of use to future investigators of this molecule.

2. Experimental Procedure

The sample, which contained 59.5 percent $C^{13}C^{12}H_6$, was purchased from Merck Sharp & Dohme of Canada, Ltd. The spectra were taken with a pressure of 3.2 mm Hg total pressure (1.9 mm $C^{13}C^{12}H_6$) and an optical path of 24 m.

The spectrometer, used in this study as well as for the normal ethane work [2], has been described previously. Because of the small amount of costly sample available, a threefold longer optical path (24 m) was required than was used for ethane. This resulted in the loss of some resolution; however, lines separated by about 0.035 cm^{-1} could be resolved. The spectra were measured by using rare gas emission lines as standards. The regions between the standard lines were measured from the fringe system formed by a Fabry-Perot interferometer [5].

*This work was supported by the Research Division of the U.S. Atomic Energy Commission.

[1] Figures in brackets indicate the literature references at the end of this paper.

3. Rotational Analysis

As in the case of normal ethane, the only parallel band of $C^{13}C^{12}H_6$ that could be resolved sufficiently well with the instrumentation available was the $\nu_2+\nu_6$ band at 2749 cm^{-1}. Substitution of one C^{13} in ethane results in a shift of about 4.1 cm^{-1} for the origin of this band. Since the sample contained about 40 percent normal ethane, the resulting spectrum consisted of a complicated mixture of lines from the two overlapping bands together with their accompanying "hot bands" arising from excited levels of the torsional vibration. The lines of ethane were easily identified when the spectra were compared with those obtained from the earlier studies on ethane. The vibrational shift was such that most of the P and R branch lines fell between those of the normal ethane. There was, however, some blending of the lines. Since blending can result in an apparent change of the frequency of a line, all blended lines were marked as such when assigned and given a weight of ½ in the following calculations. Badly overlapped lines were not used in the analysis.

As in the case of normal ethane, the quantity $(A'-B')-(A''-B'')$ was sufficiently large so that transitions from the substates $K=2$ and higher were resolved. The unresolved lines from the substates $K=0$ and 1 were not used in the calculations. The ground state rotational constants were calculated by means of combination differences from the equation

$$\begin{aligned}\Delta_2F''&=R(J-1,\,K)-P(J+1,\,K)\\&=(4B''-6D_J''-4D_{JK}''K^2)\,(J+\tfrac{1}{2})\\&\quad-8D_J''(J+\tfrac{1}{2})^3. \quad (1)\end{aligned}$$

Since no substates with K greater than 6 were identified, the value of D_{JK}'' obtained was highly uncertain. The assumption was then made that this constant is equal to that found for ethane times the ratio of the B values of the substituted ethane to that of the normal molecule or 5.8×10^{-6} cm^{-1}. With this assumed constant, the resulting ground state rotational constants found by least squares

were $B''=0.64865\pm0.00005$ cm^{-1} and $D_J''=8.4\pm1.4\times10^{-7}$ cm^{-1} where the uncertainties cited are probable errors. The values of D_J' calculated is in good agreement with that found for normal ethane ($D_J''=7\pm2\times10^{-7}$ cm^{-1}).

The upper state rotational constants were determined using the equation

$$\nu=\nu_0+[B'+B''-(D'_{JK}+D''_{JK})K^2]m+[B'-B''-D_J'+D_J''-(D'_{JK}-D''_{JK})K^2]m^2-2(D_J'+D_J'')m^3-(D_J'-D_J'')m^4+[(A'-B')-(A''-B'')]K^2. \quad (2)$$

The values of B'', D_J'', D''_{JK} obtained above were inserted into the equation, and the data were subjected to a least squares fit. As in the case of normal ethane, the $K=5$ substate was found to be perturbed. The origin of this state fell 0.03_2 cm^{-1} above the calculated value. While this difference is small, it is 3.1 times the standard deviation of the fit taken without including this substate and is therefore significant. Any changes in the other rotational constants of this state were too small to be detected. Because of this perturbation, the observed frequencies were again fit to eq (2) with the frequencies from the $K=5$ substate omitted. The constants obtained from this treatment are listed in table 2. The spectrum calculated from these constants is compared with the observed spectrum in table 1. For the $K=5$ substate, the observed origin was used instead of that calculated from eq (2).

TABLE 1. *Comparison between observed and calculated spectrum of $\nu_2+\nu_6$ of $C^{13}C^{12}H_6$*

J_K	$^qR_K(J)$		$^qP_K(J)$		J_K	$^qR_K(J)$		$^qP_K(J)$	
	Obs	Calc	Obs	Calc		Obs	Calc	Obs	Calc
	cm^{-1}	cm^{-1}	cm^{-1}	cm^{-1}		cm^{-1}	cm^{-1}	cm^{-1}	cm^{-1}
3_0	2754.164	2754.141			11_3	63.236	63.233	[b] 33.908	33.907
3_1		54.163			11_4	[b] 63.356	63.361	34.044	34.043
3_2	54.229	54.227	2745.290	2745.297	11_5	63.540	63.556	34.241	34.253
3_3	[b] 54.346	[b] 54.336			11_6	63.717	63.728	34.440	34.433
4_0	54.362	55.331			12_0	64.104	64.089	32.230	32.201
4_1		55.353			12_1		64.105		32.218
4_2	55.410	55.417	[b] 43.931	43.936	12_2	64.143	64.158	32.270	32.278
4_3	55.545	55.525	44.058	44.046	12_3	[b] 64.253	64.247	[b] 32.369	32.373
4_4	55.671	55.675			12_4	[b] 64.368	64.370	32.509	32.505
					12_5	64.558	64.560	32.696	32.710
5_0	56.528	56.501			12_6	64.715	64.723	32.890	32.883
5_1		56.522							
5_2	56.589	56.585	42.550	42.553	13_0	65.111	65.087	30.679	30.649
5_3	56.719	56.691	42.652	42.662	13_1		65.103		30.667
5_4	56.838	56.840	42.825	42.814	13_2	65.150	65.154	30.719	30.725
5_5	[b] 57.072	57.061			13_3	[b] 65.231	65.238	30.834	30.816
					13_4	[b] 65.358	65.357	30.937	30.945
6_0	57.671	57.650			13_5	65.529	65.540	31.150	31.144
6_1		57.669			13_6	65.700	65.696	31.310	31.311
6_2	57.728	57.732	41.158	41.149					
6_3	57.860	57.836	41.276	41.257	14_0			2729.112	2729.077
6_4	57.977	57.982	[b] 41.411	41.407	14_1				29.095
6_5	58.195		41.646	41.635	14_2			29.142	29.151
6_6	58.399	58.399			14_3	2766.237	2766.208	29.239	29.239
					14_4	[b] 66.319	66.321	29.363	29.363
7_0	2758.800	2758.775	2739.661	2739.638	14_5	66.508	66.497	29.542	29.556
7_1		58.795		39.657	14_6	66.638	66.645		
7_2	58.839	58.857	[b] 39.722	39.724					
7_3	[b] 58.963	58.959	39.835	39.830	15_2	67.070	67.079	27.548	27.556
7_4	59.085	59.102	39.980	39.978	15_3			[b] 27.618	27.641
7_5	59.342	59.317	40.199	40.203	15_4	[b] 67.259	67.263	27.755	27.759
7_6	59.501	59.511			15_5	67.444	67.431	27.952	27.947
					15_6	67.591	67.571	28.097	28.098
8_0	59.898	59.882	38.209	38.193					
8_1		59.901		38.213	16_0	67.976	67.952	25.894	25.872
8_2	59.950	59.961	38.255	38.277	16_1		67.964		25.888
8_3	60.087	60.061	38.388	38.381	16_2	68.010	68.009	25.935	25.940
8_4	60.191	60.201	38.537	38.527	16_3			26.030	26.021
8_5	60.396	60.412	38.751	38.749	16_4			26.137	26.134
8_6	60.589	60.600	38.944	38.944	16_5	68.330	68.342		
					16_6	68.468	68.473		
9_0	60.988	60.966							
9_1		60.984			17_0			24.268	24.238
9_2	61.024	61.043	36.794	36.809	17_1				24.252
9_3	61.152	61.140	36.913	36.912	17_2			24.298	24.302
9_4	[b] 61.277	61.276	37.055	37.055	17_3	68.990	68.985	24.385	24.379
9_5	61.476	61.483			17_4			24.487	24.487
9_6	61.664	61.666	37.468	37.463	17_5	69.236	69.234		
					17_6	69.356	69.352		
10_0	2762.045	2762.037	2735.269	2735.238					
10_1		62.045		35.258	18_2			22.649	22.644
10_2	62.079	62.103	35.315	35.320	18_3			22.707	22.716
10_3	62.203	62.197	35.433	35.420	18_4			22.818	22.818
10_4	62.322	62.330	35.560	35.560					
10_5	62.534	62.531	35.757	35.773	19_3			2721.030	2721.032
10_6	62.721	62.708	35.948	35.959	19_4			21.129	21.127
11_0	63.082	63.069	33.756	33.731	20_2			19.270	19.264
11_1		63.086		33.749	20_3			19.348	19.327
11_2	63.150	63.141	33.802	33.810					

[b] Blended line.

TABLE 2. *Rotational constants of* $C^{13}C^{12}H_6$ *derived from the combination band,* $\nu_2+\nu_6$ *in* cm^{-1}[a]

ν_0	2749.164±0.002
B''	0.64865±0.00005
D_J''	8.4±1.4×10⁻⁷
D_{JK}''	5.8×10⁻⁶ (assumed)
$B'-B''$	−0.01062±0.00001
$D_{JK}'-D_{JK}''$	3.12±0.07×10⁻⁶
$D_J'-D_J''$	~0
$D_K'-D_K''$	~0
$(A'-B')-(A''-B'')=0.0226\pm0.0005$	

[a] Uncertainties cited are probable errors.

4. Results

For a symmetric top molecule, the "r_s" distance of an atom on the symmetry axis from the center of gravity is given by the relation

$$\Delta I_0=\mu r_s^2 \tag{3}$$

where ΔI_0 is the change of the moment of inertia upon substitution, $\mu=m\Delta m/(M+2m)$, M is the mass of the original molecule, and Δm is the change of mass upon substitution. Using the B_0 value obtained earlier for ethane and the value found for the C^{13} substituted ethane above, a "r_s" value of 1.527± 0.004 A for the C—C distance is calculated. The uncertainty cited is probable error.

This value supports Lide's estimate that the "r_s" value for ethane lies in the range 1.525–1.530 A [6] and is in good, albeit somewhat fortuitous, agreement with the value 1.526 A found for the C—C bond lengths in propane and isobutane.

The authors thank Dr. B. P. Stoicheff for his suggestions and interest in this problem, and Miss Jessie Kirkland for measuring the spectra.

5. References

[1] H. C. Allen, Jr., and E. K. Plyler, J. Chem. Phys. **31,** 1062 (1959).
[2] W. J. Lafferty and E. K. Plyler, J. Chem. Phys. **37,** 2688 (1962).
[3] D. R. Lide, J. Chem. Phys. **33,** 1514 (1960).
[4] D. R. Lide, J. Chem. Phys. **33,** 1519 (1960).
[5] E. K. Plyler, L. R. Blaine, and E. D. Tidwell, J. Research NBS **55,** 183 (1955) RP 2617.
[6] D. R. Lide, Tetrahedron **17,** 125 (1962).

(Paper 67A3–208)

JOURNAL OF RESEARCH of the National Bureau of Standards—A. Physics and Chemistry
Vol. 67A, No. 3, May–June 1963

Self-Broadening of Carbon Monoxide in the 2 ν and 3 ν Bands *

Earle K. Plyler and Robert J. Thibault

(February 12, 1963)

The self-broadening of carbon monoxide has been measured for the 2 ν and 3 ν bands with pressures up to 3.5 atmospheres. A grating spectrometer of high resolving power was used for the measurements and the correction for finite slits was small. The corrections varied from 3 to 20 percent for the different conditions of measurement. The half-widths per atmosphere, $\gamma°$, decreased from 0.089 cm^{-1} for $|m|=1$ to 0.053 cm^{-1} for $|m|=21$. The half-widths are compared with those obtained by other investigators and it is shown that the results reported in this work fall in between the self-broadening values previously obtained.

1. Introduction

The broadening of the rotational lines of carbon monoxide by foreign gases has been investigated for a number of gases such as CO_2[1].[1] The observed half-width, γ, is the sum of the self-broadening of CO and the foreign gas broadening. This may be expressed as follows:

$$\gamma=\gamma^0_{CO}P_{CO}+\gamma^0_F P_F \qquad (1)$$

where γ^0_{CO} is the half-width per atm for CO self-broadening and γ^0_F is the half-width per atm of the foreign gas broadening; P_{CO} and P_F are the partial pressures in atmospheres of CO and of the foreign gas, respectively.

If a long path cell of 4 m or greater is used, the partial pressure of CO which produces optimum line blackening is a few mm (Hg) or less and the term, $\gamma^0_{CO}P_{CO}$, of eq (1) approaches zero. Whenever a long path cell is available, more accurate results for γ^0 can be obtained. If a cell with an optical path of 10 cm is used, the pressure of the CO may have to be of the same order of magnitude as the pressure of the broadening gas to obtain suitable measurements. In such cases the self-broadening of the carbon monoxide must be known before γ^0 for the foreign gas can be determined. If the foreign gas broadening is smaller than the self-broadening of CO, appreciable errors may be introduced by using inaccurate values for the CO self-broadening.

The self-broadening of CO has been measured in three different laboratories and the values differ somewhat. This work was undertaken to determine a precise set of values for the self-broadening of CO.

2. Experimental Procedures

In order to secure the best possible results, a high-resolution grating spectrometer was used double-passed in this work. A 10,000 1/in. commercial replica grating was used in the first order for the 2–0 band and in the second order for the 3–0 CO band. An optimum balance between slit-width, response time and noise level was obtained with a spectral slit of 0.08 cm^{-1}. A response of 98 percent of the total deflection was obtained in 1 sec in the 2–0 and 3–0 bands. The grating was driven at 18 sec of angle per minute of time which was about 0.06 cm^{-1}/min in the 2–0 band. Further information regarding the spectrometer and its operation can be obtained from a previous publication [2].

Several preliminary tests were made before the broadening was measured. These included slit width measurements, stray energy tests, transmission tests, and recorder linearity checks.

Many different path and pressure combinations were employed to insure the reliability of our results. These are listed in table 1. The higher pressures involved were measured with a Bourdon tube type gage with a stated accuracy to within ½ percent at 100 lb/in^2.

The correction of the observed half-widths for the finite slit width of the spectrometer was made using the correction factors proposed by Izatt [3].

TABLE 1. *Pathlengths and pressures used in measurement of CO self-broadening*

2-0 Band		3-0 Band	
Pathlength	Pressure	Pathlength	Pressure
cm	*atm*	*cm*	*atm*
4	1.65	400	2.00
4	1.83	400	2.29
4	3.45	400	3.00
9	1.00		
9	2.00		
9	2.17		
9	2.34		
9	3.00		
100	2.00		

3. Results

The half-width of a spectral line may be defined as half its physical width, measured at the frequency corresponding to half its maximum extinction, expressed in reciprocal centimeters per atmosphere. The method of measurement used in our work is essentially the same as that applied previously in this laboratory (see ref. 1). It is a very simple

*This work was supported by the Geophysic Research Directorate, Air Force Cambridge Research Laboratories.

[1] Figures in brackets indicate the literature references at the end of this paper.

method consisting of measuring the line widths at 40, 50, and 60 percent of the extinction coefficient at maximum absorption. The three values obtained are reduced to the half-width for 50 percent of the maximum coefficient by dividing by a constant which is dependent on the coefficient of extinction and line shape. These factors are 1.22 for 40 percent, 1.0 for 50 percent and 0.817 for 60 percent, assuming Lorentzian line shape. Since it is a direct method, and the slit corrections are relatively small (<20 percent in all cases and<7 percent in most), our results should certainly be considered reliable to within ± 5 percent.

An example of the data obtained, showing the effect of pressure change on self-broadened CO lines, is given in figure 1. The half-widths measured from these data are presented in the form of a table and a graph. Table 2 lists the average values obtained for both the (2–0) and the (3–0) CO bands separately, while figure 2 represents the weighted average of all values. The self-broadening, $\gamma°$, of corresponding lines (same $|m|$) of the P and the R branches agreed within experimental error and are averaged in the final results.

The self-broadening of carbon monoxide has previously been measured in three laboratories. Table 3 gives a brief summation of the conditions of measurement. The results obtained by each group are plotted in figure 3, along with the measurements reported in this paper.

TABLE 2. *Half-width, $\gamma°$, for self-broadening of carbon monoxide for the 2 ν and 3 ν bands*

$\|m\|$	$\gamma°$ (cm^{-1} atm^{-1})		Weighted average	No. of measurements
	2-0	3-0		
1	0.0870	------	0.0870	9
2	.0712	0.0732	.0716	10
3	.0651	.0665	.0654	13
4	.0605	.0643	.0616	7
5	.0567	.0582	.0572	6
6	.0553	.0569	.0560	7
7	.0546	.0568	.0555	6
8	.0543	.0564	.0551	8
9	.0548	.0556	.0551	6
10	.0553	.0552	.0552	8
11	.0533	------	.0533	4
12	.0538	.0534	.0536	7
13	.0538	.0523	.0532	5
14	.0529	.0528	.0529	4
15	.0534	------	------	4
16	.0535	------	------	5
17	.0531	------	------	5
18	.0528	------	------	5
19	.0522	------	------	4
20	.0523	------	------	1
21	0512	------	------	2

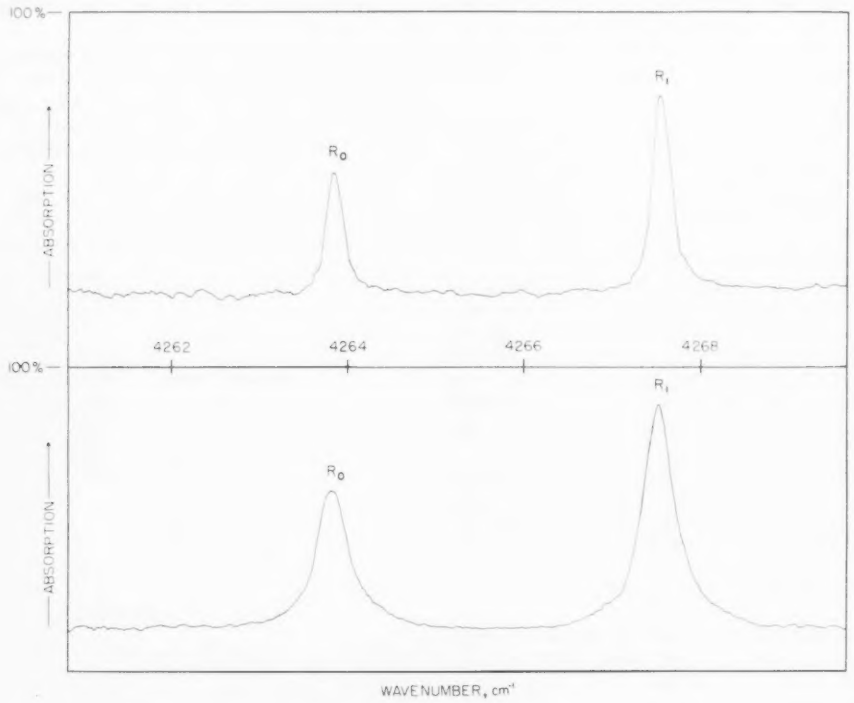

FIGURE 1. *The upper curve shows the self-broadening* CO *lines* R_0 and R_1 *of the 2 ν band under 1 atm pressure.*

The lower curve shows the same lines with 2.1 atm pressure. The absorption path length in both cases was 9.0 cm.

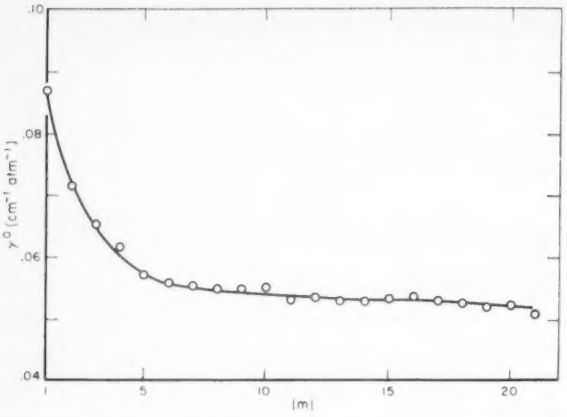

FIGURE 2. *The variation of the half-widths, γ°, for carbon monoxide as a function of the rotational number* |m|.

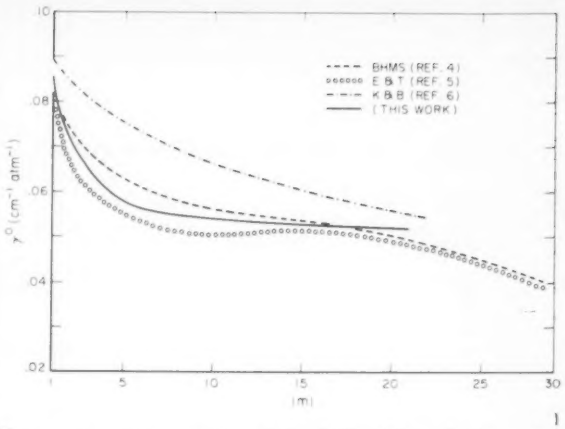

FIGURE 3. *A comparison of the half-widths, γ°, for carbon monoxide as obtained by different observers.*

TABLE 3. *The conditions of measurement of the self-broadening of* CO

Investigator	Lines reported	Pathlength	Pressure Hg	Slit width	CO band
		cm	*cm*	*cm*$^{-1}$	
Eaton & Thompson	$\|m\|$=1 to 28	0.6 to 20	1 to 30	0.5	(1-0)
Benedict et al	$\|m\|$=1 to 32	0.03 to 890	0.3 to 228	0.2	(1-0) and (2-0)
Kostkowski & Bass	$\|m\|$=1 to 22	1 to 100	380 to 760	0.25	(2-0)
This work	$\|m\|$=1 to 21	4 to 400	76 to 262	0.08	(2-0) and (3-0)

4. Discussion

The results obtained in this study fall between those of Benedict et al. [4] and those of Eaton and Thompson [5]. The greatest variation of their values from our results occurs at $|m|=7$ where the disagreement is about 8 percent. The average of the two sets of values from $|m|=1$ to $|m|=16$ fall very close to our results. The half-widths reported by Kostkowski and Bass are somewhat larger than those reported by other workers. Since their work was extended to higher pressures, the inherent overlapping in the wings of lines may have influenced their results.

It should be noted that although data were obtained for lines of $J>21$, these are not considered as reliable as the low J values, due to their low intensity, and have not been included. No quantitative conclusion can be drawn from the present work as to decrease in half-widths with higher J values; however, the variation of γ° with $|m|$ must be related to the directional properties of the intermolecular forces. In the case of self-broadening in CO, it is believed that both the quadrupole-quadrupole and anisotropic dispersion forces are of primary importance. The rapid decrease in γ° with $|m|$, and the magnitude of γ° have been approximately accounted for by a recent calculation based on these forces [7].

Quantitative measurements of the intensities of the lines of 2 ν (4260 cm^{-1}) and 3 ν (6350 cm^{-1}) bands of CO were not made. However, it was observed that the intensities of the P and R branches of the 2 ν compared with those of the 3 ν were approximately equal when a pressure of 3 atm and 400 cm path length were used for the measurement of 3 ν and 1.5 atm pressure and 4 cm path length were used for 2 ν. This indicates that the intensity of 2 ν compared to 3 ν is roughly 200 to 1.

5. References

[1] Earle K. Plyler and Robert J. Thibault, J. Research NBS **66A,** (Phys. and Chem.) No. 5 435 (1962).

[2] Earle K. Plyler and L. R. Blaine, J. Research NBS **62,** 7 (1959) RP 2922.

[3] J. R. Izatt, Progress Rep., J. Hopkins Univ., Lab. of Astrophysics and Phys. Meteorology (1960).

[4] W. S. Benedict, R. Herman, G. Moore, and S. Silverman, Astrophysics J. **135,** 1277 (1962).

[5] D. R. Eaton and H. W. Thompson, Proc. Roy. Soc. **A 251,** 475 (1959).

[6] H. J. Kostkowski and A. M. Bass, J. Quant. Spec. and Rad. Transfer **1,** 177 (1961).

[7] W. S. Benedict and R. C. Herman, Symposium on Spectral Line Shape and Molecular Interactions, Rehoboth, Sept. 1–5, 1961.

(Paper 67A3–209)

JOURNAL OF RESEARCH of the National Bureau of Standards—A. Physics and Chemistry
Vol. 67A, No. 3, May–June 1963

Thermodynamic Properties of Polyethylene Predicted from Paraffin Data

Martin G. Broadhurst

(February 13, 1963)

Thermodynamic data on the *n*-paraffins from *n*-C_5H_{14} through *n*-$C_{18}H_{38}$ have been used to obtain values for the specific heat, entropy, enthalpy, and Gibbs free energy of a large, ideal CH_2-chain crystal from 0 to 420 °K and of the liquid above 200 °K. Analytical expressions are given for the properties of the crystal and liquid above 200 °K. For the crystal, a modified Einstein function was used to adjust the melting temperature to 414.3 °K. Values between 975 and 1025 cal/mole for the heat of fusion were found to be the ones most consistent with the data. Comparison of the results with polyethylene data shows reasonable agreement.

1. Introduction

This paper concerns the empirical determination of accurate values for the thermodynamic properties of ideal CH_2-chain crystal [1] and liquid in the temperature range from 0 to 420 °K and 200 to 420 °K respectively, using published data on pure *n*-paraffins. This analysis is intended to circumvent the inherent difficulties involved in measuring polyethylene directly since (so far) even the most carefully crystallized polyethylene samples are not large, well defined CH_2-chain systems, and measurements necessarily reflect the nonnegligible effects of chain folds and "amorphous" inclusions. Wunderlich [1],[2] realizing this problem, has extrapolated specific heats to 100 percent crystallinity to obtain the crystalline CH_2 contribution to the specific heat. This method is presently limited in accuracy by a scarcity of data and variations in the chemical structures (e.g., degree of branching and molecular weight) which exist between samples of different crystallinity. Even ideally, if one had sufficient data on several polyethylene samples which differed in percent crystallinity, the extrapolated results might still reflect the presence of chain folded lamellar surfaces, unless the lamellar thicknesses were properly taken into account.

The use of *n*-paraffin data to determine CH_2 properties offers the advantages that the *n*-paraffins can be made highly pure and crystallized to a high degree of perfection. Very carefully measured specific heat data are available for pure *n*-paraffins from *n*-C_6H_{14} through *n*-$C_{18}H_{38}$ (see following section). It has been reported that the molar specific heat (C_p),[3] enthalpy (H), entropy (S), and Gibbs free energy (F) of the solid *n*-paraffins appear to be linear with chain length at constant temperature and crystal phase [2–4]. An obvious interpretation of this observation is that each CH_2 unit in the chain can be thought of as contributing a certain number of vibrational modes to the crystal without changing the frequency spectrum, and that this contribution is independent of the length of the chain in which the unit is located, so long as the local crystal structure remains unchanged. Accordingly, the properties of a CH_2 unit should be the same in a large ideal —CH_2— crystal as in the *n*-paraffins. The major limitation to the *n*-paraffin determination of the crystalline CH_2 properties are the deviations from linearity with chain length which become appreciable at temperatures near the *n*-paraffin melting points.

For the liquid phase, there is a slight but real departure from linearity which will necessitate special treatment in the determination of the liquid phase properties.

The approach used below will be: (a) To establish the best values for C_p, H, S, and F of a —CH_2— unit in both the liquid and solid phases over as wide a range of temperatures as possible, (b) to establish a consistent analytical representation of the above

[1] This means a crystal, large in all dimensions, of very long CH_2 chain molecules, which contains no chain ends or branches and only an equilibrium number of defects.

[2] Figures in brackets indicate the literature references at the end of this paper.

[3] Actually, the specific heat data refers to C_{sat_d}, the specific heat under the saturated vapor pressure of the material. For this work, the difference between C_p and C_{sat_d} for the solid and liquid phases of the *n*-paraffins is negligible.

data from 200 to 420 °K, and (c) to compare the results with actual data on polyethylene and examine the discrepancies between the predicted and observed properties.

2. Source of Data

The n-paraffin data used in this study were furnished by the United States Bureau of Mines, Bartlesville, Okla., in the form of tables of values for C_p, $H\text{-}H_0$, S, and $F\text{-}H_0$ (H_0 is the enthalpy at 0 °K). Their work on n-C_6H_{14}, n-C_7H_{16}, and n-C_8H_{18} through n-$C_{16}H_{34}$ is presented, together with details of sample purity, measurement techniques, and thermodynamic calculations, in references [5, 6, and 7] respectively, and their work on n-$C_{17}H_{36}$ and n-$C_{18}H_{38}$ is as yet unpublished. The data on n-C_7H_{16}, n-$C_{17}H_{36}$ and n-$C_{18}H_{38}$ covered the temperature range from 0 to 370 °K, and data for the remaining paraffins extended from 0 to 320 °K.

3. CH_2 Structures

The even n-paraffins[4] from C_6H_{14} through $C_{18}H_{38}$ are triclinic at all temperatures up to the melting point. The odd n-paraffins [4] from $C_{11}H_{24}$ through $C_{17}H_{36}$ are orthorhombic at all temperatures up to within 15 degrees of their melting points but undergo a solid-solid transition prior to melting. The orthorhombic CH_2 structure of the odd paraffins appears to be identical to the CH_2 structure of polyethylene, and is assumed to be identical to the structure of the ideal CH_2-chain crystal whose properties we are predicting. Although one would not expect the data for the triclinic structure of the even n-paraffins to be relevant to this work, it was found that the data obtained from the even n-paraffins varied only slightly from that of the odd n-paraffins.

In the liquid state one expects and finds no even-odd differences among the paraffins. The absolute entropies of all 13 paraffins examined here, when plotted against chain length, lie on the same, nearly linear curve and the enthalpies and free energies show a similar behavior if one takes into account the differences in zero point enthalpies between the different solid structures. For instance, the enthalpy which had to be added to F and H for the even paraffins in order to have the liquid phase values of F and H for both even and odd paraffins lie on the same nearly linear curve, when plotted versus n, was found to be 370 ± 10 cal/mole of paraffin molecules. This zero point energy difference is independent of chain length since it results entirely from the differences in packing of the chain end groups, with the triclinic phase allowing the lowest energy packing.[5]

Whereas the solid phase of very linear, high molecular weight polyethylene contains a significant volume of chain folds which cause deviations from the ideal crystalline CH_2 specific heats, the liquid state should present no such difficulties. Specific heat measurements should not be able to detect the small percentage of chain ends and branches present in the liquid. Therefore, the specific heats and absolute entropies calculated here from the liquid n-paraffin data should be close to the actual measured values for polyethylene, and a comparison of predicted and experimental properties of the liquid provides an experimental test of this work. The liquid paraffin data should not, however, be expected to reflect the presence of a glassy state even well below the temperature where the ideal CH_2-chain liquid might become a glass.

[4] Even n-paraffins and odd n-paraffins are terms used here to mean n-paraffins containing an even or odd number of carbon atoms in the molecule.

[5] See reference [3] for a further discussion of the above points.

4. Analysis of the Paraffin Data

Table 1 contains a sample of the thermodynamic data as received for the solid and liquid phases at representative temperatures.

For the solid at a given temperature, the differences between the thermodynamic values of consecutive even and consecutive odd compounds was computed and these differences were averaged over the whole range of compounds for which data were available at that temperature. The averages for the even and odd paraffins were found to be very similar, and the combined average for both even and odd compounds was divided by two to obtain the desired thermodynamic value per mole of CH_2 units.

At the higher temperatures, where the shorter paraffins are liquid, the accuracy of the computations decreases due to the decreased range of data and the premelting [6] increase in the specific heat that begins about 50 degrees below the melting point and which can be seen in the data at 200 °K in table 1. It is probable that above 200 °K, the values calculated by the above procedure will be somewhat smaller than the correct values.

For the liquid phase data, the range of temperatures amenable to computation was limited at low temperatures by the decrease in the number of liquid samples and at high temperatures (370 °K) by the termination of experimental measurements. The most reliable values are those around 300 °K where most data exist.

The differences between the thermodynamic values for consecutive even and odd paraffins are not quite as constant for the liquid as for the solid as can be seen in table 1, and an appropriate extrapolation of these differences to $n=\infty$ was considered to be preferable to using a simple average. When plotted versus $1/n$, the differences for the liquid were found to be linear within experimental error. For F, H, and S, the best linear extrapolation to $1/n=0$ was graphically determined, and the resulting intercept was chosen as the desired thermodynamic value. For C_p, this $1/n$ extrapolation gave values which exhibited excessive scatter. It was found that this scatter could be reduced by integrating the C_p data, extrapolating the integrated values to $1/n=0$ and then differentiating the extrapolated integrated values to obtain the desired extrapolated C_p values. In practice, this process merely involved

[6] We are not here concerned with the distinction between homophase premelting and impurity induced heterophase premelting.

TABLE 1. *Sample data and calculations*

Thermodynamic function	Number of carbon atoms in molecule, n																
	6	8	10	12	14	16	18	Even avg.	7	9	11	13	15	17	Odd avg.	Net avg. per CH_2	Graph. extrap. to 1/n=0
Solid phase at 100 °K																	
C_p(cal/mole °K)		24.08	28.60	33.16	37.72	42.26	46.86				31.17	35.79	40.27	44.84			
$C_p(n+2)-C_p(n)$		4.52	4.56	4.56	4.54	4.60		4.56			4.62	4.48	4.57		4.55	2.28	
S(cal/mole °K)		20.47	23.75	27.05	30.36	33.67	36.98				25.55	28.89	32.16	35.55			
$S(n+2)-S(n)$		3.28	3.30	3.31	3.31	3.31		3.30			3.34	3.27	3.39		3.33	1.66	
H(cal/mole)		1207	1414	1622	1829	2036	2243				1525	1735	1940	2151			
$H(n+2)-H(n)$		207	208	207	207	207		207			210	205	211		209	104	
$-F$(cal/mole)		840	961	1083	1207	1331	1454				1031	1154	1276	1403			
$-F(n+2)+F(n)$		121	122	124	124	123		123			124	122	127		124	62	
Solid phase at 200 °K																	
C_p(cal/mole °K)		39.18	45.86	53.01	60.29	67.63	74.98				50.67	57.78	64.94	72.31			
$C_p(n+2)-C_p(n)$		6.69[a]	7.15[a]	7.28	7.34	7.35		7.32			7.11[a]	7.16[a]	7.37		7.37	3.67	
S(cal/mole °K)		41.77	48.99	56.31	63.68	71.02	78.45				53.15	60.60	67.90	75.35			
$S(n+2)-S(n)$		7.22[a]	7.32	7.37	7.34	7.43		7.36			7.45	7.30	7.45		7.39	3.69	
H(cal/mole)		4364	5152	5954	6764	7568	8385				5615	6432	7234	8048			
$H(n+2)-H(n)$		788[a]	802	810	804	817		808			817	802	814		811	405	
$-F$(cal/mole)		3992	4646	5308	5973	6637	7304				5016	5687	6346	7022			
$-F(n+2)+F(n)$		654[a]	662	665	664	667		664			671	669	676		672	334	
Liquid phase at 300 °K																	
C_p(cal/mole °K)	46.86	60.90	75.38	90.09	105.01	120.07					82.68	97.47	112.53	127.87			
$C_p(n+2)-C_p(n)$	14.04	14.48	14.71	14.92	15.06			14.64			14.79	15.06	15.34		15.06	7.4	8.0
S(cal/mole °K)	71.05	86.67	102.27	117.87	133.41	148.86			78.86	94.50	110.02	125.59	141.11	156.68			
$S(n+2)-S(n)$	15.62	15.60	15.60	15.54	15.45			15.57	15.64	15.52	15.57	15.52	15.57		15.58	7.79	7.74
H(cal/mole)	11301	14807	18328	21854	25368	28871			12681	16204	19719	23240	26783	30320			
$H(n+2)-H(n)$	3506	3521	3526	3514	3503			3514	3523	3515	3521	3543	3537		3526	1760	1770
$-F$(cal/mole)	10014	11193	12353	13506	14654	15788			10977	12148	13287	14437	15550	16683			
$-F(n+2)+F(n)$	1179	1160	1153	1148	1134			1155	1172	1139	1150	1113	1133		1141	574	547

[a] These values are low because of premelting and were omitted from the calculations.

taking differences between the consecutive experimental H values in table 2 and dividing by 10°. For example, C_p (per mole of CH_2 units) at 305 °K was taken to equal H (per mole of CH_2 units) at 310 °K minus H (per mole of CH_2 units) at 300 °K divided by 10°. The same procedure was followed (though mathematically, less precisely) using the TS data, in order to increase the number of available C_p values.

The results of the above determinations are listed in table 2 and are represented graphically as closed circles in figures 1 through 4. The large number of digits given in the calculated value columns in table 2 is not intended to indicate significant figures but is included only for internal consistency.

5. Determination of Analytical Expressions

Linear least squares fits of the specific heats for the solid above 150 °K and specific heats for the liquid above 200 °K as a function of temperature were carried out. The calculated standard deviations were 0.15 c l/mole-°K for the solid (39 data points) and 0.84 cal mole-°K for the liquid (36 data points). Integrations of C_p and C_p/T were then carried out and the average values of the constants of integration were determined from the entropy and enthalpy data. The resulting functions fit the H and S data for the solid above 200 °K with a standard deviation of 2 cal/mole and 0.01 cal/mole-°K, respectively, and for the liquid above 200 °K with a standard deviation of 6 cal/mole and 0.02 cal/mole-°K, respectively. The Gibbs free energy was computed directly from H and S and was found to fit the free energy data above 200 °K with a standard deviation of 4 cal/mole for the solid and 9 cal/mole for the liquid.

By using the calculated analytical expressions to extrapolate up to the temperature where the free energies for the solid and liquid become equal, it was found that the predicted melting point was 397.4 °K and the predicted heat of fusion was 1132 cal/mole. Since the predicted melting point is 4 percent below its most probable value of 414.3 °K [4] and since the predicted heat of fusion seems unreasonably high, the assumption of a linear specific heat for the solid above 200 °K was concluded to be inadequate for the representation of the known data. Hence, a correction to the specific heat for the solid was sought that would decrease the free energy of the solid by a sufficient amount to increase the melting point to its previously determined most probable

TABLE 2. *Values of the molar specific heats (C_p) enthalpies ($H-H_0$), entropies (S) and Gibbs free energies ($F-H_0$) of ideal CH_2 chain crystal and liquid as derived from n-paraffin data (experimental values) and as calculated using the equations in table 3*

Temperature	C_p(cal/mole °K)		$H-H_0$(cal/mole)		S(cal/mole °K)		$-(F-H_0)$ (cal/mole)	
	exp.	calc.	exp.	calc.	exp.	calc.	exp.	calc.
	Solid phase							
°K								
10	0.025	.....	0.06	.....	0.01	.....	0.02	.....
20	.15	.....	.85	.....	.05	.....	.30	.....
30	.39	.....	3.50	.....	.16	.....	1.34	.....
40	.70	.....	9.00	.....	.32	.....	3.7	.....
50	1.03	.....	17.8	.....	.51	.....	7.8	.....
60	1.34	.....	29.5	.....	.73	.....	14.0	.....
70	1.63	.....	44.6	.....	.95	.....	22.4	.....
80	1.88	.....	62.0	.....	1.19	.....	33.2	.....
90	2.10	.....	82.0	.....	1.43	.....	46.2	.....
100	2.28	.....	104	.....	1.66	.....	61.7	.....
110	2.45	.....	128	.....	1.88	.....	79	.....
120	2.60	.....	153	.....	2.10	.....	99	.....
130	2.75	.....	180	.....	2.32	.....	121	.....
140	2.89	.....	208	.....	2.52	.....	146	.....
150	3.05	3.02	237	.....	2.73	.....	171	.....
160	3.16	3.17	268	.....	2.92	.....	200	.....
170	3.28	3.32	300	.....	3.12	.....	230	.....
180	3.40	3.48	334	.....	3.31	.....	263	.....
190	3.52	3.65	369	.....	3.51	.....	297	.....
200	3.67	3.8572	405	405.88	3.69	3.7201	334	338.14
210	3.81	4.0378	441	445.35	3.87	3.9127	371	376.30
220	3.95	4.2224	479	486.64	4.05	4.1046	410	416.39
230	4.05	4.4107	519	529.78	4.23	4.2963	453	458.39
240	4.16	4.6028	562	574.85	4.41	4.4881	496	502.31
250	4.32	4.7975	603	621.84	4.58	4.6799	541	548.15
260	.....	4.9936	647	670.76	4.77	4.8717	590	595.90
270	.....	5.1924	691	721.70	4.94	5.0640	643	645.59
280	.....	5.3909	742	774.57	5.13	5.2562	695	697.18
290	.....	5.5838	790	829.37	5.30	5.4484	748	750.67
300	.....	5.7898	.....	886.34	.....	5.6416	.....	806.15
310	.....	5.9909	.....	945.19	.....	5.8345	.....	863.15
320	.....	6.1851	.....	1005.91	.....	6.0272	.....	922.79
330	.....	6.3836	.....	1068.84	.....	6.2208	.....	983.51
340	.....	6.5795	.....	1133.64	.....	6.4142	.....	1047.20
350	.....	6.7734	.....	1200.32	.....	6.6075	.....	1112.31
360	.....	6.9629	.....	1268.71	.....	6.7999	.....	1179.27
370	.....	7.1553	.....	1339.47	.....	6.9939	.....	1248.29
380	.....	7.3421	.....	1411.78	.....	7.1865	.....	1319.13
390	.....	7.5293	.....	1486.17	.....	7.3798	.....	1390.97
400	.....	7.7141	.....	1562.37	.....	7.5727	.....	1466.73
410	.....	7.8966	.....	1640.42	.....	7.7654	.....	1543.41
414.3	.....	7.9748	.....	1674.52	.....	7.8482	.....	1576.98
420	.....	8.0761	.....	1720.26	.....	7.9578	.....	1622.03
	Liquid phase							
200	[a]6.8	6.6360	1076	1064.60	4.83	4.8676	−110	−91.08
210	6.0	6.7178	1144	1131.37	5.16	5.1934	−58	−40.77
220	6.95	6.7996	1203	1198.96	5.50	5.5078	4	12.75
230	7.0	6.8814	1274	1267.36	5.80	5.8118	62	69.35
240	6.4	6.9632	1343	1336.58	6.10	6.1064	124	128.95
250	7.05	7.0450	1405	1406.62	6.37	6.3923	187	191.44
260	7.0	7.1268	1475	1477.48	6.65	6.6702	253	256.76
270	7.25	7.2086	1544	1549.16	6.92	6.9407	324	324.83
280	7.35	7.2904	1615	1621.66	7.19	7.2044	398	395.57
290	8.4	7.3722	1688	1694.97	7.45	7.4616	470	468.90
300	7.7	7.4540	1770	1769.10	7.74	7.7129	547	544.77
310	6.75	7.5358	1845	1844.05	8.00	7.9586	628	623.13
320	7.7	7.6176	1911	1919.82	8.22	8.1992	719	703.93
330	7.6	7.6994	2000	1996.40	8.45	8.4348	794	787.10
340	7.6	7.7812	2072	2073.80	8.69	8.6660	883	872.62
350	7.55	7.8630	2152	2152.02	8.90	8.8926	968	960.40
360	7.95	7.9448	2225	2231.06	9.12	9.1153	1062	1050.44
370	8.5	8.0266	2304	2310.92	9.34	9.3341	1154	1142.70
380	.....	8.1084	2392	2391.60	9.56	9.5492	1241	1237.12
390	.....	8.1902	.....	2473.09	.....	9.7610	.....	1333.68
400	.....	8.2720	.....	2555.40	.....	9.6693	.....	1432.32
410	.....	8.3538	.....	2638.53	.....	10.1746	.....	1533.06
414.3	.....	8.3890	.....	2674.52	.....	10.2619	.....	1576.98
420	.....	8.4356	.....	2722.48	.....	10.3768	.....	1635.80

[a] This column refers to temperatures 5° higher than indicated; e.g., 6.8 is the C_p value at 205 °K.

value, and at the same time the correction was desired to have as little effect as possible on the linear thermodynamic functions for the solid below 300 °K where a good fit of the data was already obtained.

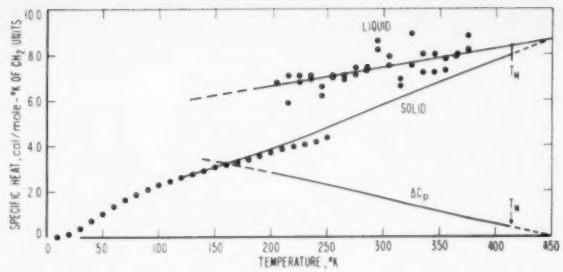

FIGURE 1. *Predicted specific heats, C_p, of an ideal CH_2-chain crystal and liquid as a function of temperature.*

The closed circles represent values calculated from *n*-paraffin data, samples of which are listed in table 1, and the solid curves were calculated from the equations in table 3.

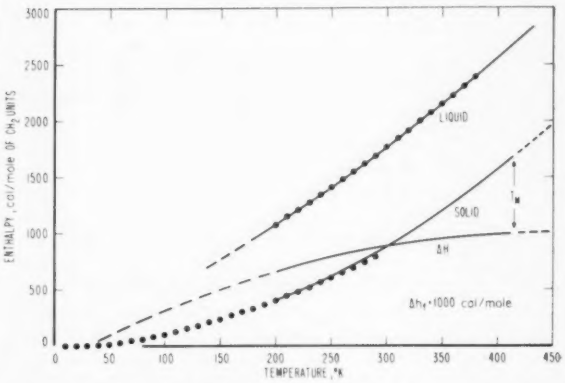

FIGURE 2. *Predicted enthalpies ($H-H_0$), of an ideal CH_2-chain crystal and liquid as a function of temperature.*

The closed circles represent values calculated from *n*-paraffin data, samples of which are listed in table 1, and the solid curves were calculated from the equations in table 3.

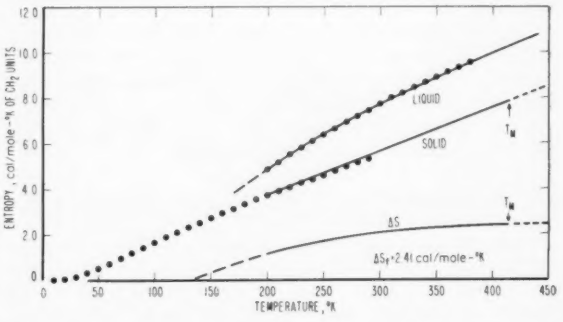

FIGURE 3. *Predicted entropies, S, of an ideal CH_2-chain crystal and liquid as a function of temperature*

The closed circles represent values calculated from *n*-paraffin data, samples of which are listed in table 1, and the solid curves were calculated from the equations in table 3.

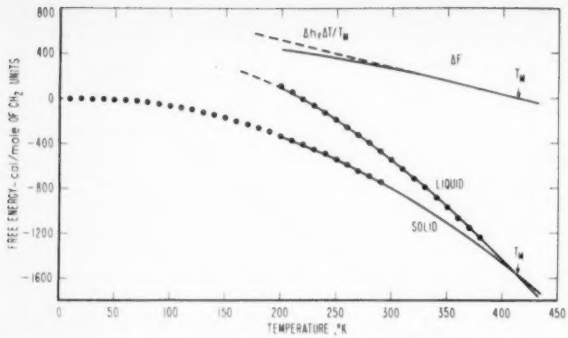

FIGURE 4. *Predicted Gibbs free energies* (F-H_0) *of an ideal* CH_2*-chain crystal and liquid as a function of temperature.*

The closed circles represent values calculated from *n*-paraffin data, samples of which are listed in table 1, and the solid curves were calculated from the equations in table 3.

Fortunately, a correction of the type implied here by the *n*-paraffin data has the same form as the specific heat contributions due to several independent CH_2 vibrations which become important above 250 °K [8, 9]. These vibrations are well represented by a summation of Einstein functions of the form $C_v = \sum_i (R\theta_i^2/T^2)[e^{\theta_i/T}/(e^{\theta_i/T}-1)^2]$. For our use, we have preserved the form of this function but have applied it to C_p rather than C_v and have made the further approximations that we can use a single term to replace the summation of several terms, and that $\theta >> T$ in the range of interest. That is, we shall assume a correction to C_p of the form,

$$\overline{C}_p = (\overline{n}R\overline{\theta}^2/T^2)\exp(-\overline{\theta}/T), \qquad (1)$$

where the bar indicates an "effective" quantity which is expected to lie somewhere between the maximum and minimum quantities in the above expression for C_p. The effective number of independent CH_2 modes is represented by $\overline{n}$, R is the molar gas constant, $\overline{\theta} = h\overline{\nu}/k$ is the characteristic temperature, h is Planck's constant, $\overline{\nu}$ is the effective frequency of vibration, k is Boltzmann's constant, and T is the absolute temperature.

It is convenient to replace the two parameters $\overline{n}$ and $\overline{\theta}$ in eq (1) by two different parameters, F_s and H_s, the corrections to the free energy and enthalpy at T_M needed to give the proper melting point and heat of fusion. This replacement is accomplished by integrating eq (1) to find the corresponding $\overline{H}$ and $\overline{F}$ and then solving the equations $H_s = \overline{H}$ at $T = T_M$ and $F_s = \overline{F}$ at $T = T_M$ for $\overline{\theta}$ and $\overline{n}$. The result is $\overline{n} = (F_s/RT_M)\exp(H_s/F_s)$ and $\overline{\theta} = T_M H_s/F_s$. If we assume $T_M = 414.3$ °K[4] then one finds that F_s must equal −48.80 cal/mole (calculated from the uncorrected ΔF at 414.3 °K) and H_s must equal (1162.10 − Δh_f) cal/mole where Δh_f is the heat of fusion at $T_M = 414.3$ °K. We have here chosen a value of $\Delta h_f = 1000$ cal/mole as reasonable, which choice gives $\overline{\theta} = 1376$ and $\overline{n} = 1.64$.

The resulting analytical expressions for the thermodynamic functions of the CH_2-chain crystal and liquid above 200 °K are shown in table 3, and the calculated values are compared to the experimental values in table 2.

TABLE 3. *Analytical expressions for the thermodynamic functions of the ideal* CH_2*-chain crystal and liquid above 200 °K, derived from* n*-paraffin data*

Function	Solid phase ($T \geq 200$ °K)	Liquid phase ($T \geq 200$ °K)
C_p (cal/mole °K)	$0.0139T + 0.916 + 22.308 \times 10^4 u/T^2$	$0.00818T + 5.00$
$H - H_0$ cal/mole)	$0.00695T^2 + 0.916T - 60 + 162.10u$	$0.00409T^2 + 5.00T - 99$
S (cal/mole °K)	$0.0139T + 0.916\ln T - 3.94 + (0.117789 + 162.10/T)u$	$0.00818T + 5.00\ln T - 23.26$
$F - H_0$ (cal/mole)	$-0.00695T^2 - 0.916T\ln T + 4.856T - 60 - 0.117789Tu$	$-0.00409T^2 - 5.00T\ln T + 28.26T - 99$
	Liquid-solid difference ($T \geq 200$ °K)	
ΔC_p (cal/mole °K)	$-0.00572T + 4.84 - 22.308 \times 10^4 u/T^2$	
ΔH (cal/mole)	$-0.00186T^2 + 4.84T - 39 - 162.10u$	
ΔS (cal/mole °K)	$-0.00572T + 4.84\ln T + 19.32 - (0.117789 + 162.10/T)u$	
ΔF (cal/mole)	$0.00186T^2 - 4.84T\ln T + 23.404T - 39 + 0.117789Tu$	

$u = \exp[-3.32172\,(414.3 - T)/T]$

6. Discussion

6.1. Reliability of the Results

It is important to have some idea of how accurately the results listed in table 2 represent the properties of an ideal CH_2-chain compound. The specific heats below 150 °K and H, S, and F below 200 °K are probably accurate to ±1 percent judging from the consistency of the averaged values (examples in table 1) and the estimate of better than 1 percent accuracy for the original data. At 200 °K the effects of premelting can be seen in table 1 as a reduction in the first two specific heat differences and the first H, S, and F differences. One is increasingly uncertain above 200 °K about the correctness of the averaged data values, and thus the calculated values are to be preferred at the higher temperatures. All reasonable attempts to alter the results by starting with different initial linear and quadratic specific heat functions did not change the predicted melting point by more than 2 degrees or the predicted heat of fusion by more than 5 cal/mole. Nor did different assumed forms of the correction term make a significant difference in the predicted thermodynamic functions. The results were found to be quite insensitive to artifacts in the data or initial assumptions. This insensitivity, while giving one confidence in the predicted values, greatly reduces the importance which one can attribute to the values of $\overline{\theta}$ and $\overline{n}$ in eq (1).

The most uncertain and sensitive parameter in the calculations is the heat of fusion, Δh_f. The best current experimental estimate of Δh_f for polyethylene by the diluent method is 970 cal/mole [10]. A reasonable calculation shows that for the ideal CH_2-chain crystal, Δh_f can be expected to be higher than for 100 A thick lamellar polyethylene by 2 to 3 percent. From our work, Δh_f=975.9 appears to be a minimum value since any lower value results in the solid specific heat exceeding the liquid specific heat below the melting point. As Δh_f is increased above its minimum value, the deviation between the calculated and experimental values in the 200 to 290 °K range increases, and the values of $\overline{\theta}$ and $\overline{n}$ in eq (1) decrease from 1580 °K and 2.70 for Δh_f=976 to 1376 °K and 1.64 for Δh_f=1000 cal/mole and 1164 °K and 0.98 for Δh_f=1025. If Δh_f is as large as 1025 cal/mole, both the deviation from the experimental data and the values of $\overline{\theta}$ and $\overline{n}$ seem unreasonable. Thus it appears likely that the correct value of Δh_f lies within ±2.5 percent of the 1000 cal/mole assumed in this analysis.

The ±2.5 percent error in Δh_f causes an uncertainty in H and S for the solid which decreases rapidly with temperature from about 1 percent at 400 °K to a negligible error at 300 °K. The effect of the uncertainty in Δh_f on the specific heat is illustrated in figure 5.

For the liquid phase, the standard deviations of the data from the calculated curve have been given in the previous section and amount to roughly 10 percent for C_p, 2 percent for F, and 0.3 percent for H and S. Hence, it seems reasonable to expect the calculated H and S values to be accurate to within ±2 percent. A comparison with polyethylene liquid data in the next section supports an estimate of ±2 percent reliability for the liquid C_p values as well as the H and S values.

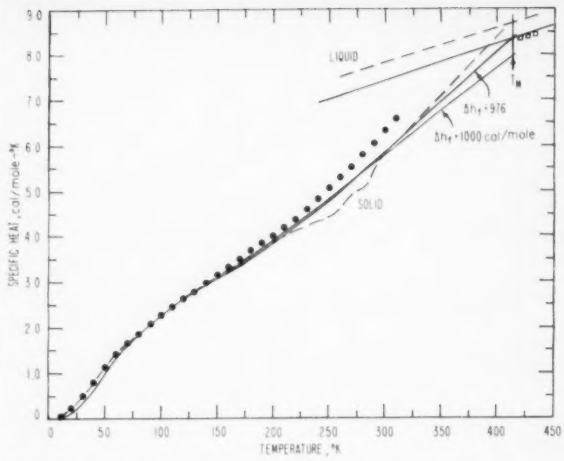

FIGURE 5. *The predicted specific heats, C_v, of an ideal CH_2-chain crystal and liquid (solid curves) for two assumed heats of fusion, compared to the extrapolated values given by Wunderlich for completely crystalline polyethylene (dashed curve) and the polyethylene data of Dainton, Evans, Hoare, and Melia (closed circles) and Passaglia and Kevorkian (open squares).*

6.2. Comparison With Experiment

Figure 5 shows a comparison of the ideal specific heat predicted here from n-paraffin data with that predicted by Wunderlich [1] from polyethylene data and with actual experimental values for crystalline Marlex 50 as reported recently by Passaglia and Kevorkian [9] and Dainton, Evans, Hoare, and Melia [11]. The specific heat values predicted here are appreciably lower than the polyethylene values up to 80 °K, slightly larger from 80 to 140 °K (this range varies somewhat with different data) and again smaller at higher temperatures. The smoothness (smaller variations in the slope) of the experimental C_p curve relative to the predicted curve below room temperature indicates that the ideal vibrational frequency distribution is broadened and the characteristic temperature is lowered in actual specimens of polyethylene—a result attributable to imperfections. Similar behavior was noted during this study in C_p data for a sample of n-$C_{32}H_{66}$ and a less pure sample of n-$C_{33}H_{68}$. Whereas the C_{33} specific heats were nearly linear with temperature from 90 to 180 °K, the C_{32} specific heats were markedly sigmoidal in the same temperature range with values below those of C_{33} at high and low temperatures and above those of C_{33} at temperatures between 100 and 150 °K. Liquid polyethylene specific heat data [9], shown as squares in figure

5, agree to within 1 percent with the predicted liquid C_p curve. The enthalpies of the liquid reported by Passaglia and Kevorkian are smaller than predicted by less than 2 percent and the entropies of the liquid are larger than predicted by less than 2 percent. These agreements are considered satisfactory.

Wunderlich's predicted H and S values for the solid at 300 °K agree to within 2 percent with those predicted from the n-paraffins. The predicted specific heats differ somewhat as shown by the dashed curve in figure 5. Dainton, Evans, Hoare, and Melia [11] used an extrapolation technique to obtain a value for the ideal entropy of polyethylene at 25 °C of 5.5 cal/mole °K in favorable agreement with 5.6 cal/mole °K predicted here.

One important result of this work concerns the thermodynamic crystallinity scale [i.e., the calculation of the crystalline fraction of a sample from the equation χ=[H (liquid) -H(sample)]/[H liquid)-H (crystal)]. The values of H (liquid) -H (crystal) calculated in this study are significantly larger than those given by Wunderlich [1], but both the crystalline and liquid enthalpies are smaller, probably because of a zero point enthalpy difference. Such a zero point enthalpy difference is expected if one assumes that the polyethylene extrapolation pertains to an ideally perfect chain folded lamellar crystal rather than the ideally perfect, large nonfolded crystal associated with the paraffin extrapolation. Whereas both types of perfect crystals would have the same zero point entropy (equal to zero by the third law), the zero point enthalpies would be different. It is interesting to note that the Marlex 50 sample measured by Passaglia and Kevorkian [9] has a volume crystallinity of 80.0 percent and an enthalpy crystallinity of 93.8 percent as determined from the values of Wunderlich and Dole [12], and using enthalpy values from this work, 97 percent or 93.5 percent, depending upon whether one uses the solid at 0 °K or the liquid above T_M as the reference state. The zero point enthalpy correction which had to be added for the latter calculation was 40 cal/mole of folds. The fact that thermodynamic crystallinities are generally higher than volume crystallinities is consistent with the assumption that much of the imperfection in highly crystalline polyethylene samples is unoccupied volume (such as might be expected to exist between lamellar fold surfaces.) Volume measurements would be sensitive to these defects whereas enthalpy measurements would not.

6.3. Observations and Suggestions

The thermodynamic properties represented in figures 1–4 exhibit several unusual features that result from the high specific heat of the solid at high temperatures (nearly equal to that of the liquid at the melting temperature). The difference (ΔH) between the enthalpies of the solid and liquid is quite constant in the melting region and the tendency of ΔH to become negative at low temperatures is not pronounced. Even though ΔS appears to tend toward zero between 100 and 150 °K, the necessity for polyethylene to form a glass to maintain a positive ΔH and ΔS is not as obvious as in most substances. It seems likely that the discontinuity in the ΔH versus temperature curve at the glass transition would be so small that it would be difficult to detect. In accord with the above, ΔF is well approximated by $\Delta h_f \Delta T/T_M$ over an unusually large range of temperatures. This simple linear approximation to Δf is in error by only 1.5 percent for ΔT=50 degrees and by less than 5 percent for ΔT=100 degrees. One would expect Δf to be much less linear than this for most substances [12]. From the above observations, it is not surprising that there is very little indication of a glass transition in the thermodynamic data for linear polyethylene.

There is no indication in the data derived from the liquid paraffins above 200 °K of the existence of the glassy state in polyethylene, and yet the glass is generally considered to be the stable amorphous state in polyethylene below about 237 °K [1]. One may conclude that the glass transition temperature is chain length dependent and that the glass becomes stable with respect to the supercooled liquid above 200° only for chain lengths greater than some minimum value. The only way one could use the n-paraffins for predicting the properties of the polyethylene glassy state would be to have data on the glassy state of the n-paraffins.

As shown in table 1, the incremental increase per CH_2 in the n-paraffin thermodynamic properties is not as constant in the liquid state as in the solid. This result seems consistent with the following argument. In the solid, even for chains with less than 10 CH_2 units, the intermolecular forces are strong enough compared to the intramolecular forces to isolate the motions of a central CH_2 unit from those of the chain ends. In the liquid the intermolecular forces are weaker and less regular so that the CH_2 behavior is sensitive to chain end effects. The nonlinearity of the incremental increase per CH_2 in the liquid thermodynamic properties with reciprocal chain length possibly indicates the presence of "entire chain" vibrational modes in the liquid even for very long chain lengths. [7]

The departure of the predicted specific heat from that measured for polyethylene in the 10 to 80 °K temperature range should be investigated further. Since all polyethylenes so far measured seem to show the same higher than predicted specific heats in this range, the anomaly would seem to be associated with some nonideal feature which all samples have in common—e.g., chain folded surfaces. It would be interesting to examine the changes in

[7] In a private communication, J. P. McCullough has suggested that the nonlinearity in the liquid state is due to a contribution from short range order which decreases exponentially with temperature above the melting point. If this were the case, the liquid data would become more linear at higher temperatures. Higher temperature specific heat data can clarify this point.

specific heat of polyethylene with lamellar thickness to see if the discrepancy could be resolved. It might also be useful to attempt to analyze the data in this paper in the manner reported recently by Wunderlich [8]. It is desirable to have more *n*-paraffin specific heat data for longer chain lengths and higher temperatures in order to increase the accuracy and temperature range of the predicted higher temperature solid and liquid thermodynamic values.

7. References

[1] B. Wunderlich, Motion in Polyethylene I, J. Chem. Phys. **37,** 1203, (1962).

[2] E. F. Westrum, Jr., and J. P. McCullough, Physics and Chemistry of the Organic Solid State, Chapter 1, *I*, A. Weissberger et al., editors, Interscience Publishers (in press).

[3] M. Broadhurst, J. Research NBS **66A,** 241 (1962).

[4] M. Broadhurst, J. Chem. Phys. **36,** 2578 (1962).

[5] D. R. Douslin and H. M. Huffman, J. Am. Chem. Soc. **68,** 1704 (1946).

[6] H. L. Finke, M. E. Gross, G. Waddington and H. M. Huffman, J. Am. Chem. Soc. **76,** 333 (1954).

[7] J. P. McCullough and J. F. Messerly, Bulletin 596, Bureau of Mines, U.S. Department of the Interior, U.S. G.P.O. (1961).

[8] B. Wunderlich, Motion in Polyethylene II (to be published).

[9] E. Passaglia and H. G. Kevorkian, J. Appl. Polymer Sci. **7,** 119 (1963).

[10] R. Chiang and P. J. Flory, J. Am. Chem. Soc. **83,** 2857 (1961).

[11] F. S. Dainton, D. M. Evans, F. E. Hoare, and T. P. Melia, Polymer, **3,** 277 (1962).

[12] B. Wunderlich and M. Dole, J. Polymer Sci. **24,** 201 (1957).

[13] J. D. Hoffman, J. Chem. Phys. **29,** 1192 (1958).

(Paper 67A3–210)

JOURNAL OF RESEARCH of the National Bureau of Standards—A. Physics and Chemistry
Vol. 67A, No. 3, May–June 1963

Spectrophotometric Determination of the Thermodynamic *p*K Value of Picric Acid in Water at 25 °C

Marion Maclean Davis and Maya Paabo

(February 12, 1963)

The thermodynamic *p*K value of picric acid was determined spectrophotometrically in water containing hydrochloric acid to repress the ionization. The *p*K value 0.33 ($K \approx 0.46$) was obtained from data at 450 mμ. Attempts to determine the *p*K value by potentiometric titrations of picric acid and by spectrophotometric measurements of picric acid solutions in the near-saturation range did not yield satisfactory results. The new *p*K value is compared with previously published values.

1. Introduction

Because of the wide-ranging importance of picric acid, numerous attempts have been made to determine its ionization constant in water. Table 1 summarizes ionization constants or *p*K values which have been reported in the literature, obtained by catalytic, conductance, distribution, or spectrophotometric methods.[1] The values obtained for K range from about 0.15 to 0.6, the corresponding *p*K range being about 0.8 to 0.2.

The principle of additivity of substituent effects, which has been applied successfully in calculating approximate *p*K values for some of the *meta*- and *para*-substituted benzoic acids (for example, see [1, 2]),[2] cannot be used for a dependable estimate of the *p*K values of di- and trinitrophenols, because the calculated acidic strengths are less than those determined experimentally—in some cases, very much less [3 to 5]. For picric acid, several different estimated *p*K values are obtained on using different combinations of the following experimentally obtained *p*K values: Phenol (10.00), *m*-cresol (10.09), 3,5-xylenol (10.19), *o*-nitrophenol (7.21), *p*-nitrophenol (7.15), 2,4-dinitrophenol (4.10), 2,6-dinitrophenol (3.71), 2,4,6-trinitro-*m*-cresol (0.81), and 3,5-dimethylpicric acid (1.38). The variability of the calculated *p*K values is evident from the following examples:

(1) The *p*K value 1.57 is obtained by using *p*K values for phenol, *o*-nitrophenol and *p*-nitrophenol.

(2) By subtracting the numerical difference between the *p*K values for phenol and *o*-nitrophenol from the *p*K value for 2,4-dinitrophenol one obtains 1.31.

(3) Subtracting the numerical difference between the *p*K values for phenol and *p*-nitrophenol from the *p*K value for 2,6-dinitropnenol gives the value 0.86.

(4) Subtracting 0.09 from the experimental *p*K value for trinitro-*m*-cresol gives 0.72.

TABLE 1. *Ionization constants previously reported for picric acid*

Temp. °C	Range of concns.[a]	Method of measurement[b]	K[c]	Equiv. value of *p*K
18	0.002079 to 0.03342	Dist.	[d] 0.164	0.785
25	----------	Cond.	[e] ~.2	----------
25	0.03 to 0.05	Cat.	.32	[f] .506
25	.00997 to .0399	Spec.	[*g] .151	[*] .820
20	.00194 to .00204	Spec.	[h] .381	.419
25	.000187 to .004347	Cond.	[i] .60±35%	.22 (0.41 to 0.09)
25	Approx. .00005	Spec.	[*] .51	[*] 0.29
25	.002358 to .004410	Cond.	[*k] .196	[*] .708
25	----------	Spec.	.42	[l] .38

[a] All concentrations appear to have been in molar units.

[b] Abbreviations used: "Cat.," catalytic effect on the hydrolysis of ethyl acetate as compared with that of HCl; "Cond.," conductance; "Dist.," distribution between water and benzene; "Spec.," spectrophotometric.

[c] An asterisk signifies that K and *p*K are claimed to be *thermodynamic* values.

[d] V. Rothmund and C. Drucker, Z. physik. Chem. **46,** 827 (1903). Dippy, Hughes, and Laxton (see footnote k), who evidently recalculated K, cite this value as 0.23, which is equivalent to *p*K 0.64. E. Schreiner (see footnote f) obtained *p*K = 0.526 at 25° from Rothmund and Drucker's data.

[e] S. M. Neale, Trans. Faraday Soc. **17,** 505 (1921). He used λ_0=376, and observed a trend from K=0.299 for v=32 liters to 0.155 at v=1280 liters.

[f] E. Schreiner, Z. anorg. allgem. Chem. **138,** 311 (1924). Assumptions made: HCl is completely dissociated; H^+ is associated with 10 H_2O; Pi^- and HPi are unhydrated. In three expts. with C_{HPi}=0.05, 0.04, 0.03, he obtained for −log K_0 the respective values 0.466, 0.534, 0.517. Emf measurements at 18° yielded *p*K = 0.540.

[g] H. von Halban and L. Ebert, Z. physik. Chem. **112,** 359 (1924). From measurements at 450 mμ (?). HPi solutions of three concentrations were used, as well as data in 0.116-*N* HCl, and the results were extrapolated by the method of least squares.

[h] H. von Halban and M. Seiler, Helv. chim. acta **21,** 385 (1938). From measurements at 436 mμ. Fourteen measurements were made with C_{HPi} ranging from 0.00194 to 0.00204, C_{HCl} ranging from 0.0084 to 0.0117. When their data are treated as in this paper, the average *p*K value obtained is 0.355.

[i] G. Kortüm and H. Wilski, Z. physik. Chem. (n.f.) **2,** 256 (1954); prelim. note, G. Kortüm, Z. Elektrochem. **57,** 874 (1953). They used λ_0=380.44, consider optical results to be surer.

[j] R. G. Bates and G. Schwarzenbach, Experientia **10,** 482 (1954). From data at 356 mμ. As in this work, hydrochloric acid was added to repress ionization of picric acid, but larger amounts were added (C_{HCl}, 0.1 molal to 4 molal). The same equation (see eq (1)) was used in calculating *p*K. Because of uncertainty about the value of D_1, *p*K values were calculated with eight assumed values of D_1, then plotted against the molality of hydrochloric acid. The best D_1 value was considered to be the one providing the best linear relation between *p*K and the molality of HCl.

[k] J. F. J. Dippy, S. R. C. Hughes, and J. W. Laxton, J. Chem. Soc. (London) **1956,** 2995. Solutions of five concentrations were measured. They used λ_0=385.5 (obtained by the extrapolation method of R. M. Fuoss (J. Am. Chem. Soc. **57,** 488 (1935)).

[l] Unpublished result of T. Riley and F. A. Long, cited by A. C. McDougall and F. A. Long, J. Phys. Chem. **66,** 429 (1962). Experimental conditions were not given.

[1] A few attempts have been made to determine *p*K by emf procedures. The results are not included in table 1, either because they were considered unsatisfactory or because they were not supported by any experimental details or data.

[2] Figures in brackets indicate the literature references at the end of this paper.

(5) Subtraction of 0.19 from the experimental pK value found for dimethylpicric acid gives 1.19.

Bearing in mind that the experimental pK values for the dinitrophenols are all lower than the values calculated assuming additivity of substituent effects, one may reasonably expect the experimental pK for picric acid, also, to be lower than values calculated in (1) to (3). The pK values calculated in (4) and (5) likewise set upper limits for the pK value to be expected for picric acid. Dimethylpicric acid, in particular, undoubtedly is weakened by steric inhibition of resonance of nitro groups with the ring, caused by adjacent methyl groups—this follows from well-known theoretical considerations, as well as from its absorption spectrum [4]. It is very likely that trinitro-*m*-cresol, too, is weakened by steric inhibition of resonance, though not to the same degree as dimethylpicric acid.

The two following additional modes of calculating a pK value for picric acid,[3] which use only experimental pK values for nitrophenols, should give a better estimate of the range within which the true pK value falls:

(6) Subtracting the difference between the pK value for *o*-nitrophenol and that for 2,4-dinitrophenol from the pK value for 2,6-dinitrophenol gives 0.60.[4]

(7) Subtracting the difference between the pK values for dimethylpicric acid and trinitro-*m*-cresol from the value for trinitro-*m*-cresol gives 0.24.

This paper reports the results obtained in applying to picric acid the spectrophotometric procedure used in determining the pK values of 3,5-dimethylpicric acid [4] and 2,4,6-trinitro-*m*-cresol [5], in which hydrochloric acid is added to repress the ionization of dilute aqueous picric acid. Absorbance measurements were also made for aqueous picric acid at higher concentrations. Attempts to measure the pK by potentiometric titration are discussed briefly.

2. Experimental Procedures

2.1. Materials

A commercial high grade of *picric acid* was recrystallized several times from benzene-cyclohexane or water, the final time from water, forming long needles. Preliminary drying to constant weight at room temperature was accomplished by leaving the crystals for approximately four hours in a desiccator through which dried air passed continually. No further measurable loss in weight occurred on heating for an hour at 100 to 110 °C. The melting point was 121.5 to 122.0 °C. The values for percent purity obtained by potentiometric weight-titrations of two samples were 99.97 and 100.02.

The *hydrochloric acid* and *sodium hydroxide* were commercial materials of highest grade, stated to meet A.C.S. specifications.

[3] These were suggested by Donald D. Wagman.

[4] The same result is obtained, of course, by subtracting the difference between the pK values for *o*-nitrophenol and 2,6-dinitrophenol from the pK value for 2,4-dinitrophenol.

2.2. Attempt to Determine pK by Potentiometric Titrations

Solutions of picric acid about 0.004 M or 0.044 M were titrated with approximately 0.46-M sodium hydroxide, using glass and sleeve-type calomel electrodes. The method of calculation was the same as in the titrimetric determination of the pK of 2,6-dichlorobenzoic acid [2]. Before the titrations the electrode system was checked with NBS 0.05-M potassium acid phthalate buffer (pH 4.01) and 0.05-M potassium tetroxalate buffer (pH 1.65). The initial pH values ranged from 1.50 to 1.54, and the average pK values from three experiments were 0.78, 0.86, and 0.74. These are *not* considered reliable values. In the first place, pK values calculated by this method are highly sensitive to the magnitude of the experimental pH values, and these were not reproducible enough. There was evidence of a tendency for picrate to crystallize near the sleeve of the calomel electrode during titrations. A second difficulty concerns the standardization of the instrument with buffer solutions before the titrations. The pH range near 1.50, which is vital for this method of determining the pK of picric acid, is outside the range of pH values in which the Hitchcock and Taylor scale of pH values (obtained with buffer solutions using cells with liquid junction) and the NBS scale (obtained using cells without liquid junction) are in excellent agreement [6]. Near pH 1.50, the two scales differ by 0.04 pH unit.

2.3. Determination of the pK Value by Spectrophotometry

Absorbances were obtained with a Beckman Model DU quartz spectrophotometer, equipped with a thermostated cell compartment [7]. The absorption cells were the same accurately made, demountable cells of various lengths used in other spectrophotometric studies [8]. When solutions contained hydrochloric acid or sodium hydroxide, the same concentration of acid or alkali was present in the sample cell and the reference cell. To increase the precision of wavelength settings, the spectrophotometer is provided with an auxiliary indicator line, as recommended in [9]. The absorbance values used are the average of at least five independent settings, which were highly reproducible, even on a steep slope of an absorption curve.

a. Determination of pK in Hydrochloric Acid Solutions of Picric Acid

In picric acid solutions as dilute as 5×10^{-5} M the concentration of nonionized molecules is negligibly small unless a stronger acid is added to repress the ionization. The pK value was calculated from the equation

$$p\mathrm{K} = -\log [\mathrm{H}^+] - 2\log \gamma_{\pm} - \log [(D-D_1)/(D_2-D)]. \quad (1)$$

In this equation $[\mathrm{H}^+]$ denotes the total hydrogen ion concentration in moles per liter, and $\gamma_{\pm}$ is taken as the mean activity coefficient of aqueous hydro-

chloric acid of equivalent molarity (see [4], footnote 4). The symbols D_1, D_2, and D apply to any picric acid solution of a given stoichiometric concentration, D_1 being the spectral absorbance (optical density) when the acid is present entirely as HPi, D_2, the absorbance when it is present entirely as Pi^-, and D, the absorbance when conversion of HPi to Pi^- or vice versa is only partial. The use of eq (1) involves the usual convention that $\gamma_+ \cdot \gamma_- = \gamma_\pm^2$ for hydrochloric acid, as well as the assumptions that $\gamma_{HPi}=1$ and γ_{Pi^-} is the same as $\gamma_\pm$ for hydrochloric acid.

A recognized problem in determining spectrophotometrically the pK values of acids as strong as picric acid is the difficulty in determining D_1 values. In the high concentrations of mineral acid needed for repressing the ionization, additional effects on the spectral absorption seem prone to occur. In the hope of meeting this difficulty, measurements were made not only at 355 mμ, which is near the wavelength of maximum absorption of Pi^-, and at 400 mμ, which is on a shoulder of the absorption curve for Pi^-, but also at 450 mμ, where it seemed fairly certain that D_1 would equal zero.

b. Attempt to Determine pK Using More Concentrated Aqueous Solutions

Using the shortest available absorption cells (0.01-cm), absorbance measurements were made at 450 mμ for five picric acid solutions ranging from 0.025 M to 0.050 M, with and without additions of sodium hydroxide. The absorbance values indicated that in all of these solutions more than 90 percent of the solute was present as Pi^-. An attempt was made to calculate pK by eq (1) (with the same assumptions as before). These calculations, which indicated that pK may be about 0.4 or less, cannot be considered reliable, both because of experimental uncertainties and because of the uncertainty as to how much the assumed activity coefficients differ from the true values.

3. Results and Discussion

3.1. Spectral Absorption Curves

Figure 1 shows a series of absorption curves obtained with 5×10^{-5}-M picric acid in water, in 0.023-M sodium hydroxide, and in aqueous hydrochloric acid ranging from 0.145 M to 8 M. The faintly dotted line shows the spectral absorption of picric acid in cyclohexane [10]. The arrows indicate the three wavelengths used in determining pK.

It is generally accepted that ionization of picric acid is essentially complete in solutions as dilute as 5×10^{-5} M. This belief finds support in our experiments, in which the absorption curves obtained in water and in 0.023-M sodium hydroxide (pH>12)

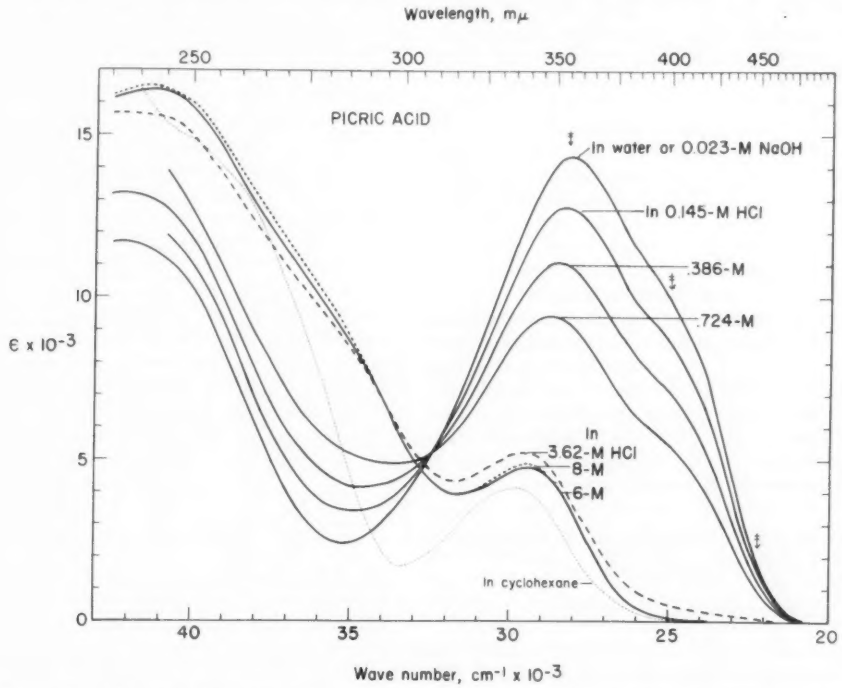

FIGURE 1. *Spectral absorption curves of picric acid (5×10^{-5} M) in water, in aqueous alkali (approx. 0.023-M, pH>12), and in aqueous acid* (HCl, *ranging from 0.145 M to 8 M*). *t*=25 °C.

The faintly dotted line indicates the spectral absorption of picric acid in cyclohexane [10]. The arrows indicate the wavelengths (355 mμ, 400 mμ, and 450 mμ) used in determining pK. The absorption in water and 0.023-M NaOH agreed very closely in the entire spectral range measured.

agreed very closely. It was thought desirable to limit the excess of alkali, as a large concentration causes an irreversible deepening of the color.[5] The alkali was added slowly, with stirring, to avoid momentary large excesses.

For all the aqueous solutions containing 0.724-*M* hydrochloric acid or less, there is a well-marked isosbestic point at approximately 307 mμ, $\epsilon = 5050$. The curves for the three highest concentrations of hydrochloric acid do not pass through this isosbestic point, but appear to be shifted toward the ultraviolet. The curves obtained with 6-*M* and 8-*M* hydrochloric acid are very similar at wavelengths longer than about 280 mμ, but in the region from about 320 mμ to 350 mμ there is a suggestion of the kind of behavior observed in determining the *p*K of dimethylpicric acid [4], when progressive decreases in the absorption on the first additions of hydrochloric acid were followed by increases in the absorption at high concentrations of hydrochloric acid.

As is well known, in the near ultraviolet and visible regions the absorption curve for aqueous picrate appears to be the envelope of at least two overlapping bands, one near 355 mμ and the other in the vicinity of 400 mμ.[6] In some solvents, these bands are more clearly distinguishable and, moreover, their positions vary with the nature of the cation (for example, [14, 15]). The absorption of the nonionized acid is also affected by the nature of the medium (see fig. 1 and [14, 15]). Physical constants determined from absorbance measurements in a region of overlapping bands could be in error if, for example, one component band were a "blue-shift" band and another, a "red-shift" band, or if both were "red-shift" bands not equally affected by a changing medium.[7] In recent years attempts have been made to account theoretically for strong absorption bands of nitroaromatic compounds, including mono- and dinitrophenols and picric acid. For example, it has been suggested that the absorption band of picrate ion near 353 mμ and the band showing as a shoulder near 400 mμ are intramolecular charge-transfer bands, in which the phenyl and nitro groups act as electron-donor and electron-acceptor groups, respectively (see [19] and references cited). This is recognized as being only a partial interpretation, which does not take into account such factors as inter- and intramolecular hydrogen bonding and steric inhibition of resonance of substituent groups with the benzene ring.

3.2. Results of *p*K Determinations in Aqueous Hydrochloric Acid

a. *p*K Value Determined at 450 mμ

Table 2 summarizes the results obtained by calculating *p*K from absorbance data at 450 mμ. The equation used and the assumptions made about activity coefficients were discussed in section 2.3a. At 450 mμ the additional assumption was made that $D_1 = 0$, justification for which is as follows:

(1) The absorbance of picric acid in 6-*M* and 8-*M* hydrochloric acid is negligibly small at 450 mμ and even shorter wavelengths (fig. 1).

(2) Under comparable experimental conditions picric acid dissolved in cyclohexane (see fig. 1) or benzene [15] has negligibly small absorbance in this region.

(3) Nonionized 2,4-dinitrophenol does not absorb measurably at wavelengths as long as 450 mμ; the close similarity of the absorption curves of 2,4-dinitrophenol and picric acid in both acidic and alkaline solutions has been pointed out [11].

Averaging all of the results from three independent experiments gives 0.33 as the *p*K value of picric acid. (The average obtained by including only the *p*K values obtained for $C_{HCl} = 0.241$ *M* or greater, where the values of log $[D/(D_2 - D)]$ are in the best range, is not significantly different from the average based on all 26 values.)

TABLE 2. *p*K *of picric acid in water at 25 °C from data at 450 mμ* [a]

Molar concentration of HCl	D	$\log \frac{D}{D_2 - D}$	$-\log[H^+]$	$-2 \log y_{\pm}$	*p*K
Expt. 1. $C_{HPi} = 5.004 \times 10^{-5}$ *M*, $b = 5$ cm					
0.0966	0.430	0.870	1.015	0.196	0.341
.145	.410	.721	0.839	.218	.336
.193	.392	.611	.714	.230	.333
.290	.359	.444	.538	.242	.336
.386	.330	.320	.413	.244	.337
.483	.304	.218	.316	.242	.340
.579	.284	.143	.237	.236	.330
.724	.250	.021	.140	.222	.341
.821	.230	−.050	.086	.210	.346
.917	.214	−.107	.038	.195	.340
.966	.206	−.137	.015	.186	.338
Expt. 2. $C_{HPi} = 5.005 \times 10^{-5}$ *M*, $b = 5$ cm					
0.193	0.392	0.611	0.714	0.230	0.333
.241	.375	.521	.618	.238	.335
.483	.308	.233	.316	.242	.325
.604	.277	.117	.219	.235	.337
.845	.229	−.053	.073	.206	.332
Expt. 3. $C_{HPi} = 5.002 \times 10^{-5}$ *M*, $b = 0.05$ cm					
0.0483	0.452	1.100	1.276	0.164	0.340
.0966	.428	0.853	0.996	.198	.341
.107	.425	.829	.955	.202	.328
.171	.401	.664	.757	.226	.319
.241	.374	.516	.611	.238	.333
.321	.352	.413	.488	.243	.318
.385	.332	.328	.411	.244	.327
.483	.307	.230	.313	.242	.325
.579	.284	.143	.235	.236	.328
.676	.251	.061	.168	.227	.334
Average *p*K					0.334
K					0.46
Relative standard deviation, %					2.1

[a] The ionic dissociation constant was derived using the equation

$$pK = -\log[H^+] - 2 \log y_{\pm} - \log [(D - D_1)/(D_2 - D)]. \quad (1)$$

See the text for discussion of assumptions made about activity coefficients. The symbols D_1, D_2, and D denote the spectral absorbances (optical densities) of solutions containing the same stoichiometric concentration of picric acid present as nonionized molecules, ionized molecules, or mixtures of the two, respectively. At 450 mμ, D_2 was found to have the value 0.488 and D_1 was assumed to be zero. The symbol b denotes the optical cell length.

[5] This reaction is discussed in [11, 12].

[6] In cases like this, Vandenbelt and Henrich's discussion and illustrations of overlapping absorption bands [13] are helpful in visualizing probable locations of the principal component bands.

[7] Recent textbooks on absorption spectroscopy, such as [16 to 18], discuss blue- and red-shifts, referring to original papers.

The good agreement of the results was unexpected, considering the uncertain validity of assumptions made in applying eq (1) and the fact that the wavelength of measurement was on a steep slope instead of on or close to the head of an absorption band (which is generally considered desirable, when feasible). However, as noted in section 2.3, no difficulty was experienced in obtaining absorbance values of high precision.

As table 2 shows, the stoichiometric concentration of picric acid was varied 100-fold in a dilute range, and the concentration of hydrochloric acid extended from about 0.05-M to 0.97-M. Since the pK values obtained under these conditions show no perceptible trend, it seems justifiable to conclude that the pK value adopted is valid at zero ionic strength.

b. pK Values Obtained From Data at 355 mμ and 400 mμ

The spectral shifts in the most highly concentrated hydrochloric acid solutions (see sec. 3.1) interfere with experimental determination of D_1 values at 355 mμ and 400 mμ. A general idea of their probable magnitudes can be obtained from the appearance of the curves and the comparative absorbance values at all three wavelengths. pK values were calculated assuming two different values of D_1 which were thought to cover the most likely range of values. The results are presented in table 3.

While the values of pK obtained from the absorbance data at 355 mμ and 400 mμ are in the vicinity of 0.3, in agreement with the results obtained at 450 mμ, the values in table 3 show a gradual increase in magnitude with increasing concentration of the hydrochloric acid. Conceivably this behavior occurred for one or more of the following reasons:

(1) Adoption of values for D_2 that were a little too low. The values adopted were believed to be close to the correct values, but, as table 3 shows, at 355 mμ an increase of only 0.005 in the value of D_2 can bring the pK values into fairly good agreement with the series obtained at 450 mμ (see values enclosed in brackets).

(2) Overlapping absorption bands of picrate ion that are not equally affected by the progressive changes in the medium (see sec. 3.1).

(3) The gradual hypsochromic ("blue") shift in the absorption curve of nonionized picric acid.

(4) Slight changes in the spectral absorption resulting from interaction of picric acid with trace impurities in the hydrochloric acid.

3.3. Concluding Discussion

As indicated above, attempts to determine the pK of picric acid in water by potentiometric titration (sec. 2.2) or by applying spectrophotometry to nearly saturated solutions (sec. 2.3b) did not yield results that were considered reliable.

However, the consistent spectrophotometric results obtained at 450 mμ with picric acid solutions covering the range 5×10^{-5} M to 5×10^{-3} M, in the presence of approximately 0.05-M to 1-M hydrochloric acid, point to the pK value 0.33 at 25 °C. The results

TABLE 3. pK of picric acid in water at 25 °C from data at 355 mμ and 400 mμ[a]

Molar concentration of HCl	λ=355 mμ; D_2=0.720			λ=400 mμ; D_2=0.498		
	D	Calcd. pK, assuming that		D	Calcd. pK, assuming that	
		D_1=0.182 [b]	D_1=0.211 [c]		D_1=0.003 [b]	D_1=0.045 [d]
Expt. 1. $C_{HPi}=5.004\times10^{-5}$ M; b=1 cm						
0.0966	0.664	0.28 [0.31]	0.30	0.451	0.23	0.28
.145	.641	.29 [.32]	.32	.430	.26	.30
.193	.622	.29 [.31]	.32	.414	.26	.30
.290	.587	.30 [.31]	.33	.383	.26	.31
.386	.554	.31 [.32]	.34	.354	.27	.32
.483	.526	.31 [.32]	.35	.328	.28	.34
.579	.498	.32 [.33]	.36	.304	.28	.35
.724	.463	.33 [.33]	.37	.271	.29	.36
.821	.444	.32 [.33]	.37	.253	.29	.37
.917	.423	.32 [.33]	.38	.235	.29	.37
.966	.416	.32 [.32]	.37	.227	.28	.37
Expt. 2. $C_{HPi}=5.005\times10^{-5}$ M; b=1 cm						
0.193	0.620	0.30 [.32]	0.33	0.410	0.28	0.33
.241	.601	.31 [.33]	.34	.395	.28	.32
.483	.525	.31 [.32]	.35	.327	.28	.34
.604	.493	.32 [.33]	.36	.299	.28	.35
.845	.439	.32 [.32]	.37	.249	.28	.37
Expt. 3. $C_{HPi}=5.002\times10^{-3}$ M; b=0.01 cm						
0.0483	0.688	0.24 [.30]	0.27	0.470	0.22	0.26
.0966	.669	.21 [.25]	.24	.449	.24	.28
.107	.669	.20 [.24]	.23	.447	.22	.26
.171	.634	.26 [.29]	.29	.421	.25	.30
.241	.607	.27 [.29]	.30	.395	.27	.32
.321	.581	.27 [.29]	.31	.374	.26	.31
.385	.564	.26 [.28]	.30	.358	.25	.30
.483	.531	.29 [.30]	.33	.330	.26	.32
.579	.506	.29 [.30]	.33	.306	.27	.34
.676	.482	.30 [.31]	.34	.286	.27	.34

[a] Calculated by the same equation as in table 2, using the same values of $-\log [H^+]$ and $-2\log \gamma_{\pm}$.

[b] This is the experimental D_1 value obtained in 6-M and 8-M HCl. The values in brackets were calculated assuming D_2=0.725.

[c] This is the D_1 value obtained by shifting the D_1 curve for 8-M HCl 5 mμ toward longer wavelengths, so that it will pass through the isosbestic point; that is, it is the experimental value for 350 mμ.

[d] This is an arbitrarily selected value.

obtained at 355 mμ and 400 mμ, though less consistent, support this choice. The pK value 0.33 is fairly close to three spectrophotometric values obtained earlier at 20° (table 1, footnote h) and at 25° (table 1, footnotes j and l).

It would be gratifying if this value agreed closely with the latest reported value (pK approx. 0.71), obtained from accurate conductance measurements (table 1, footnote k). One may speculate as to whether spectrophotometry and conductometry will always yield the same pK value, in view of recent reports ([20, 21] and references cited) that flash photolysis of certain derivatives of phenol produces shortlived excited states of considerably enhanced acidity. However, one of the pK values obtained by conductance (table 1, footnote i) is not far from the spectrophotometric value obtained in this work, and, as shown in table 1, pK values calculated from conductance measurements depend on assumptions made (for example, table 1, footnote d). Moreover, the latest conductance measurements covered a rather restricted range of concentrations of picric acid (2.358×10^{-3} M to 4.410×10^{-3} M).

4. References

[1] J. Shorter and F. J. Stubbs, J. Chem. Soc. (London) **1949,** 1180.

[2] M. M. Davis and H. B. Hetzer, J. Phys. Chem. **61,** 123 (1957).

[3] R. A. Robinson, M. M. Davis, M. Paabo, and V. E. Bower, J. Research NBS **64A** (Phys. and Chem.) No. 4, 347 (1960).

[4] M. M. Davis, M. Paabo, and R. A. Robinson, J. Research NBS **64A** (Phys. and Chem.) No. 6, 531 (1960).

[5] M. M. Davis and M. Paabo, J. Research NBS **64A** (Phys. and Chem.) No. 6, 533 (1960).

[6] R. G. Bates, Electrometric *p*H determinations, p. 74 (John Wiley & Sons, Inc., New York, N.Y., 1954).

[7] M. M. Davis and H. B. Hetzer, J. Research NBS **48,** 381 (1952) RP2326.

[8] M. M. Davis and P. J. Schuhmann, J. Research NBS **39,** 221 (1947) RP1825.

[9] K. S. Gibson and M. M. Balcom, J. Research NBS **38,** 601 (1947), section II.1, RP1798.

[10] M. M. Davis and E. A. McDonald, unpublished data.

[11] (a) J. Eisenbrand and H. von Halban, Z. physik. Chem. **A146,** 30, 101, 111 (1930); (b) J. Molnar, Compt. rend. **201,** 59, 1482 (1935).

[12] T. Abe, Nature **187,** 234 (1960).

[13] J. M. Vandenbelt and C. Henrich, Applied Spectroscopy **7,** 171 (1953).

[14] H. von Halban and B. Szigeti, Helv. Chim. Acta **20,** 746 (1937).

[15] M. M. Davis and H. B. Hetzer, J. Am. Chem. Soc. **76,** 4247 (1954); see figure 10.

[16] R. E. Dodd, Chemical spectroscopy (Elsevier Publishing Co., New York, N.Y., 1962).

[17] H. H. Jaffé and M. Orchin, Theory and applications of ultraviolet spectroscopy (John Wiley & Sons, Inc., New York, N.Y., 1962).

[18] C. N. R. Rao, Ultra-violet and visible spectroscopy (Butterworth, Inc., Washington, D.C., 1961).

[19] T. Abe, Bull. Chem Soc. Japan **35,** 318 (1962).

[20] G. Jackson and G. Porter, Proc. Roy. Soc. (London) **A260,** 13 (1961).

[21] W. Bartok and P. J. Lucchesi, Division of Physical Chemistry of the American Chemical Society, Abstracts of papers presented at Chicago, Ill., Sept. 3–8, 1961, paper No. 140.

(Paper 67A3–211)

JOURNAL OF RESEARCH of the National Bureau of Standards—A. Physics and Chemistry
Vol. 67A, No. 3, May–June 1963

Purity Analysis of Highly Purified Materials by Time-Temperature Cryometry

Gaylon S. Ross and Herbert D. Dixon

(February 13, 1963)

Visual observation of the freezing and melting of compounds in cells used for the determination of purity has uncovered some heretofore unexpected behavior. This behavior has been correlated with certain difficulties experienced in the measurement of purity, particularly when the sample is very pure. Means for partially reducing these difficulties are proposed and procedures for increasing the accuracy of purity measurements are described.

1. Introduction

The usefulness of cryometry as a method of determining the purity of a compound has been well established. The time-temperature apparatus and technique developed by Rossini and coworkers [1] [1] have been widely and successfully used. However, several years ago both Cines [2] and Mathieu [3] published comparisons between the results as obtained by the time-temperature techniques and those obtained by the use of a precision adiabatic calorimeter. Samples of various compounds were analyzed and serious differences between the two methods were found to exist. The differences in the results obtained by the two techniques were particularly significant when the more highly purified materials were analyzed. In these comparative studies, there appeared to be reasonable evidence supporting the view that, under the experimental conditions employed, the results obtained by using the adiabatic calorimeter were more reliable.

Enclosed freezing point cells [4], improved sample transfer [5], and a new method of analyzing data [6] have greatly improved the precision and accuracy of the time-temperature cryometric analysis.

This paper describes techniques used to explore further the utility of time-temperature cryometry into the region of highly purified materials, an area wherein previous work exhibited the most serious discrepancies. It will be seen from section 5, table 1, that the apparatus and techniques described give highly accurate results when used in the determination of purity of simple organic compounds.

2. The Freezing-Melting Curve

The apparatus and general experimental details discussed in this paper are modifications of those discussed in references [1, 4, and 5]. The success of any time-temperature cryometric determination of purity is dependent upon introduction of the sample without contamination, establishment of good thermodynamic and thermal equilibrium during the freezing process, and proper analysis of the experimental data. Under the experimental conditions imposed, the time-temperature freezing curve should be hyperbolic, and when materials of moderate purity are analyzed in the apparatus and by the procedures described in [4] the freezing curve exhibits normal behavior. However, with high purity material (99.99+percent), after initial recovery from supercooling, the observed temperature continues to rise until a large fraction (approximately 50 percent) of the sample is frozen. Beyond this point, the temperature falls rapidly. If the sample is melted after being about 35 percent frozen, the melting experiments produce the normal hyperbolic curves. These melting curves may be used to establish the sample purity, but in general such determinations are less accurate than those obtained from a well-performed freezing curve.

These anomalies in the freezing curves of highly purified materials have been observed for several years. At first they were thought to be associated with specific compounds, but as more materials of high purity were analyzed, it became strongly indicative that the unusual behavior was a result of the purity itself. Figure 1 depicts the general type of phenomenon observed during freezing and melting as described previously. This type of behavior has been observed with highly purified samples of benzene, titanium tetrachloride, carbon tetrachloride, dimethylphthalate, dichlorostyrene, isopropyl alcohol, certain metallo-organic compounds, and various isomers of dichloroethylbenzene.

Since the accuracy of the time-temperature cryometric measurement in the stirred cells is so dependent upon the ability to analyze the freezing curves, an investigation into the causes of the abnormal character of such curves was undertaken. For this work, unsilvered cells were used so as to permit visual observation of the freezing process. Samples of materials ranging in purity from 99.0 percent to 99.999 percent were used. It was observed that crystallization in the stirred cells always commenced on the inner surfaces of the

[1] Figures in brackets indicate the literature references at the end of this paper.

676712—63——3

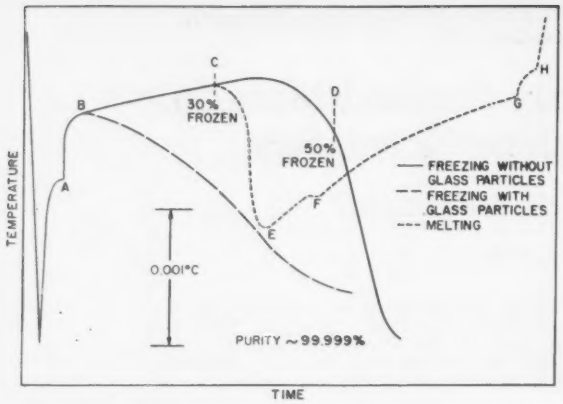

FIGURE 1. *Typical freezing and melting curves for sample of high purity, with and without addition of glass particles.*

A, change in amplification.
B, recovery from supercooling nearly complete.
C, melting experiment started.
D, bridging between thermometer well and outer cell walls, producing rapid fall of temperature.
E, low point on melting curve.
F, disruption of curve due to inclusion of solid from above liquid level.
G, major portion of crystals melted.
H, small crystalline mass in bottom of cell mixes with main body of liquid.

sample cell. A thin sheath of crystal was formed on these walls, and probably on the thermometer well and the stirrer also. There were, however, important differences between the observed behavior of the moderately pure and the very pure samples. In the case of the less pure samples, the sheath was opaque and porous. The stirrer quickly dislodged it from the cell walls and suspended the crystals in the liquid. As crystallization proceeded, these crystals remained suspended in the liquid. The liquid quickly became opaque and gave the appearance of having a very large number of small crystals in suspension.

Contrariwise, with the very pure materials, the sheath was a clear hard mass which was not dislodged by the stirrer action. Instead, it continued to grow from the wall and, encroaching upon the stirrer space, the crystal was strong enough to stop the stirrer. The crystalline mantle surrounding the thermometer well also continued to grow, but the dendritic growth disappeared. Because of poor stirring the dendritic crystals sank to the bottom and were incorporated into the crystalline mass growing there. As crystallization continued, the crystal sheath adhered tenaciously to the thermometer well. A typical time-temperature freezing curve resulting from this type of freezing behavior is shown in figure 1. An approximate temperature scale is shown, corresponding to the temperature changes which occur when a material of high purity, 99.999 percent, is frozen and melted.

The melting process was also watched. If the sample was warmed as it reached point C (fig. 1), the first effect was the melting of the outer crystalline mantle. As this solid became detached from the cell walls and was included in the liquid, much better stirring was achieved. During this initial melting period the crystalline mantle around the thermometer also became detached. At point E, the bulk of the solid has become mixed with the liquid, and continued introduction of heat caused the solid-liquid mixture to melt under conditions which approach thermodynamic equilibrium. The inclusion of large crystal masses during this melting process caused serious discontinuities in the melting curve which made analysis difficult. At point F, crystals which had been deposited above the liquid level during early stages of freezing became incorporated in the main liquid. From this point, the curve assumed the usual hyperbolic shape of the melting curve. At point G the crystalline material suspended in the liquid had completely melted. There was a slight inflection at H due to a small compact mass of crystal which had previously remained on the curved bottom of the cell. After this mass melted, the curve assumed the usual warming slope of the liquid.

One possible explanation of the abnormal behavior of the freezing curve was suggested by the above observations. After initial recovery from supercooling, a crystalline mantle was formed around the thermometer and also around the cell wall. Because of poor stirring, the mantle surrounding the thermometer was not dislodged. The thermometer was a source of heat, and it is probable that a small amount of the solid surrounding the thermometer was melted. This thin layer of liquid would be quite pure, having been formed by the melting of the very pure crystalline phase. Thermodynamic equilibrium between these two phases would occur at a higher temperature than the equilibrium between the solid and the more impure bulk liquid. The temperature of this two phase region surrounding the thermometer would continually rise until the equilibrium temperature was reached. However, at point D, the advancing crystal front from the colder outer wall joined the crystal comprising the thermometer mantle, and the temperature fell rapidly.

Because of this, attempts were made to modify the freezing behavior pattern of the highly purified materials. It was found that when one or two cubic centimeters of small glass particles (approximately 1×10^{12} particles per cubic centimeter) were added to the highly purified material (40 ml), freezing behavior similar to that obtained with the less-pure systems was observed. These particles, primarily borosilicate glass, were obtained from the sludge produced by a carbide, glass-cutting tool, and the smaller particles were separated by gravity-sedimentation techniques. They were cleaned in the same fashion as the other glass components of the cell and were placed in the cell at the time of assembly of the transfer manifold. When treated in this fashion, there was no evidence of a change of sample purity in spite of the enormous surface area. Precise details of this operation will be given later. Many different substances have been analyzed using this technique. The particles, providing they were wetted by the sample liquid, appeared to be capable of satisfactorily modifying the freezing behavior of the purest samples, producing a normal hyperbolic freezing curve. The precise role of

these particles is not known. They appear to act as crystal supports, suspended in the liquid. The crystalline mantles are quickly broken up and the large amount of suspended crystal causes thermal equilibrium to be obtained. It is probable that other materials could be satisfactorily used for this purpose; samples of diatomaceous earth added to samples of carbon tetrachloride or benzene exhibited no apparent effect.

3. Data Processing

The end result of the time-temperature freezing experiment is, of course, the determination of purity of the sample. The thermodynamic relationships, the theoretical proof that the experimental curve should be hyperbolic, and the usual methods of fitting the curve are well known and will not be discussed here. Basically, the analyst is interested in determining two numbers, the freezing temperature of the particular sample and the freezing point of the sample had there been no impurity present. Both of these numbers are obtained by fitting the data to the equation of a hyperbola. Extrapolation of this curve to the intersection of the liquidus cooling curve provides the freezing point of the sample, and further extrapolation to the asymptotic value provides the temperature at which the sample would have frozen had there been no impurity present.

When one is analyzing several samples of the same material but of different purity levels, the freezing points of the individual samples will vary as a function of the impurity present, but the extrapolated value for T_{f_0}, the freezing point of the pure material, should be invariant. This rule provides a valid test for any curve fitting technique. With this as a criterion, several hundred freezing point curves were analyzed, using a series of rather arbitrary curve-fitting rules. As a result it was found that only within the limits of 10 percent and 30 percent frozen, was the value of the experimentally determined T_{f_0} invariant with respect to the purity of the particular material. The need for the lower limit follows directly from the argument that there must be a critical ratio of crystal area to liquid volume before temperatures corresponding satisfactorily to thermodynamic equilibrium can be registered by the thermometer. The upper limit of fraction frozen is the result of increased stirring energy and decreased stirring efficiency. These limits, imposed by particular apparatus and experiment design, seem to hold for all materials analyzed to date.

Other corrections which must be considered by the analyst include factors such as the significant change in heat capacity of the sample on freezing. Because of the difficult theoretical evaluation of the effect of these corrections on the freezing point equation, perhaps the best and most elegant method of fitting the data to an empirical curve is that of Saylor [6]. In this method, a series of positive transparencies of hyperbolae whose asymptotic intersection produces an angle of from 90 to 95° are first made. These 4×5 in. transparencies are placed in a photographic enlarger. The recorded freezing curves are placed under the enlarger so that by increasing or decreasing the magnification, the projected curve can be made to coincide with the experimental curve. Special holders for the transparencies and the recorded freezing curves are used. They allow the movement of each independently, without changing the coordinate interlock between the two. When the "best fit" is obtained, the experimental curve and the coinciding projection are photographed using a 35 mm camera mounted adjacent to the projector. The developed film serves as a permanent record, and the enlarged print may be used to calculate the purity.

By applying the fitting limit rules described previously, and by selecting the correct hyperbolic transparency, the fitting and subsequent calculation of purity is made very easy. Since, usually only 30 to 35 percent of the sample is frozen, the liquid cooling slope is used. The errors introduced by this substitution are negligible.

4. Experimental Detail

When compounds are less than 99.9 mole percent pure, inadvertent contamination during transfer is a relatively minor problem. As long as the samples do not react with air or water and if the containers are reasonably clean and dry, little relative contamination results from pouring or pipetting the sample from one container to another. However, with materials which have a total impurity of less than 10 parts per million, water in the atmosphere or adsorbed on the walls of the container, cell, and transferring manifold can easily increase the amount of impurity by a factor of 10 or more. It is obvious that if complete exclusion of water and air is desired, the sample must be transferred by and analyzed in a closed, evacuated system. The following describes a technique for transferring high-purity samples from a glass ampoule, equipped with a breakoff tip, to the freezing-point cell.

4.1. The Transfer of Highly Purified Materials

The transfers were carried out in all-glass evacuated systems containing no lubricated joints. Such a system is shown in figure 2. All parts were treated with hot chromic acid, water-rinsed, cleaned with warm, concentrated nitric acid, and finally rinsed several times with distilled water. The powdered glass, mentioned previously, was treated in the same fashion as the other glassware and placed in the cell prior to final assembly. The apparatus was then assembled and dried by evacuation to 10^{-6} mm Hg while being continuously heated at 150 °C for 24 hours. Previous experience [5] indicated that even after this treatment for the 24-hour period some water was still adsorbed on the inner glass surfaces.

The manifold was flame-sealed at constriction F after evacuation. Then the breakoff tip of ampoule I was broken and a portion of material similar in composition to the sample was distilled throughout the system. This wash liquid was returned to the ampoule after several hours of refluxing. As much

of this material as possible was poured back into the ampoule by turning the entire apparatus manually. The remaining material was distilled into the ampoule by cooling container I with liquid nitrogen. This ampoule was then removed by sealing at E. The breakoff tip of ampoule A was broken, and the desired amount, usually 40 ml, was poured into the graduated tube J. After both A and J were cooled to liquid nitrogen temperature, the sample ampoule A was removed by sealing at D. The melted sample was poured into the cell and again frozen. Next the measuring tube J was removed by sealing at K. The breakoff tip L was used in removal of the sample from the cell after the analysis had been completed.

Previous experience [5] had shown that the pouring operation is to be preferred to distillation since there can be no change in composition induced in transfer by pouring, but if the impurity is sufficiently nonvolatile serious compositional changes could occur during a transfer by vacuum distillation. The powdered glass may selectively adsorb some of the impurity present in the wash sample. Whether this happens is not known but since the wash sample was similar in composition to the sample being analyzed there was no evidence of a detrimental adsorption-desorption process taking place when the sample is introduced.

4.2. The Freezing-Point Cell and Thermometric System

Freezing-point cells of the type described previously [4, 5] were used. The cells were closed so that samples could be analyzed in the absence of air and water vapor. The double helically wound stirrers were constructed of platinum-iridium, and stirring was achieved by means of a reciprocally moving external electromagnet which was coupled with the platinum-encased iron armature attached to the stirrer shaft. Figure 2 depicts a cell attached to the filling manifold. Constant-temperature freezing or warming baths were used. These baths were selected so that their temperatures differ from the freezing point of the sample by approximately 50°. The freezing rates were controlled by evacuation of the outer jacket of the cell to the appropriate pressure as determined by a Pirani gage.

A 25-ohm, bifilar, helical, glass-sheathed platinum resistance thermometer was used. The G–2 Mueller Wheatstone bridge used in this work was modified as described in [7]. The extreme stability which was achieved as a result of these modifications allowed automatic recording of the bridge output without the necessity of frequent zeroing. With this apparatus temperature differences of 0.00002 °C were detectable.

The freezing curves were recorded automatically in order to obtain a continuous record, to eliminate the tedious manipulation of dials, and to reduce operator bias. A considerable gain in both precision and accuracy was achieved by this recording method. The output from the nearly balanced Wheatstone bridge was amplified using a high-gain, d-c amplifier

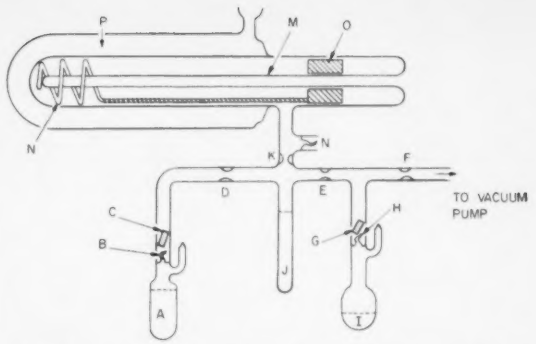

FIGURE 2. *Freezing point cell and transfer manifold.*

A, degassed sample to be analyzed. Approximately 40 ml.
B, H, breakoff glass seals separating contents of ampoule from rest of system.
C, G, glass-enclosed iron bars. They are lifted by externally operated magnets and then dropped to rupture the seals.
D, E, F, K, constricted portions of the glass manifold.
L, side arm containing breakoff tip. Used to remove sample.
J, graduated sample measuring tube.
I, ampoule containing the degassed sample used as a preconditioning wash liquid.
M, thermometer reentrant well.
N, double helical platinum-iridium stirrer.
O, platinum-enclosed, iron toroid connected to coiled stirrer by platinum-iridium rod.
P, silvered vacuum jacket.

equipped with two duplicate sets of gain controls with external-switching mechanisms.

In our experience it has been extremely helpful to program automatically the freezing sequence. For this purpose the recorder was equipped with four switches. There were two limit switches at the opposite ends of the chart, a switch that was direction-activated by the appropriate direction change of the recorder pen, and a switch that could be preset to operate at any selected portion of the recorder span. These switches, together with a stopping switch and a repeating, adjustable cycle switch, were used to program the freezing-point experiment. Programming of the freezing or melting sequence can be a valuable, timesaving aid for the analyst who is engaged in the determination of purity of many samples of one material wherein the expected range of purity is quite small. The precision obtained by programming is always improved in comparison to the nonprogramed experiment sets. However, the basic accuracy is not necessarily improved, and the decision of whether to program or not should be made upon the number of replicate analyses expected.

The programing mechanisms may be of any variety of forms. Figure 3 depicts a real freezing curve showing the programing points. Through ABC one set of amplifier gain controls is adjusted so that a single recorder span corresponds to 5 °C. At point B the direction-sensitive switch is actuated. This starts a timed sequence of events. After a preset period of time (point C) the amplifier gain controls are switched to high sensitivity by advancement of the stepping switch. Again after a preset interval, the appropriate dial on the Mueller bridge is turned (point D) by one of a pair of electromagnets so as to determine the sensitivity. The selection of this point is important in that it should be prior to 10

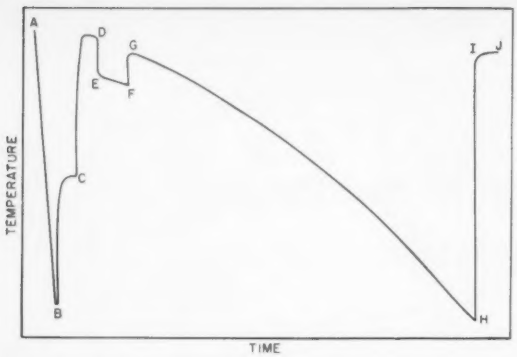

FIGURE 3. *Programed freezing curve with benzene as the sample.*

A, Start of recorded experiment. Sensitivity—1 span/5 °C
B, Spontaneous nucleation of sample. Direction switch activated.
C, Recovery from supercooling nearly complete. Gain changed. Sensitivity—0.01 °C/span.
D, Sensitivity check initiated.
E–F, Change in bridge dial.
G, Return of bridge dial to original setting.
I, Current to bridge interrupted.
J–H, Bridge zero.

percent frozen but after the highest recorded temperature has been reached. At time F the dials are automatically returned to their original position, by the other electromagnet. Point H represents approximately 35 percent frozen, and at this point the limit switch interrupts the bridge current, producing the zero plot from points I to J. The zero should not be taken in this fashion until the experiment is complete, since interruption of bridge current causes hysteresis effects which are not completely eliminated until approximately 10 minutes have elapsed.

5. Experimental Results

The most rigid test of the reliability of the general method described in this paper was imposed by participation in a cooperative project on purity control organized by the Commission on Physicochemical Data and Standards, International Union of Pure and Applied Chemistry. In this program 20 laboratories analyzed replicate samples of benzene to which controlled amounts of contaminant had been added. The list of participants included government, university, and industrial laboratories from 6 countries. The results of this investigation, as yet not published, were reported before the Calorimetry Conference in August 1961 at Ottawa, Canada. Table 1 lists the most probable purity value for each sample as decided by the Committee, together with the results as obtained by this method. It is sufficient to point out that there is excellent agreement from purity ranges of 99.999 mole percent down to 99.0 mole percent, and to note that among the several participants using the Glasgow, Streiff, Rossini technique, the methods suggested herein were the only ones which gave excellent agreement for all samples and, incidentally, agreed with those results obtained from application of precision adiabatic calorimetric techniques.

TABLE 1[a]

Sample designation	Most probable purity	Purity found	Estimated standard deviation (6 experiments per sample)
	Mole %	*Mole %*	
A–7	99.999	99.999	±0.0002
A–16	99.999	99.999	0.0002
A–28	99.999	9.9999	0.0003
B–7	99.907	99.895	0.0018
B–16	99.907	99.894	0.0008
B–28	99.907	99.915	0.0012
C–7	99.797	99.808	0.005
C–16	99.797	99.796	0.001
C–28	99.797	99.760	0.004
D–7	98.822	98.824	0.011
D–16	98.832	98.932	0.025

[a] The complete results of this investigation will be published formally by the International Union of Pure and Applied Chemistry.

6. Summary

This paper discusses in detail the changes in technique which were necessary to extend the time-temperature cryometric method of purity determination to the realm of very highly purified materials. These changes in technique are summarized as follows:

(1) The samples were transferred and analyzed in closed, evacuated systems.

(2) The systems were rigorously cleaned, dried, and preconditioned with a portion of the sample to be analyzed.

(3) Ground glass was added to insure the attainment of equilibrium in the freezing cell.

(4) The time-temperature curves were automatically recorded.

(5) When large numbers of replicate analyses were performed, the freezing experiments were programed.

(6) Selection rules were devised to insure that the best portion of the time-temperature curve was used in the curve-fitting.

(7) The optical projection method of curve-fitting was employed to eliminate operator bias and give more reliable results.

7. References

[1] A. R. Glasgow, Jr., A. J. Streiff, and F. D. Rossini, J. Research NBS **35,** 355 (1945).

[2] M. R. Cines, Physical Chemistry of Hydrocarbons, Ch. 8, (Academic Press, Inc., New York, N.Y., 1950).

[3] M. P. Mathieu, Acad. Roy. Belg., Classe Sci. Mem. **28,** (1953), Fasc. 2, No. 1945.

[4] A. R. Glasgow, Jr., and M. Tenenbaum, Anal. Chem. **28,** 1907 (1956).

[5] A. R. Glasgow, Jr., G. S. Ross, A. T. Horton, D. Enagonio, H. D. Dixon, C. P. Saylor, G. T. Furukawa, M. L. Reilly, and J. M. Henning, Anal. Chim. Acta **17,** 54 (1957); reprinted in W. M. Smit, Purity Control by Thermal Analysis (Elsevier Publishing Co., Amsterdam, 1957).

[6] C. P. Saylor, Anal. Chim. Acta **17,** 35 (1957); reprinted in W. M. Smit, Purity Control by Thermal Analysis (Elsevier Publishing Co., 1957).

[7] G. S. Ross and H. D. Dixon, J. Research NBS **65C** 271 (1960).

(Paper 67A3–212)

JOURNAL OF RESEARCH of the National Bureau of Standards—A. Physics and Chemistry
Vol. 67A, No. 3, May–June 1963

Synthesis of Isomers of Eugenol [1]

Gerhard M. Brauer, Richard Warren Morris,[2] and Willard B. Howe[2]

(February 12, 1963)

In connection with an investigation of the correlation between structure and reactivity of eugenol isomers, *o*-eugenol, 3-allyl-2-methoxyphenol and chavibetol were synthesized. A five-step synthesis was found to be most suitable for the preparation of 3-allyl-2-methoxyphenol. An improved separation of chavibetol from eugenol was achieved by gas chromatography.

1. Introduction

Slurries of zinc oxide and eugenol (I) harden to form a cementitious product which has found many applications in dentistry. A prior investigation of the setting mechanism showed that the hardened mass consists of zinc oxide embedded in a matrix of chelated zinc eugenolate [1].[3] It therefore appeared of interest to study the properties and reactivity of all eugenol isomers capable of forming chelates with metal oxides, i.e., *o*-eugenol (II), 3-allyl-2-methoxyphenol (III) chavibetol (IV) and their respective propenyl isomers.

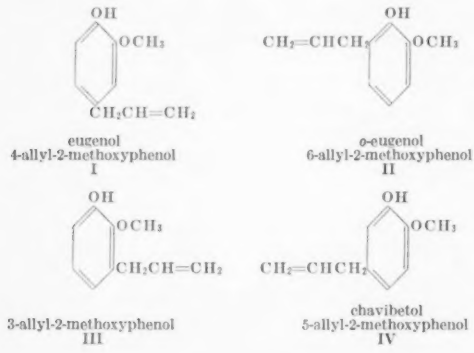

eugenol
4-allyl-2-methoxyphenol
I

o-eugenol
6-allyl-2-methoxyphenol
II

3-allyl-2-methoxyphenol
III

chavibetol
5-allyl-2-methoxyphenol
IV

The present paper describes methods for synthesizing some of these compounds. In a subsequent paper the structure of the isomers will be correlated with their ultraviolet and infrared absorption spectra, ionization constants and reactivity with metal oxides.

Three procedures were considered for the synthesis of 3-allyl-2-methoxyphenol (III). (1) Partial demethylation of 1-allyl-2,3-dimethoxybenzene (a preparation analogous to that described by Hirao [2] and Schöpf and coworkers [3] for the synthesis of Chavibetol). The isomeric products II and III appeared to be difficult to separate by techniques other than gas chromatography. (2) Claisen rearrangement of allyl 2-benzoyloxyphenyl ether followed by methylation and by subsequent hydrolysis of the benzoyl group. However, the rearrangement gave 1-allyl-2,3-dihydroxybenzene instead of the desired intermediate. (3) The procedure outlined in figure 1; this synthesis proved to be successful.[4]

The preparation of IV was also attempted by several methods. The synthesis of pure chavibetol described by Hirao [2] and Schöpf and coworkers [3] proved to be laborious in the separation of chavibetol from its eugenol isomer. This separation has now been greatly facilitated by the use of gas chromatography.

2. Experimental Procedures

2.1. o-Eugenol (6-Allylguaiacol)[5] (II) and o-Eugenol Benzoate

o-Eugenol was synthesized from guaiacol in 67-percent yield by the procedure of Allen and Gates [5]. The infrared spectrum is given in figure 2. *o*-Eugenol benzoate was prepared by refluxing *o*-eugenol with benzoyl chloride. The solution was poured into cold water and the mixture extracted with ether. The ether solution was washed successively with dilute NaOH and HCl and evaporated. After recrystallizations from aqueous ethanol and from ether the solid melted at 59 to 60 °C.

Anal: Calcd. for $C_{17}H_{16}O_3$: C, 76.1; H, 6.0. Found: C, 76.6; H, 6.0.

2.2. 3-Allyl-2-methoxyphenol (3-Allylguaiacol) (III)

o-Hydroxyacetanilide (*2'-Hydroxyacetanilide*) (*V*).

[1] The research work was supported by grants from the Office of Navy Research, Contract ONR P.J.–NR 105-210 (1-29-59), the Army Dental Corps and the Dental Sciences Division of the School of Aviation Medicine.
[2] Guest worker, U.S. Army.
[3] Figures in brackets indicate the literature references at the end of this paper.
[4] Since completion of this work, the preparation of III from *o*-nitrophenol [4] has come to our attention.
[5] Throughout this paper the systematic names employed by *Chemical Abstracts* are given parenthetically at the first mention of the compound in the experimental section.

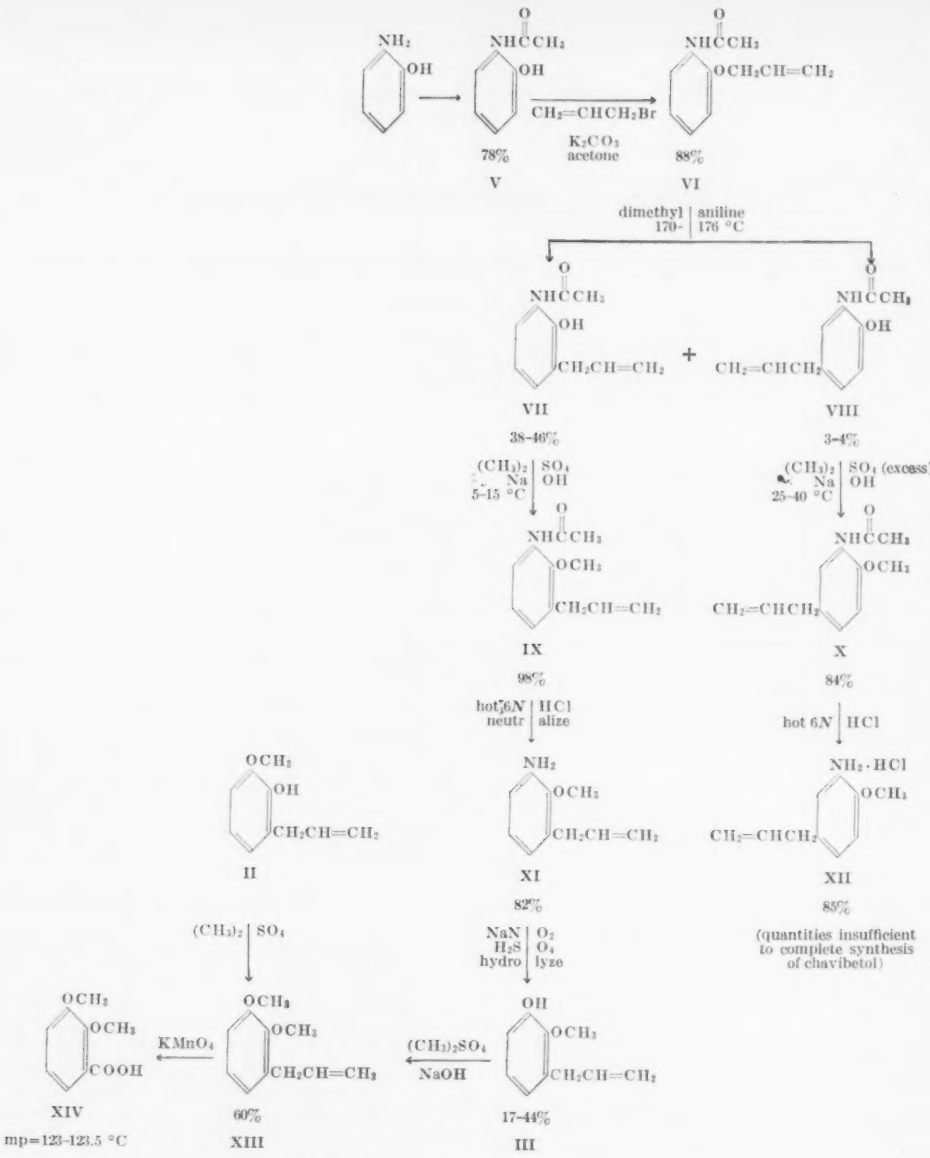

FIGURE 1. *Synthesis of 3-allyl-2-methoxyphenol (III).*

This compound was synthesized from 283 g (2.59 mole) of *o*-hydroxyaniline according to the procedure of Fierz-David and Kuster [6] and recrystallized from acetone. Yield: 307 g (78 percent).

o-Hydroxyacetanilide Allyl Ether (*2'-Hydroxyacetanilide Allyl Ether*) (*VI*). This compound was synthesized as described by Tiffany [7]. Yield: 88 percent.

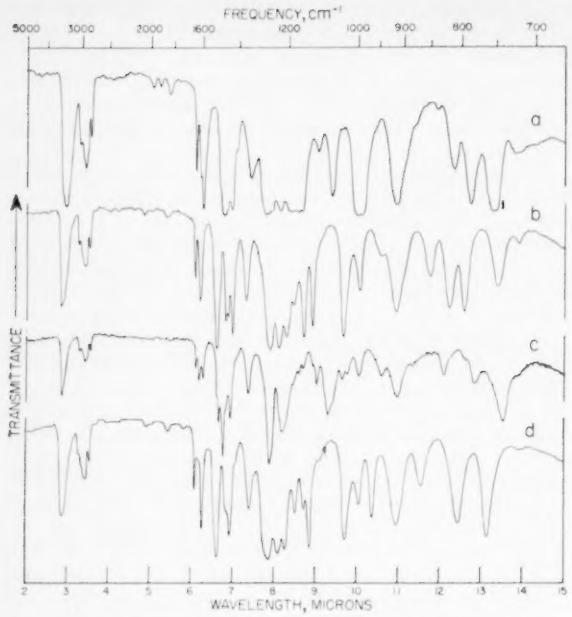

FIGURE 2. *Infrared absorption curves of eugenol and its isomers.*

Top to bottom: (a) 3-allyl-2 methoxyphenol, (b) eugenol, (c) *o*-eugenol, (d) havibetol.

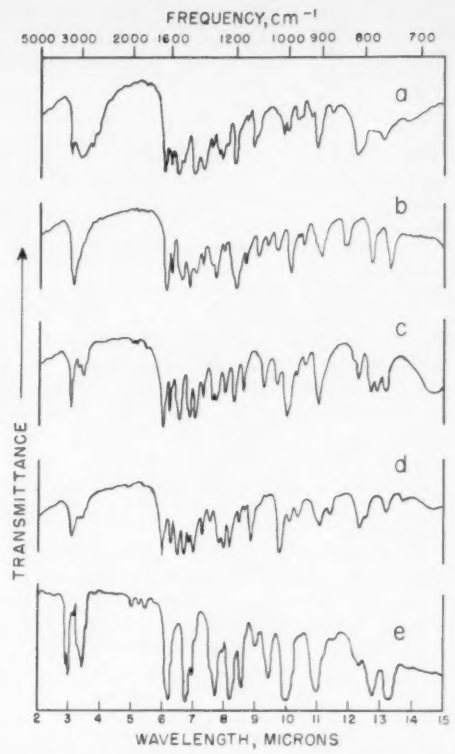

FIGURE 3. *Infrared absorption curves of intermediates.*

Top to bottom: (a) 3-allyl-2-hydroxyacetanilide, (b) 5-allyl-2-hydroxyacetanilide, (c) 3-allyl-2-methoxyacetanilide, (d) 5-allyl-2-methoxyacetanilide, (e) 3-allyl-2-methoxyaniline. Materials (a) through (d) were in the form of potassium iodide pellets; material (e) was a liquid.

3-Allyl-2-hydroxyacetanilide (3'-Allyl-2'-hydroxyacetanilide) (VII) and 5-Allyl-2-hydroxyacetanilide (5'-Allyl-2'-hydroxyacetanilide) (VIII). The Claisen rearrangement of VI was conducted in dimethylaniline at 170 to 176 °C [7]; time of reflux varied from 1½ to 4 hr. The two isomers were fractionally recrystallized and separated as described previously [7]. Faster separation was obtained by repeated fractional precipitation from 1 *N* NaOH by the addition of 0.5 *N* H_2SO_4 [8]. Yield of VII, 38 to 46 percent, mp 114 to 115 °C; yield of VIII, 3 to 4 percent, mp 115 to 116 °C. The purity of the isomers was determined by mixed melting points.

The infrared spectra of the isomers are shown in figures 3a and 3b. The spectra are useful in detecting isomerization of the allyl group to the propenyl, a change which takes place readily. Presence of the allyl group is indicated by the out-of-plane vibrations of the $=CH_2$ and $=CH-$ groups which give rise to two strong absorptions, one between 9.97 and 10.12 μ and the other between 10.93 to 11.09 μ [9]. Intramolecular hydrogen bonding between the phenolic hydrogen and the carbonyl is indicated by the shift of the acetamido carbonyl absorption (usually occuring near 5.99 μ) to 6.09 μ.

3-Allyl-2-methoxyacetanilide (3'-Allyl-o-acetanisidide) (IX). 3-Allyl-2-hydroxyacetanilide (156 g, 0.82 mole) dissolved in 500 ml of water containing 39.2 g (0.98 mole) of NaOH was cooled to 5 °C, and nitrogen was passed over the solution. Dimethyl sulfate (100 ml, 1.055 moles) was gradually added during 1 hr to the stirred solution, which was kept at 5 to 12 °C. Additional dimethyl sulfate (30 ml, 0.32 mole) was added during a period of 2½ hr. The reaction mixture, warmed to room temperature, was made alkaline and extracted with ether. On evaporation of the extract and crystallization of the residue from ligroin or 50-percent aqueous ethanol, colorless platelets were obtained. Yield: 163 g (98 percent), mp 86 to 87 °C.

Anal: Calcd. for $C_{12}H_{15}NO_2$: C, 70.3; H, 7.4; N, 6.8. Found: C, 70.4; H, 7.2; N, 6.9.

The infrared spectrum is given in figure 3c.

3-Allyl-2-methoxyaniline (3'-Allyl-o-anisidine) (XI) and its Hydrochloride. 3-Allyl-2-methoxyacetanilide (46.6 g, 0.23 mole) was refluxed for 80 min with 45 ml of 6 *N* HCl. The solution was made alkaline with 10-percent NaOH, and the oily layer was separated. Ether extracts of the aqueous layer were added to the brown oil. After evaporation of the ether the remaining oil was distilled at 3.5 mm in the presence of a little hydroquinone (to minimize polymer formation). The liquid turned brown on standing in air. Yield: 30.3 g (82%). For further purification some of the product was fractionated in a Piros-Glover spinning-band still (bp 78 to 80 °C at less than 1 mm); $n_D^{25} = 1.553$.

Anal: Calcd. for $C_{10}H_{13}NO$: C, 73.6; H, 8.0; N, 8.6. Found: C, 73.5; H, 8.0; N, 8.3.

The absence of characteristic infrared absorption bands (fig. 3c) for *cis* and *trans* —CH=CH— indicates that little, if any, of the propenyl isomer was present.

The hydrochloride was prepared by dissolving 1 g of XI in 15 ml of ether and bubbling hydrogen chloride through the solution for 5 min. The white solid, obtained on recrystallization from hot ethanol containing a drop of concentrated HCl, melted with decomposition at 178 to 179 °C.

Anal: Calcd. for $C_{10}H_{14}ClNO$: C, 60.2; H, 7.1; N, 7.0. Found: C, 59.9; H, 7.4; N, 6.9.

3-Allyl-2-methoxyphenol (3-Allylguaiacol) (III). 3-Allyl-2-methoxyaniline was diazotized, and the resulting diazonium salt converted to the phenol. Reverse diazotization appeared to give slightly better yields than the usual addition of sulfuric acid followed by nitrite. Yields improved when only small quantities of diazonium salt were decomposed; however, they varied considerably from one preparation to another.

3-Allyl-2-methoxyaniline (5 g, 0.03 mole) was suspended in 25 ml of water, and solutions of 1.15 g of NaOH in 6.5 ml of water and of 4 g of $NaNO_2$ in 15 ml of water were added successively. The entire solution, cooled to 0 °C, was then quickly added, with stirring, to 4.5 g of concentrated H_2SO_4 (previously cooled to 0 °C) and kept in an ice bath. The excess nitrite was decomposed by the addition of urea until a negative test for nitrite was obtained with starch-iodide paper. The resulting cold solution was stored in a refrigerator until needed.

A solution prepared from 150 g of anhydrous Na_2SO_4, 108 ml of concentrated H_2SO_4 and 100 ml of water, in a three-necked flask equipped for steam distillation, was kept at 135 to 150 °C by a surrounding oil bath. The cold solution of the diazonium salt was slowly added from a separatory funnel while steam was passed through the flask; the volatile products were thus steam-distilled immediately after decomposition of the diazonium salt.[6] The distillate was extracted with ether, the ether extracts were washed with 10-percent, aqueous $NaHCO_3$, and the phenol was extracted from the ether layer with 10-percent aqueous NaOH. After ether extraction of the acidified solution and evaporation of the solvent 0.85 to 2.2 g (17 to 44%) of 3-allyl-2-methoxyphenol was obtained; bp 92 to 93 °C/4 mm, $n_D^{26}=1.535$.

Anal: Calcd. for $C_{10}H_{12}O_2$: C, 73.1; H, 7.4. Found: C, 72.9; H, 7.3.

The infrared spectrum (fig. 2) shows absorption bands in the regions in which the —CH=CH_2 group absorbs, namely, 5.39 to 5.55 μ; 7.04 to 7.09 μ; 7.69 to 7.76 μ; 10.05 to 10.15 μ; and 10.93 to 11.05 μ. [11]. The areas in which the *trans* —CH=CH— group absorbs (7.67 to 7.72 μ and 10.31 to 10.42 μ) fall on the sides of two of these bands, and hence it is not possible to state with certainty that there is no absorption due to *trans* —CH=CH— groups. Absence of an absorption band near 14.49 μ indicates that there is very little, if any, *cis* —CH=CH— present. Before the final fractionation the phenol contained a considerable amount of ethanol. The mechanism of the formation of this product is not known.

To establish the identity of III it was converted to 2,3-dimethoxybenzoic acid (*o*-veratric acid) (XIV) via 1-allyl-2,3-dimethoxybenzene (XIII). 3-Allyl-2-methoxyphenol (1.5 g, 0.09 mole) dissolved in 16 ml of 15-percent NaOH was cooled, and 2.0 ml of dimethyl sulfate was rapidly added to the stirred solution. After 15 min 2 ml of dimethyl sulfate was added, and the solution was refluxed for 2 hr; 5.5 ml of 10-percent NaOH was then added, the solution refluxed for 2 more hr, cooled, and extracted with ether. The ether extract was dried and evaporated, and the residue distilled at 65 to 68 °C/2.5 mm. Yield: 1.0 g (60 percent), $n_D^{25}=1.524$. The same physical constants were obtained for XIII, synthesized from *o*-eugenol according to the procedure of Mauther [12].

For the conversion of XIII to XIV, 1 g of 1-allyl-2,3-dimethoxybenzene was refluxed for 1½ hr with 3.6 g of powdered potassium permanganate dissolved in 40 ml of water. The mixture was filtered through a fritted glass funnel, and the filtrate was evaporated to about 20 ml, cooled, and acidified with dilute H_2SO_4. The resulting precipitate, after successive recrystallizations from benzene and water, melted at 123 to 123.5 °C. The melting point was unchanged by mixture with authentic 2,3-dimethoxybenzoic acid.

Conversion of III to 2-Methoxy-3-propenylphenol. 3-Allyl-2-methoxyphenol (III) was refluxed with alcoholic KOH for 16 hr by a method analogous to the preparation of isochavibetol [2]; bp 109 °C/7mm, $n_D^{25}=1.556$. As indicated by the infrared spectrum the product was an impure mixture of *cis* and *trans* 2-methoxy-3-propenylphenol.

2.3. Chavibetol (5-Allylguaiacol) (IV)

Eugenol methyl ether (1-allyl-3,4-dimethoxybenzene) was synthesized in 88-percent yield according to the procedure of Luff, Perkin, and Robinson [13]. Demethylation of this compound with Grignard reagent, conducted as suggested by Schöpf and coworkers [3] gave a mixture of eugenol and chavibetol.

It was found that these impure eugenol-chavibetol mixtures could be separated by gas chromatography with a diisodecyl phthalate column heated to 175 °C and a hydrogen flame detector. Larger quantities of the isomers were most conveniently separated by a chromatograph designed for synthetic work; this employed Apiezon J on a C–22 firebrick column, with a column temperature of 180 °C and a pressure of 10 lb/in^2. The infrared spectrum of chavibetol is shown in figure 2.

The chavibetol was characterized by conversion to isochavibetol (mp 95 to 96 °C) as described by Hirao [2].

[6] Because of tar formation, the solution of the diazonium salts was introduced. In later reactions, through a cold-finger addition tube (as suggested by Lamboov [10]); the tube reached to within 1 cm of the surface of the hydroysis mixture.

2.4. Preparation of Intermediates in Attempted Synthesis of Chavibetol

Prior to the gas chromatographic separation described in section 2.3, the preparation of chavibetol from VIII (fig. 1) was attempted. Although the preparation was not completed for lack of material, two new intermediates (X and XII) were obtained. The following sections describe their preparation.

5 - Allyl - 2 - methoxyacetanilide (5 - Allyl - o - acet - anisidide) (X). 2-Acetamido-4-allylphenol (5 g, 0.026 mole) was dissolved in 25 ml of 5.5-percent aqueous NaOH (0.034 mole). During a 15-min period, 3.8 ml (0.04 mole) of dimethyl sulfate was added, while the solution was stirred in an atmosphere of nitrogen. During 90 min, 3 ml of dimethyl sulfate was added, together with sufficient NaOH solution to keep the mixture alkaline. The mixture was then heated at 40 °C for 45 min, and extracted with ether. After drying and evaporation of the solvent, the residue was recrystallized from ligroin to yield long, colorless needles, mp 56.5 to 57 °C; yield; 4.50 g (84 percent).

Anal: Calcd. for $C_{12}H_{16}NO_2$: C, 70.3; H, 7.4; N, 6.8. Found: C, 70.3; H, 7.6; N, 6.5. The infrared spectrum is given in figure 3d.

5-Allyl-2-methoxyaniline Hydrochloride (5'-Allyl-o-anisidine Hydrochloride) (XII). 5-Allyl-2-methoxyacetanilide (3.8 g, 0.019 mole) dissolved in 10 ml of 6*N* HCl was refluxed for 45 min, and the solution was concentrated by evaporation under reduced pressure. The resulting precipitate on recrystallization from an aqueous solution acidified with a little HCl gave colorless needles (mp 170 to 172 °C); yield (including recovery from mother liquor); 3.15 g (85 percent).

Anal: Calcd. for $C_{10}H_{14}ClNO$: C, 60.2; H, 7.1; N, 7.0. Found: C, 60.2; H, 7.2; N, 6.8.

A solution of the hydrochloride (3 g in 15 ml of water) was made slightly alkaline with 2-percent NaOH and extracted with ether. After evaporation of the solvent a liquid remained which sublimed during attempted vacuum distillation. The crystalline product, on successive recrystallization from 70-percent aqueous ethanol and ligroin, gave colorless scales, mp 47 °C. The presence of an absorption band at 10.32 μ suggests that some isomerization to the *trans* propenyl group had taken place. Elementary analysis indicated that the compound was impure.

2.5. Synthesis of Allyl 2-Benzoyloxyphenyl Ether and Its Behavior in a Claisen Rearrangement

In one of the alternative procedures for the synthesis of 3-allyl-2-methoxyphenol, allyl 2-benzoyloxyphenyl ether was synthesized and its Claisen rearrangement investigated.

Allyl 2-Benzoyloxyphenyl Ether (XV). Catechol monobenzoate was prepared in 55-percent yield by benzoylation of catechol at 6 °C according to the procedure of Donadio [14]. A solution prepared from catechol monobenzoate (168 g, 0.78 mole), anhydrous K_2CO_3 (110 g, 0.80 mole), allyl bromide (103 g, 0.85 mole) and 750 ml of dry acetone was refluxed overnight with stirring. The product was extracted with ether, and the extract washed successively with 5-percent NaOH and water. After evaporation of the solvent the compound was recrystallized from an ether-petroleum ether mixture; yield; 121 g (61%); mp 44 °C.

Anal: Calcd. for $C_{16}H_{14}O_3$: C, 75.6; H, 5.6. Found: C, 75.6; H, 5.7.

Behavior of Allyl 2-Benzoyloxyphenyl Ether on Claisen Rearrangement. Attempts were made to obtain 2-allyl-6-benzoyloxyphenol by Claisen rearrangement of allyl 2-benzoyloxyphenyl ether. The allyl ether (10 g, 0.04 mole) was refluxed at 180 to 200 °C in a nitrogen atmosphere for 30 min.

Separation of the reaction products yielded considerable quantities of starting materials, benzoic acid, and a phenol which distilled at 107 to 115 °C/7mm. The distillate (n_D^{26}=1.5588) crystallized on storage in a refrigerator; yield: 2.2 g (37%).

The phenol was identified as impure 1-allyl-2,3-dihydroxybenzene by (1) its infrared spectrum, which showed the presence of allyl and phenol groups and the absence of ester linkages, (2) a positive test for a catechol derivative [15], and (3) methylation with dimethyl sulfate and subsequent permanganate oxidation to 2,3-dimethoxybenzoic acid.

The authors thank Miss M. Kathryn Wharton, Applied Polymer Standards and Research Section for the infrared analyses, E. Deardorff of the Standards Reference Materials Section for the elementary analyses, R. J. Vanapeldoorn, Walter Reed Army Institute of Research for assistance in the gas chromatographic separation, and Dr. Harriet Frush for many valuable suggestions.

3. References

[1] H. I. Copeland, G. M. Brauer, W. T. Sweeney, and A. F. Forziati, J. Research NBS **55,** 133 (1955) RP2611.
[2] N. Hirao, Bull. Chem. Soc. Japan **11,** 179 (1936).
[3] C. Schöpf, E. Brass, E. Jacobi, E. Jorde, W. Mocnik, L. Neuroth, and W. Salzer, Ann. **544,** 30 (1940).
[4] M. Pal'gi, J. Gen. Chem. U.S.S.R. **28,** 2275 (1958).
[5] C. F. H. Allen and J. W. Gates, Org. Syntheses, Collective Vol. III, p. 418.
[6] H. E. Fierz-David and W. Kuster, Helv. Chim. Acta **22,** 82 (1939).
[7] B. D. Tiffany, J. Am. Chem. Soc. **70,** 592 (1948).
[8] Z. Budesinsky and E. Rockova, Chem. Listy **48,** 427 (1954).
[9] D. C. Shrewsberry, Spectrochim. Acta **16,** 1294 (1960).
[10] J. P. Lambooy, J. Am. Chem. Soc. **72,** 5327 (1950).
[11] L. J. Bellamy, Infra-red Spectra of Complex Molecules, 2d ed. (John Wiley & Sons, New York, N.Y., 1958).
[12] F. Mauther, J. Pract. Chem. **148,** 95 (1937).
[13] B. D. W. Luff, W. H. Perkin, Jr., and R. Robinson, J. Chem. Soc. **97,** 1138 (1910).
[14] R. E. Donadio, Master's thesis, University of Detroit, Detroit, Mich., June 1952, p. 13–14.
[15] F. Feigl, Spot Tests in Organic Analysis, 6th ed., p. 416 (Elsevier Publishing Co., New York, 1960).

(Paper 67A3-213)

JOURNAL OF RESEARCH of the National Bureau of Standards—A. Physics and Chemistry
Vol. 67A, No. 3, May–June 1963

Analysis of Families of Curves

John Mandel and Frank L. McCrackin

(January 2, 1963)

A systematic approach is presented for fitting empirical expressions to data depending on two variables. The problem can also be described as the simultaneous fitting of a family of curves depending on a parameter.

The proposed method reduces a surface fitting problem to that of fitting a few functions of one variable each. First, the surface is expressed in terms of these one-variable functions, and using an extension of two-way analysis of variance, the accuracy of this fit is assessed without having to determine, at this point, the nature of the one-variable functions. Then, the one-variable functions are fitted by customary curve-fitting procedures.

For illustration, the method is applied to two sets of experimental data.

1. Introduction

A frequently occurring situation in scientific work is one in which the relationship between two quantities is examined for a series of values of a third quantity. For example, in the thermodynamic studies of gases the pressure-volume relationship may be examined at various temperatures. The results of such experiments are often presented in terms of a one-parameter *family* of curves. Alternatively, one may describe the problem as the fitting of a surface in a space of three dimensions.

An analysis of a set of data (or curves) of this type follows one of two possible lines: either a model is postulated on the basis of physicochemical hypotheses, in which case the main purpose of the analysis is to verify the adequacy of this model, and possibly to estimate certain constants occurring in the model; or there exists no pertinent theory, in which case the problem consists in finding a satisfactory empirical representation of the data. Thus, in our example, one might postulate Van der Waals equation:

$$\left(p+\frac{a}{V^2}\right)(V-b)=RT \tag{1}$$

where p, V, and T represent pressure, volume, and temperature, R, the gas constant, and a and b two constants to be inferred from the data. The postulation of this equation would put the problem in the first category. On the other hand, the experimenter may desire to determine the form of the equation that best represents his data, without committing himself to any specific preconceived equation such as (1). In that case, which constitutes a problem of the second category, the choice of a suitable equation may present considerable difficulties. There exist few, if any, guidelines to assist one in the selection, and trial and error is the only way by which a particular equation is finally chosen. A widely used statistical procedure for fitting curves and surfaces is the method of least squares. Application of this method requires that some specific functional form be agreed upon *prior* to the fitting process. This process serves to estimate the unknown parameters and to evaluate the adequacy of the fit in terms of the smallness of the residuals. There is no assurance, by this method, that a much better fit might not be achieved by an entirely different functional form. Also, if the fit turns out to be inadequate, the method of least squares yields little, if any, information regarding the direction in which one ought to search for a more appropriate model.

In this paper, the empirical fitting of a family of curves is attacked in a systematic way. Mathematical expressions are used involving functions that depend each on one variable only. The nature of each of these functions is left entirely open in the initial fitting process, and the adequacy of the fit is judged without having to specify the nature of these functions. Thus, one need not estimate the values of any parameters before judging the success of the fit.

The specific examples presented in this paper are used only to illustrate the mathematical approach and not to propose alternative equation of state, either for rubber or for ethylene.

2. Generalized Model

For the sake of clarity, we shall discuss the problem first in terms of eq (1). Rewriting eq (1) as:

$$p=\left(\frac{-a}{V^2}\right)+\left(\frac{R}{V-b}\right)T \tag{2}$$

we see that for any particular value of V, it represents simply a linear relationship between p and T.

Thus, for any value of V, a plot can be made of p versus T, and a straight line fitted to the plotted points. If data are available for different values of V, this method will result in a collection of straight lines, one for each value of V. The slope of the straight line, corresponding to any given value of V, is $\frac{R}{V-b}$ and the intercept is $\frac{-a}{V^2}$. Thus, by studying the relationship between the experimentally determined slopes and the corresponding values of V, one can obtain an estimate of the parameter b. Similarly, from the intercepts an estimate of a can be obtained.

So far, no new technique of analysis has been introduced, and the procedure is entirely contingent on the linearity of p in terms of T. Note, however, that in fitting each straight line, no use has been made of the fact that the slope depends on V in accordance with the function $\frac{R}{V-b}$ or that the intercept is inversely proportional to V^2. It is only in the estimation of b and a that consideration has been given to these facts.

Suppose, now, that the experimenter is not committed to eq (2) as the only possible representation of his data, or that, in fact, he knows this equation to be unsatisfactory for that purpose. It is then possible to suggest an immediate generalization of eq (2), far less restrictive than this equation, that may be more adequate as a representation of the data.

We note that eq (2) belongs to the general class.

$$p=f(V)+g\ (V)h(T) \tag{3}$$

where f and g are two distinct functions of volume only, while h is a function of temperature only. Equation (3) is more general than eq (2) in that no assumptions are made regarding the form of the functions f, g, and h. For example, $h(T)$ may be a quadratic, or an exponential, or any other desired function of T. Nor is it necessary to assume that $f(V)$ and $g(V)$ obey the functional forms $\frac{-a}{V^2}$ and $\frac{R}{V-b}$ required by Van der Waal's equation. Any dependence of h on T and of f and g on V is admissible in the general formulation of eq (3).

We will adopt as our generalized model that represented by eq (3). First we describe a method for fitting the model represented by eq (3) and for evaluating the adequacy of the fit. Then we illustrate the usefulness of this model by applying it to two sets of experimental data.

3. Analysis of the Generalized Model

Let the data be in the form of a rectangular array, in which each row is associated with a particular value of V, and each column with a particular value of T. Each cell of the array then contains the value of pressure corresponding to the volume and temperature values represented by the row and column intersecting in that cell. Such an arrangement is shown in table 1.

TABLE 1. *Schematic of* p-V-T *data*

	Temperature			
Volume	T_1 T_2 . . . T_j . . . T_n			
V_1				
V_2				
.				
.				
.				
V_i	. . . . . $p_{V_iT_j}$			
.				
.				
V_m				
Average	$\bar{p}_{T_1}$	$\bar{p}_{T_j}$	$\bar{p}_{T_n}$	$\bar{\bar{p}}$

The main difficulty in fitting eq (3) lies in our ignorance of the function $h(T)$. Indeed, eq (3) expresses for any given value of V, a linear relation between p and $h(T)$. If $h(T)$ is known for each T, the straight line corresponding to each value of V can at once be plotted and the nature of the functions $f(V)$ and $g(V)$ can then be determined by studying the slopes and intercepts of the lines as functions of V. Let us note, however, that a similar analysis can be made as soon as we have a set of values linearly related to $h(T)$. For if a function $H(T)$ is defined by

$$H(T)=\alpha+\beta h(T) \tag{4}$$

eq (3) can be written

$$p=A(V)+B(V)H(T) \tag{5}$$

with

$$A(V)=f(V)-\frac{\alpha}{\beta}g(V) \tag{6a}$$

$$B(V)=\frac{g(V)}{\beta} \tag{6b}$$

Then eq (5) also represents, as does eq (3), a linear relationship between p and $H(T)$ for each value of V. If $H(T)$ is known, the functions $A(V)$ and $B(V)$ may then be determined from the linear fits of p versus $H(T)$, for different values of V. Now when $h(T)$ is unknown, there exist nevertheless many functions $H(T)$ the values of which can be inferred from the data for all T values represented in the table. One of these functions is given by the column averages $\bar{p}_T$ of table 1. This follows at once by averaging both members of eq (3) over all rows, for any given value of T:

$$\bar{p}_T=\bar{f}+\bar{g}h(T). \tag{7}$$

This function belongs indeed to the class of $H(T)$ defined by eq (4). For reasons of statistical convenience, a preferable choice is given by

$$C_T=\bar{p}_T-\bar{\bar{p}} \tag{8}$$

where $\bar{\bar{p}}$ is the grand average of all $\bar{p}_T$ values in the table. When $H(T)$ is selected to be C_T, as defined by eq (8), we will refer to the corresponding representation by eq (5) as the "standard form." Thus, the standard form is given by:

$$p=A_V+B_VC_T \tag{9}$$

where C_T is defined by (8) and:

$$A_V=f(V)-\frac{\bar{f}-\bar{\bar{p}}}{\bar{g}}\,g(V) \tag{10a}$$

$$B_V=\frac{g(V)}{\bar{g}} \tag{10b}$$

From (10b) it follows that the average of B_V over all rows is equal to unity. On the other hand, eq (8) shows that the average of the C_T over all columns is equal to zero. Thus:

$$\bar{B}=1 \text{ and } \bar{C}=0. \tag{11}$$

It is easily verified that these two conditions are necessary and sufficient for assuring that the representation is in the standard form. Therefore, a function of two variables, as represented in table 1, may be approximated, in the form of eq (9), by three single—variable functions. The function C_T of temperature is first computed from the column averages of table 1 by eq (8). A linear fit of each row of the table versus C_T then gives the values of the functions A_V and B_V as the intercepts and the slopes of the fitted lines.

An analytical formula for the function of two variables may now be obtained by fitting empirical formulas to the curves C_T versus T, A_V versus V, and B_V versus V.

4. Statistical Model

So far we have not considered errors of measurement. Let us now assume that the experiment has been conducted in such a way that V and T are controlled and p is a measurement subject to experimental error. Then eq (3) becomes:

$$p=f(V)+g(V)h(T)+\epsilon' \tag{3a}$$

where ϵ' is a random error of zero expectation. For greater generality, the first member in eq (3a) can be replaced by any suitable function of p. In work dealing with equations of state, such as pressure-volume-temperature relationships, it is customary to study the quantity pV. Replacing p by pV in the left-hand side of (3a) would visibly not change the functional nature of the right-hand side of this relation and it would generally result in greater homogeneity in the variance of the error term. Representing the measured quantity, or any appropriate function of it (as in this case pV) by $Z_{V,T}$, we have the general relation

$$Z_{V,T}=f(V)+g(V)h(T)+\epsilon \tag{12}$$

which can be written in the standard form:

$$Z_{V,T}=A_V+B_VC_T+\epsilon \tag{13}$$

where $\bar{B}=1$ and $\bar{C}=0$. Specifically, C_T is defined by

$$C_T=\bar{Z}_T-\bar{\bar{Z}} \tag{14}$$

where $\bar{Z}_T$ is the column average for column T and $\bar{\bar{Z}}$ the grand average in table 1, the cell entries of which are $Z_{V,T}$. In regard to the errors, ϵ, we will assume that they are normally and independently distributed constituting a sample from a normal population of zero mean, and variance equal to σ^2.

Under these assumptions, the values $Z_{V,T}$ and $\bar{Z}_T$ (from which the C_T are calculated) are no longer statistically independent, nor are $\bar{Z}_T$ and C_T independent. It has, however, been shown [1][1] that the following analysis is not invalidated by this circumstance.

5. Statistical Analysis

Denote by m the number of rows of table 1, and by n the number of its columns. For each row, a straight line is fitted to the set of points (Z, C) using the usual method of linear regression. This yields the estimates,

$$\hat{A}_V=\frac{\sum_T Z_{V,T}}{n} \tag{15}$$

$$\hat{B}_V=\frac{\sum_T Z_{V,T}C_T}{\sum_T C_T^2} \tag{16}$$

and an estimate of the variance about the regression line:

$$\hat{V}(\epsilon)=\frac{\sum_T[Z_{V,T}-(\hat{A}_V+\hat{B}_VC_T)]^2}{n-2}. \tag{17}$$

Since the variance of ϵ is assumed to be the same for all values of V, the m estimates given by eq (17) for the m values of V may be pooled. How this is to be done will be shown in the discussion on the analysis of variance. Note, however, that an inspection of the m values of $\hat{V}(\epsilon)$ is of considerable interest, especially for the detection of trends related to the magnitude of V. A pooled value is meaningful only in the absence of such trends.

From (17), or from a pooled value of $\hat{V}(\epsilon)$, estimates of the standard errors of $\hat{A}_V$ and $\hat{B}_V$ may be obtained by the usual formulas.

[1] Figures in brackets indicate the literature references at the end of this paper.

6. Case of Concurrence

Among the many possibilities for the structure of a family of curves, two special cases deserve particular attention. The first concerns a family of "parallel" curves. In this case, the straight lines resulting from the application of the method described in this paper will also be parallel. Their slopes are then independent of V and all equal to unity so that the model reduces to the "additive" type.

$$Z_{V,T}=A_V+C_T+\epsilon=A_V+\overline{Z}_T-\overline{\overline{Z}}+\epsilon. \tag{18}$$

The second special case is that in which all the curves of the family pass through a common point. We denote this situation as the "concurrent" case. When the curves are concurrent, then so are the straight lines resulting from our analysis. Now a necessary and sufficient condition for a collection of straight lines of the type

$$Z=f(V)+g(V)h(T) \tag{19}$$

to concur, is that a linear relation exist between $f(V)$ and $g(V)$. For if $h(T_0)$, Z_0 are the coordinates of the common point, the following identity must hold for all V;

$$Z_0=f(V)+g(V)h(T_0)$$

or

$$f(V)=Z_0-[h(T_0)]g(V). \tag{20}$$

This equation expresses a linear relation between $f(V)$ and $g(V)$, since Z_0 and $h(T_0)$ are numerical constants. Conversely, if this linear relation holds, then the entire set of straight lines passes through the point $[h(T_0), Z_0]$, and hence is concurrent.

The importance of the concurrent model is that in it, the algebraic expression of the structure of the family of curves becomes quite simple. Indeed, replacing in eq (19), the quantity $f(V)$ by its expression given by eq (20), we obtain

$$Z=[Z_0-h(T_0)g(V)]+g(V)h(T)$$

or

$$Z-Z_0=g(V)[h(T)-h(T_0)]. \tag{21}$$

Thus, in the case of concurrence, the measured quantity is essentially the product of two functions, the first involving V only, and the second only T.

We will show in the next section how the concurrence of a family of curves is revealed by the analysis of variance.

7. Analysis of Variance

The theoretical basis of the analysis of variance is discussed in reference [1]. The analysis is based on the standard form of the model, as given by eq (13), which can be rewritten as

$$Z_{V,T}=A_V+C_T+(B_V-1)C_T+\epsilon. \tag{22}$$

To each of the four terms in this expression corresponds a sum of squares, computed as indicated in table 2a.

TABLE 2a. *Analysis of variance*

Term in eq (22)	Degrees of freedom	Sum of squares	Mean square
A_V	$m-1$	$SS_A=n\Sigma_V\hat{A}^2_V$	$\frac{SS_A}{m-1}$
C_T	$n-1$	$SS_C=m\Sigma_T C^2_T$	$\frac{SS_C}{n-1}$
$(B_V-1)C_T$	$m-1$	$SS_{B\times C}=\Sigma_V(\hat{B}_V-1)^2\Sigma_T C^2_T$	$\frac{SS_{B\times C}}{m-1}$
	$(m-1)(n-2)$	$SS_\epsilon=\Sigma_V\Sigma_T[Z_{V,T}-(\hat{A}_V+\hat{B}C_T)]^2$	$\frac{SS_\epsilon}{(m-1)(n-2)}$

It is seen from table 2a that the usual interaction term is here partitioned into two parts, $(B_V-1)C_T$ and ϵ. Thus, only $(m-1)(n-2)$ degrees of freedom are available for random error, the remaining $(m-1)$ being allocated to the important "slope effect." The analysis thus provides an answer to the question of how the m estimates given by eq (17) are to be pooled: the total number of degrees of freedom for the pooled estimate is $(m-1)(n-2)$ (rather than $m(n-2)$, because of the correlation between the m separate estimates). The $m-1$ degrees of freedom corresponding to the term $(B_V-1)C_T$ provide a means for testing the "parallelism" of the family of curves. In the case of parallelism the mean square corresponding to the $(B_V-1)C_T$ term will not be significantly larger than the ϵ mean square and the model underlying the set of curves becomes the simple additive model of ordinary analysis of variance.

The existence of a point of concurrence is tested by a further partitioning of the interaction sum of squares. The test is based on the theorem proved in the preceding section that a necessary and sufficient condition of concurrence is the existence of an exact linear relation between $f(V)$ and $g(V)$. In view of eqs (10a) and (10b), this implies a linear relation between A_V and B_V. But then the correlation between these two quantities is unity. Consequently, the test for concurrence is carried out as follows. First, compute the correlation coefficient $r_{\hat{A},\hat{B}}$ between the quantities $\hat{A}_V$ and $\hat{B}_V$. Then partition the $(B_{V-1})C_T$ term as shown in table 2b. If the mean square for concurrence is significant with respect to that for nonconcurrence *and* the latter is comparable in magnitude to the ϵ mean square, there is good evidence that the family of curves pass through a common point. Of course, one can also plot the m points $(\hat{A}_V, \hat{B}_V)$; if an exact straight line (to within ϵ error) results, there is concurrence in the family of curves.

TABLE 2b. *Test for concurrence*

Term in eq (22)	Degrees of freedom	Sum of squares	Mean square
$(B_V-1)C_T$	$m-1$	$SS_{B\times C}$	$\frac{SS_{B\times C}}{m-1}$
Concurrence	1	$SS_{conc}=[SS_{B\times C}][r^2_{\hat{A},\hat{B}}]$	SS_{conc}
Nonconcurrence	$m-2$	$SS_{nonconc}=[SS_{B\times C}][1-r^2_{\hat{A},\hat{B}}]$	$\frac{SS_{nonconc}}{m-2}$

8. Further Generalization of the Model

Suppose that application of the proposed method to a particular one-parameter family of curves has been unsuccessful. In terms of eq (13), this would be shown by the failure to obtain straight-line relationships when $Z_{V,T}$ is plotted versus C_T, for particular values of V. A natural extension of the procedure is to try a model of the type

$$Z_{V,T}=A'_V+B'_VC_T+D_VC_T^2 \tag{23}$$

that is, to fit a quadratic, rather than a linear relation, to Z as a function of the column averages. If necessary, a polynomial of degree higher than two can be tried. Experience shows that the quadratic model represented by eq (23) may give very satisfactory results where the simpler linear model fails. For computational convenience, it is often advantageous to make the quadratic fit by the method of orthogonal polynomials in C_T, despite the fact that the C_T can, of course, not be expected to be equidistant. The relative advantage of using orthogonal polynomials increases with the number of rows in the table, since all rows are fitted versus a constant set of polynomials in C_T. For the quadratic model, the method of orthogonal polynomials yields the equation

$$Z_{V,T}=A_V+B_VC_T+D_V[Q(C_T)] \tag{24}$$

where A_V and B_V and C_T are identical with the corresponding quantities used in the linear fit, and $Q(C_T)$ is defined by:

$$Q(C_T)=C_T^2-\left(\frac{\sum_T C_T^3}{\sum_T C_T^2}\right)C_T-\left(\frac{\sum_T C_T^2}{n}\right) \tag{25}$$

where n is the number of values of T (number of columns). The estimate of D_V is given by

$$\hat{D}_V=\frac{\sum_T Z_{V,T}[Q(C_T)]}{\sum_T [Q(C_T)]^2}. \tag{26}$$

The improvement of the quadratic fit over the linear one can be assessed by the corresponding reduction in the sum of squares in the analysis of variance. Denoting the reduction in the sum of squares due to the quadratic term by SS_D, we have:

$$SS_D=(\sum_V \hat{D}_V^2)\sum_T [Q(C_T)]^2. \tag{27}$$

The corresponding number of degrees of freedom is $m-1$, where m represents the number of V values (number of rows).

9. Application to the Compression of Vulcanized Rubber

The data in table 3 are taken from a study of the compression of natural rubber-sulfur vulcanizates [3]. Tabulated are specific volume measurements for pressure values ranging from 1 to 10,000 atm over a temperature range extending from 20 to 80 °C. The analysis was made using the program for the IBM 7090 computer, to be described in the last section. The analysis of variance is shown in table 4. This analysis corresponds to a fit of the data by the empirical formula

$$V=A_p+B_pC_T+\epsilon \tag{28}$$

where V is the measured specific volume, A_p and B_p are two functions of pressure, and C_T is a function of temperature. The symbol ϵ represents an "error-term," including the effect of experimental error as well as that of any inadequacy of eq (28) to represent the data. It is seen that the standard deviation corresponding to this error term is 0.00094. Since the values of specific volume are all of the order of 0.85, the coefficient of variation of the error term is about 0.11 percent.

TABLE 3. *Specific volume of rubber*

Pressure	Temperature, °C				
	21.0	38.5	50.2	64.0	81.5
atm					
1	0.93397	0.94143	0.94826	0.95639	0.96667
1000	.91678	.92204	.92673	.93344	.94077
2000	.89941	.90189	.90464	.90953	.91360
3000	.88447	.88645	.88880	.89231	.89436
4000	.87214	.87336	.87572	.87864	.87937
5000	.86056	.86188	.86424	.86697	.86680
6000	.85038	.85134	.85410	.85654	.85636
7000	.84113	.84201	.84480	.84717	.84708
8000	.83263	.83345	.83608	.83828	.83828
9000	.82647	.82563	.82859	.82996	.83074
10000	.81834	.81829	.82129	.82249	.82360

TABLE 4. *Specific volume of rubber—analysis of variance*

Term in eq (28)[a]	Degrees of freedom	Sum of squares	Mean square
A_p	10	0.0878718	0.008787
C_T	4	.0009200	.000230
$(B_p-1)C_T$	10	.0004684	.000047
ϵ	30	.0000264	.00000088

[a] (Equation (28) may be written as follows:

$$V=A_p+C_T+(B_p-1)C_T+\epsilon.$$

The values of A_p, B_p, and C_T are listed in table 5. Their relation to pressure and temperature are shown in figures 1, 2, and 3. It is interesting to compare the results of this analysis with those of the conventional analysis of variance for a two-way table. In such an analysis, the effect of "slopes" would not have been separated from that of random interaction. Consequently, the trend shown in figure 2 would have been ignored; i.e., the curve in this figure would have been replaced by a horizontal straight line. The "error-term" would have been inflated by the trend of figure 2 and would have yielded a mean square of 12.37×10^{-6} (the pooled mean square for the last two terms in table 4) corresponding to a standard deviation of error of 0.0035, and a coefficient of variation of roughly 0.4 percent.

TABLE 5. *Specific volume of rubber—parameters*

Pressure	A_p	B_p	Temperature	C_T
1	0.9494	2.7737	21.0	−0.005370
1000	.9280	2.0484	38.5	−.003416
2000	.9058	1.2497	50.2	−.000191
3000	.8893	0.8905	64.0	+.003306
4000	.8758	.6899	81.5	+.005621
5000	.8641	.6149		
6000	.8537	.6020		
7000	.8444	.5986		
8000	.8357	.5658		
9000	.8283	.4576		
10000	.8208	.5167		

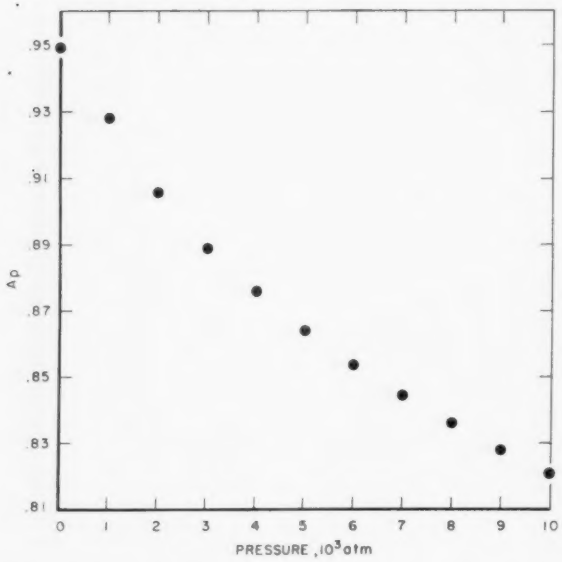

FIGURE 1. *Compression of vulcanized rubber, parameter* A.

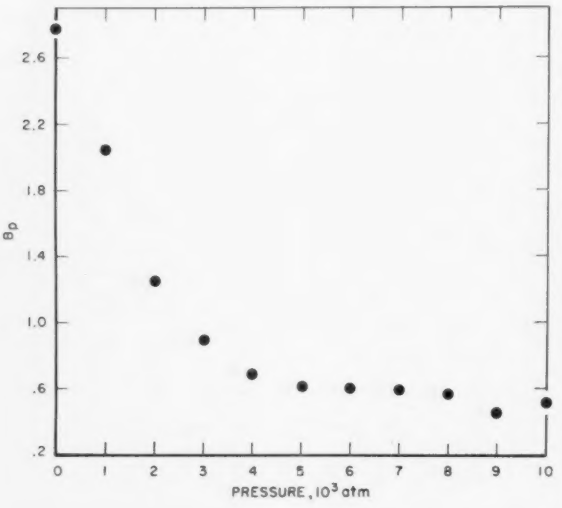

FIGURE 2. *Compression of vulcanized rubber, parameter* B.

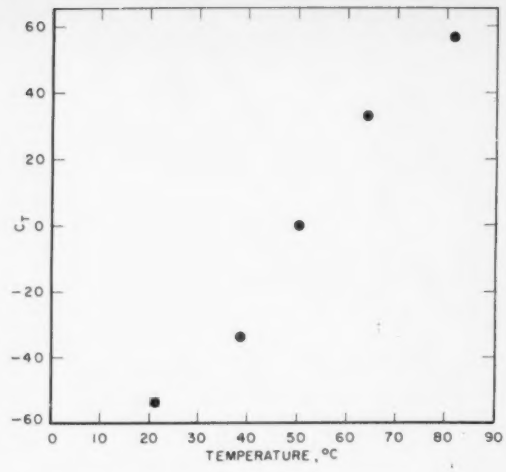

FIGURE 3. *Compression of vulcanized rubber, parameter* C.

By means of figures 1, 2, and 3, the effects of pressure and temperature on specific volume have been quantitatively separated. Figures 1 and 2 represent the effect of pressure; by fitting empirical curves to these graphs, isotherms can be obtained for each of the temperatures included in the study. Figure 3 represents the effect of temperature. It exhibits a possible discontinuity of slope which, if real, would be interpreted as a so-called "glass transition."

In the next section we will discuss another application, for which an analytic expression will be derived to represent the data.

10. Application to the Isotherms of Ethylene

The data for this illustration are taken from a published study of the isotherms of ethylene [2], for temperatures between 0 and 150 °C and pressures up to 3,000 atms. The data for 0 °C were incomplete. A complete rectangular array could be extracted from the data, covering 6 values of temperature (columns), and 40 values of density (rows). However, in order to demonstrate the capabilities of the proposed fitting process, only 13 densities were selected from this set. These data are shown in table 6; they were analyzed by the IBM 7090 program. An examination of the residuals revealed, however, a marked increase in variance with an increase in density. Therefore, the analysis was repeated, after "weighting" the rows, representing densities, by an appropriate factor. This "weighting by rows" is a simple procedure. Let

$$Z \equiv pV = A_d + B_d C_T + \epsilon_{d,T} \tag{29}$$

and let the variance of $\epsilon_{d,T}$ be given by

$$V(\epsilon_{d,T}) = \frac{K}{\omega_d}. \tag{30}$$

Then, multiplying eq (29) by $\sqrt{\omega_d}$ we have:

$$(\sqrt{\omega_d})(Z_{d,T})=(\sqrt{\omega_d}A_d)+(\sqrt{\omega_d}B_d)C_T+(\sqrt{\omega_d}\epsilon_{d,T}).$$

TABLE 6. *Equation of state for ethylene* [a]

Density	Temperature, °C					
	25	50	75	100	125	150
19.0407	0.97365	1.07743	1.18010	1.28137	1.38277	1.48309
47.875	.80607	0.92622	1.04361	1.15894	1.27309	1.38615
90.841	.60885	.75053	0.88775	1.02243	1.15528	1.28704
133.083	.47510	.63254	.78765	0.94127	1.09356	1.24486
186.001	.37578	.55506	.73693	.91911	1.10127	1.28330
205.88	.35635	.54767	.74293	.93895	1.13521	1.33117
238.60	.35108	.56984	.79304	1.01706	1.24101	1.46466
266.25	.38459	.63473	.88799	1.14112	1.39357	1.64500
291.80	.46332	.74881	1.03528	1.32004	1.60310	1.88420
315.34	.59374	.91664	1.23807	1.55592	1.87086	2.18230
375.30	1.31315	1.74911	2.17600	2.59290	3.00240	3.40630
415.87	2.2661	2.7896	3.2984	3.7906	4.2745	4.7487
437.03	2.9648	3.5354	4.0890	4.6228	5.1463	5.6596

[a] The tabulated value is pV.

Denoting $(\sqrt{\omega_d})(Z_{d,T})$ by $Z^*_{d,T}$ we obtain

$$Z^*_{d,T}=A^*_d+B^*_dC_T+\epsilon^*_{d,T} \tag{31}$$

where

$$A^*_d=\sqrt{\omega_d}A_d \tag{32a}$$

$$B^*_d=\sqrt{\omega_d}B_d \tag{32b}$$

and

$$V(\epsilon^*_{d,T})=\omega_d\frac{K}{\omega_d}=K. \tag{33}$$

Thus, eq (31) now represents a family of curves with constant error-variance; the C_T are redefined in terms of the $Z^*_{d,T}$ and A_d and B_d are computed from A^*_d and B^*_d using eqs (32).

In the present case, the weights ω_d were chosen in accordance with the relation

$$\sqrt{\omega_d}=\frac{1}{\hat{A}_d} \tag{34}$$

where A_d is of course simply the average of all pV values in the row corresponding to density d. It follows from this choice and eq (32a), that the estimate of A^*_d is equal to unity for all values of d.

Equation (31) was fitted to the data and gave a coefficient of variation of 0.3 percent. Since the data are believed to have a better precision than is indicated by this coefficient of variation, the fitting process was repeated, using the quadratic model:

$$Z^*_{d,T}=A^*_d+B^*_dC_T+D^*_d[Q(C_T)]+\epsilon^*_{d,T} \tag{35}$$

where $Q(C_T)$ is defined by eq (25) and D^*_d is estimated by a formula similar to eq (26). In terms of the unweighted data, the coefficient of the quadratic term is D_d, where

$$D^*_d=\sqrt{\omega_d}D_d. \tag{32c}$$

The analysis of variance is given in table 7. It should be noted that the latter is in terms of the weighted values, in accordance with eq (35). Thus, the residual variance is a measure of $V(\epsilon^*)$, not $V(\epsilon)$. Furthermore, because $A^*_d=1$ for all d, the mean square corresponding to this term is zero. From eqs (30) and (33) we infer that:

$$\sigma_{\epsilon^*}=\sqrt{\omega_d}\sigma_\epsilon$$

which, in view of eq (34) becomes

$$\sigma_{\epsilon^*}=\frac{\sigma_\epsilon}{\hat{A}_d}. \tag{36}$$

TABLE 7. *Equation of state for ethylene—analysis of variance*

Term in eq (35)	Degrees of freedom	Sum of squares	Mean square
A^*_d	12	0	0
C_T	5	7.53538	1.50708
$(B^*_d-1)C_T$	12	0.70968	0.05914
$D^*_d[Q(C_T)]$	12	.0004263	.0000355
ϵ^*	36	.0090178	.000000494
Residual error, using eq (31)	48	0.0094441	0.00000925

Thus, σ_{ϵ^*} is roughly equal to the coefficient of variation of pV. From the analysis of variance it is seen that this coefficient of variation is equal to approximately 0.3 percent using the simple model of the type of eq (13), and that it is reduced to about 0.07 percent when the more complicated model involving a term in C_T^2 is used. This model can be written

$$Z_{d,T}=A_d+B_dC_T+D_d[Q(C_T)]+\epsilon$$

or

$$Z_{d,T}=A'_d+B'_dC_T+D_dC_T^2+\epsilon. \tag{37}$$

The values of A'_d, B'_d, D_d and C_T resulting from the analysis are given in table 8.

The analysis could be terminated at this point. Using table 8 and eq (37), a value of $Z_{d,T}$ can be computed for any value of d and any value of T within the ranges of these variables covered by the data. This can be done by numerical interpolation carried out on the functions A'_d, B'_d, D_d, and C_T.

TABLE 8. *Equation of state for ethylene—parameters*

Density	A'	B'	D	Temperature	C
19.0407	1.229967	0.559646	-0.177346×10^{-2}	25	−0.457050
47.875	1.100321	.636773	-1.353445×10^{-2}	50	−.272819
90.841	0.954057	.744060	-2.150476×10^{-2}	75	−.089140
133.083	.863068	.845462	-0.591976×10^{-2}	100	.092803
186.001	.825883	.998293	2.786081×10^{-3}	125	.273447
205.88	.838570	1.072784	3.599158×10^{-3}	150	.452757
238.60	.902332	1.225498	3.916304×10^{-3}		
266.25	1.011673	1.386588	2.926550×10^{-3}		
291.80	1.174651	1.562422	1.179659×10^{-3}		
315.34	1.393917	1.746246	-1.032038×10^{-3}		
375.30	2.380897	2.298531	-7.853346×10^{-3}		
415.87	3.540819	2.724986	-13.286168×10^{-3}		
437.03	4.351878	2.957346	-16.109714×10^{-3}		

To obtain a complete empirical representation of the data, one further step is required. The quantities A'_d, B'_d, and D_d must be expressed as calculable functions of the density d, and C_T as a calculable function of the temperature T. This was done by fitting polynomial expressions to each of these functions, using the data in table 8. In particular, the quantity C_T was satisfactorily fitted by

$$C_T = c_0 + c_1 T + c_2 T^2.$$

A reduction in the overall number of coefficients is achieved by introducing the quantity

$$C''_T = \frac{C_T - c_0}{c_1} = T + \frac{c_2}{c_1} T^2. \tag{38}$$

Then, as can readily be verified, eq (37) can be written in the form

$$Z_{d,T} = A''_d + B''_d C''_T + D''_d (C''_T)^2 + \epsilon. \tag{39}$$

It was found that satisfactory fits were obtained by using a fourth-degree polynomial for D'' and fifth-degree polynomials for A'' and B''. The coefficients of the fitted polynomials are listed in table 9.

TABLE 9.—*Equation of state for ethylene coefficients of fitted polynomials*[a]

Degree of term in polynomial	A''	B''	D''	C''
0	1.03565	3.37538×10^{-3}	1.75818×10^{-6}	0
1	-9.33337×10^{-3}	4.59160×10^{-5}	-1.07282×10^{-7}	1
2	4.43017×10^{-5}	-3.05037×10^{-7}	1.13865×10^{-9}	-1.406662×10^{-4}
3	-1.23357×10^{-7}	9.77568×10^{-10}	-3.71113×10^{-12}	
4	8.03331×10^{-11}	-2.03756×10^{-12}	3.55256×10^{-15}	
5	2.71884×10^{-13}	-9.87817×10^{-16}		

[a] For A'', B'', and D'' the polynomials are in terms of the density d; for C'', the polynomial is in terms of the temperature T. The equation fitted to the data is $pV = A'' + B''C'' + D''(C'')^2$.

Using these functions, "calculated" values (denoted as $\hat{Z}_{d,T}$) are obtained for $Z_{d,T}$ according to the equation

$$\hat{Z}_{d,T} = \hat{A}''_d + \hat{B}''_d \hat{C}''_T + \hat{D}''_d (\hat{C}''_T)^2 \tag{40}$$

in which $\hat{A}''$, $\hat{B}''$, $\hat{D}''$, and $\hat{C}''$ are given by the polynomials whose coefficients are listed in table 9. Values of $\hat{Z}_{d,T}$ for the thirteen densities and six temperatures are given in table 10. A comparison of these values with those of table 6 shows that 90 percent of the fitted values agree with the observed data to within 0.5 percent or better, and that of the remaining ones, all but two agree to within 1 percent. The largest relative deviation is 1.23 percent.

The fitting procedure has therefore been very successful for these data. Since all the data are fitted by a single algebraic expression, interpolation for either pressures or temperatures not used in the fit should be accurate. To test this point, eq (40) was used for interpolation at densities not used in the fitting procedure. It may be recalled that the data used for the fit constituted a selection of 13 densities from a total available set of 40 densities. Values of pV were now calculated for all six temperatures and the following additional densities: 111.849, 153.349, 221.48, 245.75, 310.08, 355.43, and 456.85. This last value is outside the range covered by the fit and involves therefore an extrapolation process. The remaining six densities involve only interpolation. Thus, the fitted surface was tested for 42 individual values by interpolation or extrapolation. The results showed that for 35 of these 42 values, the difference "observed minus fitted" was less than 0.5 percent of the observed value. All but three of these differences were smaller than 1 percent of the observed values. The largest difference was equal to 1.21 percent of the observed value. Thus, the values obtained by interpolation are of the same order of precision as those directly fitted. This appears to be generally true for the procedure proposed in this paper, provided that the fits used for the single-variable functions A, B, C, and D are all of sufficient accuracy.

TABLE 10. *Equation of state for ethylene calculated values*

Density	Temperature, °C					
	25	50	75	100	125	150
19.0407	0.97650	1.07924	1.18138	1.28291	1.38382	1.48413
47.875	.80066	0.92173	1.04053	1.15710	1.27147	1.38367
90.841	.61040	.75035	0.88793	1.02317	1.15611	1.28676
133.083	.48047	.63589	.79020	0.94342	1.09554	1.24656
186.001	.37525	.55591	.73715	.91892	1.10118	1.28389
205.88	.35326	.54715	.74194	.93757	1.13401	1.33119
238.60	.34075	.56859	.79126	1.01471	1.23889	1.46376
266.25	.38248	.63477	.88716	1.13962	1.39210	1.64457
291.80	.46452	.75090	1.03614	1.32021	1.60311	1.88481
315.34	.59742	.92027	1.24037	1.55772	1.87233	2.18421
375.30	1.31369	1.74885	2.17557	2.59397	3.00415	3.40623
415.87	2.26312	2.78469	3.29348	3.78971	4.27354	4.74519
437.03	2.96876	3.53605	4.08850	4.62635	5.14983	5.65916

It is interesting to compare the results of this fit with the equally empirical fitting process used by Michels and Geldermans [2]. These authors fitted each isotherm individually, requiring a total of 42 coefficients for the six isotherms, as contrasted with the 18 coefficients (listed in table 9) required by the present procedure. The residuals obtained by Michels and Geldermans are somewhat smaller than those obtained by the present fit. On the other hand, the procedure used in this paper leads to a single algebraic expression to fit the entire surface. Differentiation is possible both with respect to density and temperature whereas Michels and Geldermans' fit does not allow for differentiation with respect to temperature.

11. Computer Program

A program has been written to fit data to the linear or quadratic models on the IBM 7090 computer. The program was written in Fortran. The original data, fitted parameters, residuals resulting from the fitting procedures, and analysis of variance are printed. Row or column weighting may be used.

Provision is also made for transforming the data, for combining rows or columns of the data, for applying specified corrections to individual data, for reversing rows and columns of the data, and for omitting specified rows and columns from the original set of data. The rows and columns of the data are identified by alphabetical or numerical labels so the output is easily interpreted without any coding.

12. Further Generalizations

Measurements dependent on two variables are not always given in the form of a complete two-way array, such as table 1. It is often possible, in such cases, to construct such a table by interpolation or curve fitting procedures carried out on subsets of the data within which one of the two variables is held constant.

The presentation in this paper has been in terms of one-parameter families of curves. The method can, however, be used for the analysis of families of curves involving more than one parameter. Applications of this type are now being made.

13. Summary

A systematic method has been presented for the empirical fitting of data depending on two variables. Essentially, the method reduces the fitting of surfaces to that of functions of single variables. In the basic model these single-variable functions are completely arbitrary, allowing for great flexibility in applying the method. The adequacy of the model can be evaluated without having to introduce algebraic expressions for the single-variable functions. To obtain a complete algebraic representation of the surface, it is then merely necessary to fit the single-variable functions by any appropriate method.

In certain cases it may be desirable to omit this last step, and still retain a workable model which will express the surface in terms of tabulated functions of single-variables. In that case, numerical interpolation methods must be applied to these tabulated values.

The first example used to illustrate the method deals with the effects of pressure and temperature on the specific volume of certain types of rubber. A quantitative separation of these effects was obtained in terms of tabulated values of three single-variable functions. The fit by means of these functions was within experimental error.

A second example concerned the equation of state of ethylene. The entire set of data was represented by a single algebraic expression and a good fit was obtained. Eighteen coefficients were required by this fit, as against 42 coefficients necessitated by the procedure commonly used for data of this type.

The statistical analysis required for the application of the proposed procedure is presented. In addition to providing estimates for the parameters of the model, the analysis allows for testing the significance of the pertinent effects.

Thanks are expressed to Miss Mary Nan Steel for her valuable assistance in conducting the programming and the computations on the electronic computer and for tabulation and graphing of the data.

The assistance of Charles Weir in supplying the compression data on rubber is also gratefully acknowledged.

14. References

[1] Mandel, John, Non-additivity in two-way analysis of variance, J. Am. Stat. Assoc. **56,** 878–888 (1961).

[2] Michels, A. and Gelderman, M. Isotherms of ethylene up to 3000 atmospheres between 0° and 150 °C, Physica **9,** 967–973 (1942).

[3] Weir, C. E., private communication.

(Paper 67A3–214)

JOURNAL OF RESEARCH of the National Bureau of Standards—A. Physics and Chemistry
Vol. 67A, No. 3, May–June 1963

A Controlled Atmosphere Chamber

Charles L. Gordon and Rolf B. Johannesen

(February 12, 1963)

An inert atmosphere chamber for the transfer of reactive materials is described. It has the advantages of being inexpensive, easily cleaned, and can be evacuated.

1. Introduction

Many chemical compounds must be kept under an inert atmosphere while being transferred or sampled. Descriptions of a number of different inert-atmosphere transfer chambers or so-called dry-boxes have been published. These can be classed in three types. The simplest is the inexpensive transfer chamber maintaining protection from the ordinary atmosphere by a continuous flow of an appropriate inert gas. Suitably equipped plastic bags [1, 2, 3, 4, 5],[1] a section of pipe [6], the open bell jar [7], a reaction vessel [8] and a refrigerator shell [9] are of this type.

A second type is the dry-box with a constantly maintained atmosphere [10, 11, 12, 13, 14] which may be regenerated and recirculated. These dry boxes are most elaborate and include electrical outlets and even gas cocks. They are not easily purged when some organic vapors are introduced. A device sometimes used to eliminate the long flushing time required is to expel the contaminated vapor in the chamber by an inflating balloon [11].

A third type can be evacuated so that repurification of the inert gas or long equilibration periods [15, 16] can be avoided.

The chamber described here is less expensive to build than many of those described in the literature cited or commercially available and has a greater versatility for small operations in the laboratory. It is of the evacuable type mentioned above. For the occasional transfer and bottling of various samples this type of chamber offers the least expensive method in which the atmosphere can be purged completely when vapors from one sample would contaminate the next material to be transferred.

Another advantage of the chamber described here is the ease with which the whole chamber or any portions of it can be disassembled and cleaned. The bell jar itself can be further protected against surface deposits by lining it with a removable plastic film [17].

2. Chamber

The chamber is illustrated in figure 1. It consists of two main parts, the commercially available plastic bell jar, A, which measures 16 in. inside diameter and 14 in. inside height, and the base plate, B, which is a 20 in. square brass plate ½ in. thick.

[1] Figures in brackets indicate the literature references at the end of this paper.

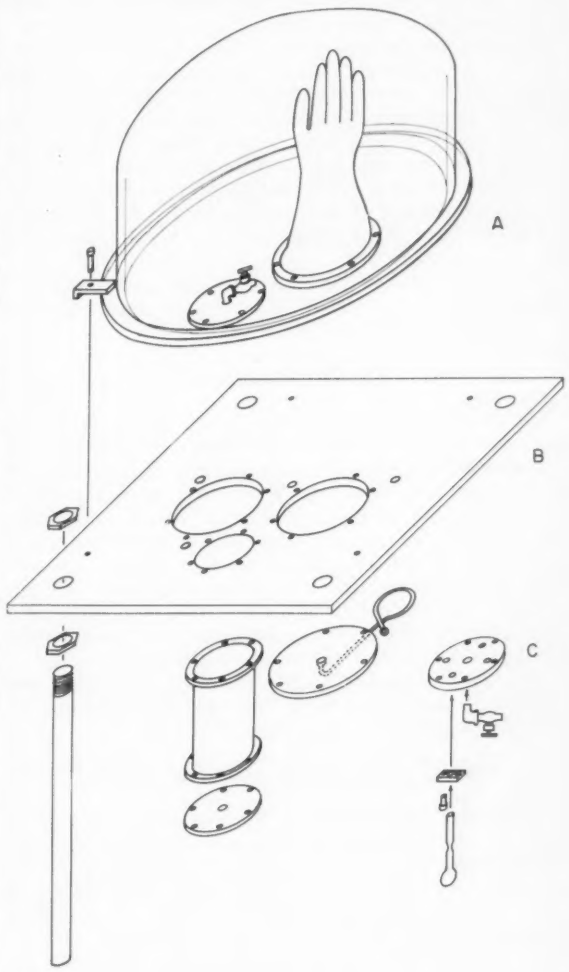

FIGURE 1. *Assembly of the inert atmosphere chamber.*

Parts which are duplicated are here shown only once.
A. Plastic bell jar.
B. Base plate.
C. Sampling attachment.

The base plate has several openings: two 5-in. diameter holes for the gloves, one 3-in. hole for an antechamber, and four holes threaded for ¼-in. pipe, each closed by a needle valve for control of evacuation and admission of the inert atmosphere. A design using the base plate in a vertical position with a shelf on it for a working area is more convenient. However, the sampling technique described later can not be used.

The base plate has four legs (18 in. long) attached at its corners, which hold it up sufficiently high above the table top that the operator's arms can be freely moved about under the chamber while his hands are inside the chamber. Also sufficient room is available for the introduction from below of equipment into the antechamber. All the flat metal-to-metal seals are gasketed by cutouts from a 1/16 in. neoprene sheet.

On both the top and bottom faces of the base plate, sets of six equally spaced, blind-tapped (¼–20) holes are provided, surrounding each of the glove openings and the ante-chamber opening. These tapped holes are for the ¼–20×½ Hex Socket Head Cap Screws used to fasten the glove retaining rings and the inside antechamber plate on the top of the base plate. The tapped holes on the underside are for fastening the glove port cover plates and the antechamber by the same means.

Neoprene gloves [18, 19] are clamped over the glove holes by means of ¼ in. thick brass rings of 6 in. outside, and 5 in. inside, diameter.

3. Atmosphere

For many uses oil-pumped helium, or argon, direct from the tanks is sufficiently inert. In our use for transferring samples of titanium salts, the gas needed to be purified further. Therefore, a tower filled with a mixture of glass beads and titanium trichloride in the lower half and a mixture of glass beads and potassium hydroxide pellets in the upper half was inserted in the gas line, the gas passing from bottom to top. This was followed by a trap packed loosely with glass wool which was immersed in liquid nitrogen (for final drying of helium or hydrogen, only).

For short periods the inert gas in the chamber can be maintained by a filled balloon [20] attached to the exit valve.

4. Operation of the Chamber

The gloves are folded on the top of the base plate and the antechamber plate is placed over the antechamber opening. Any apparatus which is to be needed and which can withstand evacuating is placed on the base plate and the bell jar is placed in position. The lids for the glove openings are secured in position under the base plate and are attached to the vacuum line. The antechamber with its outside lid is made fast to the bottom of the base plate. The whole apparatus and antechamber is evacuated, flushed once with dry helium, reevacuated and a flow of dry helium is then put through the chamber and allowed to escape through the antechamber to the air.

Small pieces of apparatus which cannot stand evacuation are introduced to the chamber through the antechamber, allowing the apparatus to remain in the antechamber sufficiently long to flush out all air. When using the antechamber in this way there is a distinct advantage in using a gas lighter than air so that the density difference is favorable for keeping air from entering the antechamber.

In some instances when hydrogen or helium is used and where the sweeping out of the residual air is not critical the gas can be admitted to the top of the bell jar by placing a bent tube on the gas inlet opening. Slow displacement of the air from the top of the chamber downward is thus accomplished.

5. Sampling Attachment and Technique

A disk 4¼ in. in diameter was made from ½ in. thick brass plate with six ¼ in. holes matching the set used to attach the antechamber. Four 10-mm holes and four small plates for clamping were made as indicated in the figure at C. The clamping gasket was made by carefully cutting small rectangles of neoprene sheet to match these rectangular clamping plates and cutting a hole in each slightly under 10-mm in diameter by means of a cork borer.

A stock of 10-mm tubing which would just pass through the 10-mm holes was obtained by selection from ordinary stock tubing. Pieces of this tubing about 8 in. in length were cleaned and a bulb with a breakable tip blown on one end. When positioned in the clamp, clamping gasket, and attachment plate, the seal of the tube to plate was made vacuum tight by tightening the clamp.

With the four hole plate as shown, four samples could be sealed off at a time. This can be done as follows: Four tubes marked at both ends are weighed and clamped in the plate with the open ends uppermost and projecting not more than ⅜ in. above the plate. The plate with its gasket is next attached to the base plate in place of the antechamber and the valve connected to the vacuum line. The inside antechamber plate with its gasket (and with its valve closed) is placed over the antechamber hole which now has the sample tubes projecting into it from below. The valve in the sample tube plate is opened and the sample tubes evacuated, after which the inert atmosphere is introduced by closing the valve to the vacuum and opening the inside antechamber plate valve. The inside plate is released and lifted away from the antechamber opening. The samples are then introduced into the tubes after which the pressure in the chamber is reduced and the sample tubes sealed off. The sample weight is obtained as the difference between the sum of the weights of the two parts of the sealed off tube and the original weight of the tube, all corrected for buoyancy.

A controlled atmosphere chamber constructed as described above has been used for about 6 years in these laboratories and has proved to be quite satisfactory in the handling of materials which are susceptible to contamination by moisture or oxygen.

Even such sensitive material as finely divided titanium trichloride has been handled without contamination. The ease of cleaning spilled materials and the rapidity with which the apparatus can be reassembled, as mentioned above, have enhanced the value in our day to day use.

6. References

[1] Webb, L. A., and Softky, S. D., Rev. Sci. Instr. **24,** 472–3 (1953).
[2] Clark, T. J., Conn, P. K., and Hein, R. E., Chemist-Analyst **44,** 55–6 (1955).
[3] Franklin, A. J., and Voltz, S. E., Anal. Chem. **27,** 865 (1955).
[4] Occone, L. R., and Simkin, J., J. Chem. Educ. **39,** 463 (1962).
[5] Shore, S. G., J. Chem. Educ. **39,** 465 (1962).
[6] Cassatt, W. A., Jr., and Meinke, W. W., Nucleonics **13,** No. 5, 63–4 (1955).
[7] Fiebig, E. C., Spencer, E. L., and McCoy, R. N., Anal. Chem. **29,** 861 (1957).
[8] Naff, M. B., Chemist-Analyst **50,** 54 (1961).
[9] Weyland, H. H., and Schwartz, D., J. Chem. Educ. **37,** 536 (1960).
[10] Tyree, S. Y., Jr., J. Chem. Educ. **31,** 603–5 (1954).
[11] Sherfey, J. M., Ind. Eng. Chem. **46,** 435–40 (1954).
[12] Kelman, L. R., Wilkinson, W. D., Shuck, A. B., and Goertz, R. C., Nucleonics **14,** No. 3, 61–5, No. 4, 65–71, and No. 5, 77–82 (1956).
[13] Gibb, T. R. P., Jr., Anal. Chem. **29,** 584–7 (1957).
[14] Johnson, R. E., J. Chem. Educ. **34,** 80–2 (1957).
[15] Ketchen, E. F., Trumbore, F. A., Wallace, W. E., and Craig, R. S., Rev. Sci. Instr. **20,** 524 (1949).
[16] Thomas, G. R., and Lichtin, N. N., Rev. Sci. Instr. **23,** 738–40 (1952).
[17] Nelson, P. R., Jr., and Slawek, J. E., Jr., Rev. Sci. Instr. **29,** 253 (1958).
[18] Rowan, J. H., Anal. Chem. **28,** 402–3 (1956).
[19] Norton, F. J., J. Appl. Phys. **28,** 34–9 (1957).
[20] Vanderwerf, C. A., Chemist-Analyst **43,** 107 (1954).

(Paper 67A3–215)

JOURNAL OF RESEARCH of the National Bureau of Standards—A. Physics and Chemistry
Vol. 67A, No. 3, May–June 1963

Publications of the National Bureau of Standards*

Selected Abstracts

The construction of calorimeters for the measurement of absorbed dose, B. Petree and G. Ward, *NBS Tech. Note 163 (November 1962), 25 cents.*
Direct measurements of energy locally absorbed in irradiated materials can be made with adiabatic calorimeters of suitable design. Design criteria imposed by requirements of accuracy include limitations on size and complexity. Small calorimeters of simple design with precision better than one percent at dose rates above one rad per second have been developed. Details of fabrication, auxiliary equipment and performance are described.

An atlas of whistlers and VLF emissions, A survey of VLF spectra from Boulder, Colorado, D. L. Jones, R. M. Gallet, J. M. Watts, D. N. Frazer, *NBS Tech. Note 166 (PB181454) (January 1963), $2.25.*
Naturally occurring VLF noises are classified and spectrograms illustrating each class are presented.
The report is divided into six sections. The first section consists of the systematic classification of VLF noises. Samples of whistlers are VLF emissions are shown in the second and third sections, respectively. The next section gives examples of interactions between these two classes. Section 5 consists of some exceptionally active periods during magnetic disturbances. The last section is a synoptic survey for the 4 months, March through June, 1957. A spectrogram is given for every observation period containing any VLF activity.
Most of the data was recorded at the Sunset Field Station of the National Bureau of Standards, Boulder, Colo., during 1956–57.
The above National Bureau of Standards Technical Note is available by purchase from the Office of Technical Services, U.S. Department of Commerce, Washington 25, D.C. (please order by PB number).

Growth rates of potassium crystal from the vapor phase, R. L. Parker, *J. Chem. Phys.* **37,** *NO. 8, 1600–1605 (Oct. 1962).*
Measurements of the growth rate of potassium (110) faces, for low vapor supersaturations σ between 3.1 and 0.11 (the lowest value studied) have given unit condensation coefficients for all supersaturations. This results is in agreement with the theory of Burton, Cabrera, and Frank, and gives the values $\beta Co=1$, $\sigma_1 \leq 0.046$ for potassium. No evidence of 2-dimensional surface nucleation was found. Careful attention to the reduction of impurities, through the use of ultrahigh vacuum techniques, was shown to be necessary in studying this system. Results of earlier work by Hock and Neumann on potassium can be well described by an application of the Cabrera-Vermilyea theory of impurity effects, with an effective partial pressure of active gases of 1×10^{-11} mm Hg. In the present experiments this value is less than 3×10^{-13} mm Hg. The unit condensation coefficients are shown to be in disagreement with a theoretical prediction of Hirth and Pound.

The NBS photoelectric pyrometer of 1961, R. D. Lee, *Book Temperature, Its Measurement and Control in Science and Industry* **3,** *Pt. 1, 507–151 (Reinhold Publ. Corp., New, N.Y., 1962).*
A photoelectric pyrometer is described which differs from a visual optical pyrometer mainly in that radiance matches are detected photoelectrically instead of visually. Its precision for a radiance temperature measurement at 1063 °C is 0.02 deg C or less (sample standard deviation), accomplished with a spectral passband, centered on 6530 A, that has a width at half-height of 110A. The instrument is undergoing test for accuracy and stability preparatory to calibration in accordance with the International Practical Temperature Scale above 1063 °C. The investigation to date has uncovered possible inaccuracies of 0.1 to 0.2 deg C related to the size of the source used. The origin is still not known. However, the radiance match is correctable, if different sized sources are to be used in the primary calibration and subsequent temperature measurements without resorting to direct measurements of the area of the sources. Stability experiments with four aged pyrometer lamps with a constant current comparable to a radiance temperature of 1063 °C showed the most stable lamp to change by 0.3 deg C in 700 hours and the least stable to change by 0.5 deg C in 150 hours. The magnitude of these instabilities is unexpected and is being investigated further.

Heat transfer in intensively outgassed powders, R. C. Little, F. G. Carpenter, and V. R. Deitz, *J. Chem. Phys.* **37,** *No. 8, 1896–1898 (Oct. 15, 1962).*
Cooling curves were determined for powders intensively outgassed at 600° and then immersed in liquid oxygen. The behavior of these indicated a much slower thermal transport than has been reported. The cooling rate increased sharply when an adsorbing gas (A, Kr, N_2) was introduced to the evacuated powder. The greatest change in cooling rate was observed when the added gas resulted in steady-state fractional coverage in the range between 0.01 and 0.06. The great enchancement of heat transfer by small amounts of added gas indicated a significant contribution to heat transfer by surface transport in a mobile adsorbed gas film.

Rates of thermal degradation of organic polymers, S. L. Madorsky, *SPE J.* **18,** *No. 12, 1482–1490 (Dec. 1962).*
The use of plastics in modern industry, particularly in space technology and at temperatures far above the ordinary, makes it imperative to have an understanding of the chemistry and kinetics of their thermal degradation. The chemical phase of this problem has been treated in an earlier article in the SPE Journal. In this article, the kinetics phase is discussed primarily from the angle of rates, activation energies, and order of the reactions involved.

Vacuum ultraviolet photochemistry. V. Photolysis of isobutane, H. Okabe and D. A. Becker, *J. Am. Chem. Soc.* **84,** *No. 21, 4004–4007 (1962).*
The photolysis of isobutane was carried out at room temperature at 1470 Å and 1236 Å. Certain specifically labeled deuterium compounds were used to gain information on the mechanisms of product formation. From isotopic analysis of products, hydrogen, methane and ethane, in the photolysis of an equimolar mixture of isobutane+isobutane-d_{10} the following conclusions were drawn.
(1) Hydrogen is formed both from atomic and molecular processes. The atomic process becomes more important at the shorter wavelength (1236 Å). From scavenger experiments, it was found that approximately half the hydrogen is formed by the atomic process at 1470 Å. (2) Methane is predominantly formed by a molecular process at 1470 Å and 1236 A. (3) Ethane is formed primarily by the combination of methyl radicals. From the photolysis of isobutane-a-d, it was concluded that (a) there is no apparent preference of the position (primary or tertiary) for the expulsion of atomic hydrogen at 1470 A. However there is some discrimination with regard to position for the hydrogen produced by molecular elimination. (b) The primary and tertiary hydrogen participate almost equally in the intramolecular production of methane. Reactions responsible for the formation of other products, ethylene, propane, propylene, isobutene, neopentane, and isopentane, are discussed.

Traces of products of angular momentum matrices. II. Sperical basis, E. Ambler, J. C. Eisenstein, and J. F. Schooley, *J. Math. Phys.* **3,** *No. 4, 760–771 (July–Aug. 1962).*

Closed formulas are given for Tr $J_\alpha{}^p J_\beta{}^q J_\gamma{}^r$ . . . where α β, γ . . . are equal to $+1$,0 or -1, and p, q, r are non-negative integers for which $p+q+r+ \ldots \leq 9$. The procedures used in evaulating the traces are described. In order to facilitate numerical evaluation from existing tables, simple relationships are given between traces in the spherical basis and traces in the Cartesian basis. The use of these tables for evaluating expectation values of certain operators is discussed in relation to other methods based on the coupling and recoupling theory of angular momentum.

A study of stability of high temperature platinum resistance thermometers, J. P. Evans and G. W. Burns, Book, *Temperature, Its Measurement and Control in Science and Industry* **3,** *Pt. 1, 313–318 (Reinhold Publ. Corp., New York, N.Y., 1962).*
The National Bureau of Standards is studying the performance of platinum resistance thermometers in the range 630.5° to 1063 °C. A number of thermometers with temperature sensing resistors of several designs, various protecting tube materials, and two types of platinum wire have been constructed. Thermometer stability was tested by heating the thermometers for long times at high temperatures and periodically determining the thermometer resistance at 100° and 0 °C. The constancy of the ratio of these resistances, R_{100}/R_0, is taken as an indicator of thermometer stability. It is shown that stable thermometers can be made. The stability of the thermometers is found to be affected by the rate of cooling from high temperatures. This cooling rate effect is explained by the quenching-in of point defects in platinum.

The present state of atomic spectra, C. M. Moore-Sitterly, *Japan Anal.* **11,** *No. 11, 1199–1202 (1962).*
Summary of lecture given on September 5, 1962, at the University of Tokyo to the Spectroscopical Society of Japan

Correlation factors for impurity diffusion—fcc lattice, J. R. Manning, *Phys. Rev.* **128,** *No. 5, 2169–2174 (Dec. 1962).*
The correlation factor f for an isolated impurity atom diffusing by a vacancy mechanism in a face-centered cubic lattice is calculated in terms of five vacancy jump frequencies near the impurity, w_0, w_1, w_2, k_1, and k_2, as defined by Lidiard (Phil. Mag. **46,** 1218 (1955)). In general, the correlation factor can be expressed as $f=(2w_1+7Fk_1)/(2w_2+2w_1+7Fk_1)$, where F is a function of k_2/w_0. In the limit where $k_2/w_0 \to 0$, F goes to unity. In the limit where $k_2/w_0 \to \infty$, F goes to 2/7. When the five frequencies above are the only vacancy jump frequencies in the crystal, an expression for F as a function of k_2/w_0 can be found from a Bardeen-Herring calculation. It is found that

$$F=1-\frac{S}{7}\left\{\frac{11.56+50.10\Delta+40.00\Delta^2}{10.521+4.69\Delta+12.06\Delta^2+8.00\Delta^3}\right\},$$

where $S=k_2/12w_0$ and $\Delta=(k_2-w_0)/12w_0$. This method can be extended to other lattices. Applications to data in the literature are discussed.

Experimental proof of the absence of equilibrium in a helium arc, A. T. Hattenburg and H. J. Kostkowski, *Book, Temperature, Its Measurement and Control in Science and Industry* **3,** *Pt. 1, 587–592 (Reinhold Publ. Corp., New York, N.Y., 1962).*
An atmospheric pressure helium arc containing 6×10^{15} electrons per cubic centimeter on its axis was investigated by spectroscopic methods to determine the extent of local thermodynamic equilibrium. Relative intensity measurements of a number of singlet and triplet neutral helium lines did not indicate the absence of equilibrium. However, the radial increase of the temperature determined from the absolute intensity measurement of the 5016A helium line, combined with the radial decrease of temperature obtained from electron density determinations and the Saha equation, did establish the lack of local thermodynamic equilibrium in this source.

Dissociation constant of t-butylammonium ion and related thermodynamic quantities from 5 to 35°, H. B. Hetzer, R. A. Robinson, and R. G. Bates, *J. Phys. Chem.* **66,** *2696 (1962).*
The acidic dissociation constant of *t*-butylammonium ion has been determined from 5° to 35° by e.m.f. measurements of hydrogen-silver bromide cells without liquid junction. At 25°, $-\log K_{bk}=10.685$, and the temperature coefficient of the dissociation constant gives the values $\Delta H^\circ=60{,}070$ *j* mole^{-1} and $\Delta S^\circ=-3.1$ *j* mole^{-1} deg.$^{-1}$. These thermodynamic constants are compared with the corresponding values for the acidic dissociation of the protonated forms of the aminoalcohols related structurally to *t*-butylamine.

Measurement of electron density and temperature in dense plasmas by application of line broadening theory, J. B. Schumaker, Jr., and W. L. Wiese, *Book, Temperature, Its Measurement and Control in Science and Industry* **3,** *Pt. 1, 575–579 (Reinhold Publ. Corp., New York, N.Y., 1962).*
The electron density and temperature in arc plasmas have been determined by the deliberate introduction of a trace of hydrogen as a thermometer. The electron density is obtained by spectrophotometric measurement of the line profile of one of the Balmer lines and comparison with the theoretical profiles recently calculated by Griem, Kolb, and Shen. The temperature is then calculated from the electron density using the usual equilibrium equations of statistical mechanics for reacting gases.

Germanium vacuum ultraviolet Ritz standards, V. Kaufman and K. L. Andrew, *J. Opt. Soc. Am.* **52,** *No. 11, 1223–1237 (Nov. 1962).*
The number of germanium Ritz standards below 2000Å has now been increased to approximately 100 lines with estimated uncertainties not exceeding 0.0008Å, 68 of which have estimated uncertainties of 0.0003Å. This extension is the end product of a systematic Fabry-Perot interferometric investigation which has extended the former interferometric region of 2019Å–4685Å to 12069Å. Ninety-five interferometrically determined levels of Ge I are given, 72 of which have been improved by this effort.
Twenty-three lines of Ge II were also measured interferometrically, leading to a few improved energy levels of this spectrum and to estimated splittings of the $ng^2G(n-5,6,7)$ terms. An improved Series Limit of Ge II calculated from the $4f^2F-ng^2G$ series is 128535.8 cm^{-1}.

Vapor phase growth kinetics of Hg and K whiskers by field emission, R. L. Parker and S. C. Hardy, *J. Chem. Phys.* **37,** *No. 8, 1606–1609 (Oct. 1962).*
Using the method originated by Gomer, we have studied the growth kinetics of mercury and of potassium whiskers, as they grow from the vapor phase in an electron field emission tube. To the best of our knowledge, the work on potassium represents the first use of an alkali metal as a field emitter. Most of our results on mercury whiskers agree with those obtained earlier by Gomer, including the positive exponential length growth (110), orientation, attainment of terminal lengths, and the surface diffusion coefficients; there are some differences, however.
The results for potassium whiskers show some features similar to those found for mercury, and some new features. The former include positive exponential growth, and the attainment of therminal lengths. New features include the absence, usually, of symmetric emission patterns; a very low activation energy for surface self-diffusion; the fact that the whiskers cannot be pulled off but instead appear to shorten gradually if the field is raised; and finally, an interesting sensitivity of the growth processes to illumination of the whiskers with visible light.

The determination of absolute temperatures from sound velocity measurements, G. Cataland, M. H. Edlow, and H. H. Plumb, *Book, Temperature, Its Measurement and Control in Science and Industry* **3,** *Pt. 1, 129–132 (Reinhold Publ. Corp., New York, N.Y., 1962).*
Absolute temperatures were derived from determinations of the velocity of sound in a gas and the acoustical interferometer was used for the velocity measurements. For an ideal gas, the velocity of sound is directly proportional to the square root of the absolute temperature: in the case of a real gas, corrections must be made which involve virial coefficients of the gas in a pressure expansion. Since these corrections are

a function of pressure, it is desirable that velocity measurements for absolute temperature determinations be conducted at the lowest practical pressures (the real gas approaches the state of an ideal gas).
An acoustical interferometer has been constructed at the National Bureau of Standards and has been used, with helium gas as a thermometric material, to determine absolute temperatures at 4.2 °K. When temperatures thus derived are compared with absolute temperatures associated with liquid helium vapor pressures, the difference between the two temperatures is 10 millidegrees. While this result is of a preliminary nature, it does justify continued investigations for determining absolute temperatures by sonic methods.

The role of temperature in our measuring system, A. G. McNish, *Book, Temperature, Its Measurement and Control in Science and Industry* **3,** *Pt. 1, 129–132 (Reinhold Publ. Corp., New York, N.Y., 1962).*
Temperature is taken, together with length, mass, and time, as one of the completely independent quantities which form the basis of our measuring system. This is noteworthy in that temperature is an intensive quantity while the other three are extensive quantities. The unit of temperature, like the units of length, mass, and time, is independent of all units of the system, being like them, embodied in its proper standard It is possible to construct a system in which temperature is not regarded as an independent quantity but one expressible in terms of length, mass, and time. However, in such a system the unit of temperature could not be realized with anything like the accuracy required for good measurements. This is because the relationship between temperature and length, mass, and time has not yet been measured with an accuracy approaching that with which each of these quantities itself can be measured. Specifically, the gas constant has never been very accurately determined.
The present practice of regarding temperature as an independent quantity affords a procedure for the most accurate measurement of temperature.

Microwave Doppler measurements of the ionization front in cylindrical shock waves from exploding wires, D. L. Jones and R. M. Gallet. *Exploding Wires* **2,** *127–144 (1962).*
Strong cylindrical shock waves from exploding wires have been measured by microwave Doppler techniques. The results obtained simultaneously on two or three independent frequencies are in very good agreement and show that the ionization front is well defined. The Taylor-Lin similarity blast wave theory for the shock wave propagation is well verified over distances up to 6 or 7 centimeters under the present conditions. Systematic results for the determination of shock wave energy and the efficiency for shock production in air over a range of pressures, wire diameters, and stored electrical energy are presented. Relative to optical methods used in the same problem the present technique is more sensitive and perhaps more precise.
It is remarkable that very good reflections are still consistently obtained when the shock Mach falls below 3 in air. From the calculated temperature and ionization in the shock front, the expected electron density should then be negligible. This effect is probably a result of the preexcitation of the gas ahead of the shock front, caused by ultraviolet radiation from the wire explosion or from the advancing shock front itself. There is also a relatively weak precursor ionization, for which recent microwave absorbtion measurements have indicated electron densities of the order of 10^{12} cm^{-3} several centimeters ahead of the front. The good reflection at low Mach numbers permits one to show that the similarity theory is still valid until Mach number 4 or below, and permits one also to record the departure form this relation at larger radii.

Temperature dependence of elastic constants of vitreous silica, S. Spinner, *J. Am. Ceram. Soc.* **45,** *No. 8, 394 (Aug. 1962).*
The relation between the elastic moduli and temperature from room temperature to about 1300 °C was determined for a group of vitreous silica specimens by a dynamic resonance method. All the curves were approximately parabolic in shape, reaching a maximum around 1050 to 1200 °C. At the maximum value, Young's modulus was more than 11 percent higher and the shear modulus about 9 percent higher than their room temperature values. Poisson's ratio was then computed to rise from about one-sixth at room temperature to about one-fifth at the temperature of maximum elastic modulus. Small but significant differences were observed in the temperature-modulus curves for specimens from different manufacturers.

Comments on the limits to the refractive index at ground level as a radio-meteorological parameter, B. R. Bean and G. D. Thayer, Proc. *IRE* **48,** *No. 8, 1498–1501 (Aug. 1960).*
A summary discussion on the use of net rate processes and the equivalent 2-level atom in non-LTE computations.

Rate of spherulitic crystallization with chain folds in polychlorotrifluoroethylene, J. D. Hoffman and J. J. Weeks, *J. Chem. Phys.* **37,** *No. 8, 1723–1741 (Oct. 1962).*
Parameters related to the recently proposed "kinetic" viewpoint of homogeneous nucleation and growth of lamellar polymer crystals with chain folds are obtained. The nucleation constant K_g is analyzed to obtain $\sigma\sigma_e = 184$ erg^2/cm^4 (σ=lateral surface free energy, σ_e=end (chain folded) surface free energy). A similar value of $\sigma\sigma_e$ is obtained form bulk crystallization studies. The homogeneous nucleation process was identified at $\Delta T_h = 70$ °C, and a value of $\sigma^2\sigma_e = 950$ erg^3/cm^6 calculated from K_g in $I = (NkT/h)\exp(-\Delta F^*)\exp[-K_g/T^2(\Delta T)^2]$. Combination of $\sigma^2\sigma_e$ and $\sigma\sigma_e$ gives $\sigma = 5.2$ erg/cm^2 and $\sigma_e = 36$ erg/cm^2, the latter corresponding to a work on chain folding, q, of 3.9 kcal/mole of folds. A value of $\sigma = 5.1$ erg/cm^2 is obtained independently using an empirical method. Further, an independent estimate of $\sigma_e = 35 \pm 7$ erg/cm^2 is obtained for PCTFE from lamellar thickness studies, after accounting for the increase of thickness that occurs sebsequent to initial growth using melting point data. The overall role of q in homogeneous nucleation and growth in linear polymers is discussed using PCTFE and polyethylene as examples. The "kinetic" chain fold theory gives a consistent picture of surface free energies, rates of homogeneous nucleation and growth, melting behavior, variation of initial step height with temperature, and formation of chain-folded lamellae.

An experimental investigation of overall heat transfer coefficients for condensing and boiling hydrogen films, K. D. Timmerhaus, D. E. Drayer, and J. W. Dean, *Intern. Develop. Heat Transfer (ASME)* **2,** *270–278 (1961).*
Overall heat rransfer coefficients for condensing and boiling hydrogen films have been determined for temperature gradients ranging from 0.38° to 6.0 °F for a single smooth vertical brass tube. Temperature difference between the condensing and boiling films was regulated and observed by changes in vapor pressure. Overall heat transfer coefficients under these experimental conditions are plotted not only as a function of the temperature difference but also of the heat flux and are compared as far as possible with known values in the literature. Further investigations are being made to evaluate the individual heat transfer coefficients and the effect of surface conditions on the overall heat transfer coefficient.

The photolysis and radiolysis of $CH_3N_2CH_3$ and $CH_3N_2CH_3$-$CD_3H_2CD_3$ mixtures, R. E. Rebbert and P. Ausloos, *J. Phys. Chem.* **66,** *No. 11, 2253–2258 (Nov. 1962).*
Azomethane has been photolyzed in the solid, liquid, and gaseous phases. In the gas phase photolysis, evidence has been obtained for the formation of ethane by a molecular elimination from azomethane. The quantum yield of the formation of nitrogen in the liquid phase is lower than unity and decreases with decrease in temperature, benzene quenches and 2,3-dimethylbutane enhances the decomposition yield. The effect of collisional deactivation, molecular elimination and free radical recombination in the cage on the total yield of ethane is discussed.
Radiolysis experiments on mixtures of $CH_3N_2CH_3$-$CD_3N_2CD_3$ were performed in the liquid and solid phases. The results indicate that ethane is mainly formed by cage and intercage recombination in the γ-ray spur. A decrease in temperature and addition of solvents has a reducing effect on the relative yield of CH_3CD_3. Evidence for energy transfer from benzene to azomethane was obtained.

A molecular-orbital study of the geometry of HO_2, M. E.

Boyd, *J. Chem. Phys.* **37,** *No. 6, 1317–1325 (Sept. 1962).*
Determination of the energy of HO_2 as a function of the HO_1O_2 angle for fixed values of $R(H\text{-}O_1)$ and $R(H\text{-}O_2)$ have been carried out using LCAO–MO–SCF calculations on closed shell ions. All one-electron and one and two center two-electron integrals used were evaluated accurately while three center integrals were approximated. An isosceles triangle configuration is favored by these calculations and gives a value of the ionization potential of 9.5 e.v. and dissociation energy of 4.4 e.v., consonant with experimental results.
Approximation by means of ionic calculations used here is shown to be valid for the purposes of this discussion.

Isotope effect in the recrystallization of D-mannose-1-*t* phenylhydrazone, F. Weygand, H. Simon, K. D. Keil, H. S. Isbell, and L. T. Sniegoski, *Anal. Chem.* **34,** *1753–1755 (Dec. 1962).*
An isotope effect previously reported in the recrystallization of D-mannose-1-*t* phenylhydrazone has been reinvestigated and confirmed. The ratio of the rate of crystallization of the isotopic to that of the nonisotopic form (k*/k) was found to be 0.88.

Reaction of methyl-d_3 radicals with isobutane, isobutane-2-*d* and propane, W. M. Jackson, J. R. McNesby, and B. deB Darwent, *J. Chem. Phys.* **37,** *No. 8, 1610–1615 (Oct. 1962).*
The relative rates of abstraction by CD_3 radicals of primary, secondary, and tertiary H atoms have been measured. Using a standard rate constant for abstraction of D from acetone-d_6, the following rate constants are obtained.

			k(mole^{-1} cc sec^{-1})
(2)	$CD_3+CD_3COCD_3$	$CD_4+CD_2COCD_3$	$3.5\times10^{10}\,T^{1}_{2}\exp(-11{,}100/RT)$
(3)	$CD_3+(CH_3)_3CD$	$CD_4+(CH_3)_3C$	$0.88\times10^{10}\,T^{1}_{2}\exp(-9200/RT)$
(4)	$CD_3+(CH_3)_3CD$	$CD_3H+CH_2CD(CH_3)_2$	$4.38\times10^{10}\,T^{1}_{2}\exp(-11{,}100/RT)$
(10)	$CD_3+(CH_3)_3CH$	$CD_3H+(CH_3)_3C$	$0.70\times10^{10}\,T^{1}_{2}\exp(-7600/RT)$

Isotope effects obtained are, for secondary H and D in propane:

$$k_H/k_D = 1.04 \exp(1400/RT),$$

and for tertiary H and D in isobutane:

$$k_H/k_D = 0.80 \exp(1600/RT)$$

These isotope effects are within experimental error of that given by the general expression for the deuterium isotope effect previously proposed

$$k_H/k_D = \exp(1500/RT)$$

and are in excellent correspondence with the theorectical treatment of Johnston and Rapp.

Theory and methods of optical pyrometry, H. J. Kostkowski and R. D. Lee, *Book, Temperature, Its Measurement and Control in Science and Industry* **3,** *Pt. 1, 449–481 (Reinhold Publ. Corp., New York, N.Y., 1962).*
A detailed review of the theoretical methods of optical pyrometry and the application of these methods at the National Bureau of Standards in realizing and dispersing the International Practical Temperature Scale above 1063 °C is presented. In the theoretical presentation, the concepts of effective and mean effective wavelengths are introduced, and various equations relating these parameters to each other and other physical quantities are derived. The important features of precision visual optical pyrometers are discussed and a number of blackbody sources and tungsten strip lamps described. Detailed experimental procedures and results of of primary and secondary calibrations of optical pyrometers at NBS are given. Finally, recommendations for achieving high precision and accuracy and the fundamental limitations in visual optical pyrometry are presented.

Measurement of effective temperatures of microwave noise sources, J. S. Wells, W. C. Daywitt, and C. K. S. Miller, *IRE Intern. Conv. Record, Pt. 3, 220–238 (1962).*
This report describes a system now in operation for the purpose of calibrating microwave noise sources at three selected frequencies in the range 8.2 to 12.4 Gc. Included are a discussion of the reference standard noise source, an error analysis of the standard source and the comparison system, and evidence of system performance. Results of measurements indicate that the excess noise ratio of a specific commercial argon filled noise source is 15.6 db at 9.8 Gc.

The calibration of temperature standards on the international practical temperature scale of 1948, J. P. Evans, *Proc. 17th Ann. Instrument.—Automation Conf. Exhibit, Instr. Soc. Am. Preprint No. 21–1–62 (New York, N.Y., Oct. 1962).*
The International Practical Temperature Scale of 1948 is maintained in this country by the National Bureau of Standards. This paper describes techniques used at NBS to calibrate temperature measuring devices on the scale and methods of transferring the scale to industrial temperature standards.

The structure of lithium dipotassium trimetaphosphate monohydrate, E. D. Eanes and H. M. Ondik, *Acta Cryst.* **15,** *Pt. 12, 1280–1285 (Dec. 1962).*
$LiK_2P_3O_9\cdot H_2O$ is monoclinic, space group $P2_1/c$, with cell dimensions: $a=8.669\pm0.003$, $b=14.497\pm0.004$, $c=7.634$A, ±0.006, $\beta=99°53'\pm3'$, $Z=4$. The structure was determined from a three-dimensional Patterson function, and refined by electron-density syntheses and complete matrix least squares. The final R value for 1,011 independent observed reflections is 0.099.
The trimetaphosphate anion consists of three orthophosphate tetrahedra joined at corners to form a six-membered ring of alternate phosphorus and oxygen atoms in a chair configuration. The phosphate tetrahedra are nearly regular. The two potassium ions have irregular coordination figures. One is surrounded by six oxygen atoms from five different anions and the water molecule. The other is surrounded by eight oxygens, two oxygens from each of four different anions. The lighium ion is found at the center of a fairly regular tetrahedron formed by three oxygens and the water. The cation polyhedra are linked at edges and corners to produce equal cohesion in all directions, thus accounting for the lack of cleavage.

An improved resistance thermometer bridge, J. P. Evans, *Book, Temperature, Its Measurement and Control in Science and Industry* **3,** *Pt. 1, 285–289 (Reinhold Publ. Corp., New York, N.Y., 1962).*
Details of an improved Mueller bridge are given. The bridge has a range 0 to 422 ohms in 1 microhm steps. The important new features are (1) the addition of a decade with 1 microhm steps; (2) the use of mercury wetted contact switches for the 1, 0.1, and 0.01 ohm decades as well as for the 10 ohm decade and the 100 ohm coils; (3) the use of totally enclosed wafer type switches for the four lower decades; (4) the inclusion of a circuit which permits the instrument to be used as a four terminal decade resistor; (5) provision for digital readout of the bridge dial settings; and (6) electrical guarding and shielding of the measuring circuit so that sensitive electronic null detectors may be used.

Resistance thermometry in the liquid helium temperature region, M. H. Edlow and H. H. Plumb, *Book, Temperature, Its Measurement and Control In Science and Industry* **3,** *Pt. 1, 407–411 (Reinhold Publ. Corp., New York, N.Y., 1962).*
Carbon and impurity doped germanium resistors have been investigated for use as precision secondary thermometers in the liquid helium temperature region. Three germanium resistors supplied by Bell Telephone Laboratory (86Ω, 59Ω, and 21Ω) have been thermally cycled from 300 °K to 4.2 °K and their resistances have been found to be reproducible to within 1 millidegree when temperatures were derived from a controlled surface vapor pressure, and within 1/3 millidegree (except for one that had been repaired) when temperatures were derived from a vapor pressure thermometer whose tubing is jacketed through most of the liquid helium. Five impurity-doped germanium resistors supplied by Texas Instruments, Inc., have been thermally cycled from 300 °K to 4.2 °K and yield reproducibilities ranging from 2 to 10 millidegrees. Preliminary calibrations of the Bell Laboratory 59Ω and 21Ω and the Texas Instruments Inc. 125Ω resistors have been made from 4.21 °K to 2.16 °K at every .1 °K. The

data were fitted to a curve of the form log $R+k$/log $R=A+B/T$ by means of the 704 computer. The standard deviations of the data from this equation for the 125Ω and 59Ω resistors are $\leqq 1$ millidegree; for the 21Ω resistor, the standard deviation is $\leqq 3.3$ millidegrees.

A National Bureau of Standards gas thermometer, L. A Guildner, *Book, Temperature Its, Measurement and Control in Science and Industry* **3,** *Pt. 1, 151–155 (Reinhold Publ. Corp. New York. N.Y., 1962).*
At the National Bureau of Standards a constant-volume gas thermometer will be used to determine differences between the International Practical Temperature Scale of 1948 and the Kelvin thermodynamic scale. The gas thermometer thermometer bulb is a 500 cc shpere of platinum-20% rhodium alloy. It is connected to a pressure-sensitive diaphragm for separating the gas thermometer from a mercury manometer. With large menisci, the positions of the mercury crowns can be accurately detected by capacitance. The height of mercury is measured by Hoke end standards. A "tilt meter" measures variations of the manometer base from level.
Intensive effort is being made to reduce random and systematic errors. The bulb is thermostated uniformly by a copper furnace. The physical characteristics of the gas thermometer will be determined experimentally. Measurements will be made with a second thermometer bulb and with more than one gas. Determinations will be made for different masses of each gas in order to extrapolate to zero pressure.
It is planned to measure near the fixed points and at intermediate temperatures from 100 °C to 960 °C. A final set of measurements will determine the ratio of the thermodynamic temperatures of the steam and triple points of water.

Quartz crystals at low temperatures, P. R. Simpson and A. H. Morgan, *Proc. 13th Annual Symp. Frequency Control, p. 207–231 (Aug. 1959).*
The results of measurments performed at NBS Boulder Laboratories on certain characteristics of high precision quartz crystal oscillator units at temperatures below the normal ambient range are described with particular emphasis on frequency stability. Included are some details on the cryogenic ovens used, their tenperature control devices and performance. The oscillators developed for driving the crystal units and the frequency measuring systems employed will also be discussed. Various disturbing influences such as recharging the cryostats with refrigerant, shock, and vibration, filament voltage variations on the oscillator tubes, and others, will be mentioned.

Precursor electrons ahead of cylindrical shock waves, D. L. Jones, *Phys. Fluids* **5,** *No. 9, 1121–1122 (Sept. 1962).*
The presence of electrons ahead of shockwaves, produced by exploding wires, has been detected by microwave absorption in argon, helium, nitrogen and air. Operating pressures have ranged from 1 to 50 centimeters of mercury. Electron densities of the order of 10^{12} cm^{-3} have been observed several centimeters ahead of the shock front.

The thermal conductivity of solid nitrogen, H. M. Roder, *Letter to Editor Cryogenics* **2,** *No. 5, 302–304 (Sept. 1962).*
The thermal conductivity of solid nitrogen from 4° to about 28 °K was measured in an apparatus designed for detecting the effect of nitrogen free radicals, N*, trapped in the solid. The thickness of the sample was calculated from capacitance measurements assuming the dielectric constant to be given by the Clausius-Mossotti equation. Use of the capacitance method was justified by vertification of the Clausius-Mossotti equation down to 4 °K.

High pressure transition in RbF, G. Piermarini and C. E. Weir, *J. Chem. Phys.* **37,** *No. 8, 1887–1888 (Oct. 15, 1962).*
X-ray diffraction data on RbF show that at high pressures the face centered cubic NaCl type structure is transformed to the simple cubic CsCl structure. The pressure is estimated to be between 9 and 15 kb. The f.c.c. unit cell parameter of 5.64 Å changes to a value of 3.27 Å in the s.c. form. No alkali fluoride has been previously observed to undergo a transition under pressure.

Absorption bands of carbon dioxide from 2.8 to 4.2μ, E. K. Plyler, E. D. Tidwell, and W. S. Benedict, *J. Opt. Soc. Am.* **52,** *No. 9, 1017–1022 (Sept. 1962).*
The high-resolution spectrum of CO_2 has been studied between 2.8 to 4.2μ, using up to 48 meter-atmospheres path to develop weak bands. Accurate band constants have been obtained for the transitions 13^10-000, 05^10–000, and 101–02^20, and fragments of new weak bands have been detected near 3509 cm^{-1}. Estimates of band intensities are given, including a discussion of the highly abnormal intensity distribution in the weak perpendicular bands.

Synthesis of higher ketoses by aldol reactions. I. Three D-heptuloses, R. Schaffer and H. S. Isbell, *Org. Chem.* **27,** *3268–3270 (Mar. 1962).*
The 5,7-*O*-ethylidene acetals of D-*altro*, D-*manno*-, and D-*gluco*-heptulose have been prepared directly from reaction of 2,4-*O*-ethylidene-D-erythrose with 1,3-dihydroxy-2-propanone. The ethylidene acetals of D-*altro*-heptulose and D-*manno*-heptulose were separated and isolated in crystalline form. The product having the D-*gluco* configuration was hydrolyzed to crystalline D-*gluco*-heptulose. The over-all yield of crystalline products was 44.5 percent. The synthesis demonstrates the utility of aldehydo-aldoses (having alkali-stable substituents) for the preparation of higher ketoses by the aldol synthesis.

Complex formation of monomeric amides with lithium perchlorate, A. F. Diorio, E. Lippincott, and L. Mandelkern, *Nature* **194,** *No. 4848, 1296–1297 (Sept. 1962).*
The interaction of anhydrous lithium perchlorate with *N*-methylpropionamide was investigated by means of an infrared spectroscopic technique in order to elucidate the nature of the interaction of lithium salts with the peptide linkage of protein systems.
Upon addition of $LiClO_4$, the amide I absorption band attributed to C=O stretch is lowered in wave number; the single bond observed with the pure amide becomes a doublet. The strong band at 3300 cm^{-1} attributed to the N–H stretching mode is completely replaced by a strong band at 3400 cm^{-1}.
It is concluded that the lithium ion interacts with the carbonyl group directly, with a disruption of the hydrogen bonded network of the pure liquid amide. These results indicate that the disruption of the ordered structure observed in protein systems could be a result of a similar binding phenomenon not involving water.

The thermodynamic temperature scale, Its definition and realization, C. M. Herzfeld, *Book, Temperature, Its Measurement and Control in Science and Industry* **III,** *Pt. I, 41–50 (Reinhold Publ. Co., New York, N.Y., 1962).*
A temperature scale based on thermodynamics is conceptually straightforward. The usual definition is given, and the realization of the scale by means of gas thermometry is discussed. The scale can be extended by appeal to the statistical mechanical interpretation of thermodynamics. Ways of doing this for high and low temperatures, using radiation and magnetic methods respectively, are presented.
Statistical mechanical arguments make possible the use of the concept of temperature for systems differing greatly from those contemplated in classical thermodynamics.

The thermodynamic scale of temperature below 1 °K, R. P. Hudson, *Book, Temperature, Its Measurement and Control in Science and Industry* **3,** *Pt. I, 51–57 (Reinhold Publ. Co., New York, N.Y., 1962).*
Following a brief discussion of the principles of magnetic thermometry, a description is given of the main methods used to derive the relation between the "magnetic scale" and the absolute scale of temperature. Experimental results published since 1953 are summarized. An account is given of the measurement of absolute temperature using the anisotropy of radiation emitted from oriented radioactive nuclei. Recent work on the intercomparison of "nuclear orientation scales," and on the comparison of one such scale with a magnetic scale, is reviewed. There follows a short account of the adaptation of the magnetic cooling method to nuclear paramagnetics and the production of temperatures of the order of one microdegree Kelvin.

Hyperfine structure and intercombination line intensities in the spectra of magnesium, zinc, cadmium, and mercury, R. H. Garstang, *J. Opt. Soc. Am.* **52,** *No. 8, 845–851 (Aug. 1962).*
The transition probabilities of the lines $1s_0=3p_0$ and $1s_0=3p_2$ of the $s^2=sp$ arrays in Mg I, Zn I, Cd I and Hg I, which arise by the interactions of the nuclear moments with the electrons, are computed for each odd isotope individually and for the naturally occurring isotopic mixture. The individual hyperfine structure component transition probabilities are given for the $1s_0-3p_2$ lines. Part of the intensity of the lines arises from the interaction of $3p_0$ or $3p_2$ with $3p_1$ and part from the interaction of $3p_0$ or $3p_2$ with $1p_1$, the former being more important for $1s_0-3p_0$ and the latter for $1s_0-3p_2$. Spin-spin and spin-other-orbit interactions in Mg I are calculated for the 3s3p ^{3}P term and compared with observations.

Nuclear photoeffect in deformed nuclei, E. Hayward, *Rendiconti Della Scuola Intern. Fisica "Enrico Fermi"* **XV,** *214–222 (Academic Press Inc., New York, N.Y., 1962).*
The relationships between the total absorption and scattering cross sections for spherical and deformed nuclei are discussed. Recent results obtained using targets of holmium and erbium are presented.

Relaxation of nonequilibrium distributions, K. E. Shuler, *Book, Temperature, Its Measurement and Control in Science and Industry* **III,** *Pt. 1, 27–34 (Reinhold Publ. Corp., New York, N.Y., 1962).*
A review is presented of the relaxation of nonequilibrium distributions through interactions with a heat bath. As a specific example, the relaxation of an ensemble of harmonic oscillators has been considered in some detail.

Interpretation of rate experiments with resolved quantum levels, T. Carrington, *Discussions Faraday Soc., No. 33, 44–51 (1962).*
It is now possible to study the steady state flourescence and chemiluminescence of small molecules in resolved quantum levels, and in other experiments to observe the time history of the vibfational or rotational relaxation of molecules suddenly produced in a non-equilibrium distribution. These experiments require interpretation in terms of rates or probabilities of vibrational or rotational energy exchange involving specified quantum states. If it is assumed that the state of a molecule after a collision depends only on its state immediately before the collision, and not on its previous history, or on the time at which the collision occurs, the sequence of collisions suffered by one molecule becomes a Markov chain and the appropriate mathematical formalism may be directly applied. This establishes a relationship between the observable transition rates and the more abstract concept of probability of transition per collision. The mathematical results are illustrated in discussing certain experiments.

Other NBS Publications

J. Research NBS 67C (Eng. and Instr.), No. 2 (Apr.–June 1963), 75 cents.

Temperature dependence of the elastic constants of thoric specimens of varying porosity. S. Spinner, L. Stone, and F. P. Knudsen.

Residual stresses and their relaxation on the surfaces of sections cut from plastically deformed steel specimens. C. J. Newton.

Permeation rates of electrolytic hydrogen and deuterium through iron. J. W. Pitts.

Steady state heat conduction in cylinders with multiple continuous line heat sources. B. A. Peavy.

A radial-flow apparatus for determining the thermal conductivity of loose-fill insulations to high temperatures. D. R. Flynn.

Analysis of a microwave radiometer for precise standardization of noise sources. G. D. Ward and J. M. Richardson.

Realistic evaluation of the precision and accuracy of instrument calibration systems. C. Eisenhart.

J. Research NBS 67D (Radio Prop.), No. 3 (May–June 1963), 70 cents.

Effects of radio wave propagation through mid-latitude 6300 A arcs. J. R. Roach.

Comparison of observed atmospheric radio refraction effects with values predicted through the use of surface weather observations. B. R. Bean and G. D. Thayer.

Ionospheric scattering effects in long-distance propagation. H. A. Whale.

Concerning solutions of the VLF mode problem for an anisotropic curved ionosphere. J. R. Wait.

On the statistical theory of electromagnetic waves in a fluctuating medium (1). K. Furutsu.

Reception of skywave signals near a coastline. J. B. Andersen.

Analysis and synthesis of nonuniform transmission lines or stratified layers. G. Latmiral, G. Franceschetti, and R. Vinciguerra.

Resonant characteristics of a corrugated sphere. J. R. Wait and C. M. Jackson.

Impedances of long antennas in air and in dissipative media. D. W. Gooch, C. W. Harrison, Jr., R. W. P. King, and T. T. Wu.

Reflection of VLF radio waves from an inhomogeneous ionosphere. Part I. Exponentially varying isotropic model. J. R. Wait and L. C. Walters.

NBS viscometer calibrating liquids and capillary tube viscometers, R. C. Hardy, NBS Mono. 55 (Dec. 26, 1962), 20 cents.

Handbook for CRPL Ionospheric Predictions Based on Numerical Methods of Mapping, S. M. Ostrow, NBS Handb. 90 (Dec. 21, 1962), 40 cents (Supersedes Circ. 465).

1962 Research Highlights of the National Bureau of Standards, Annual Report, NBS Misc. Publ. 246 (Dec. 1962) 70 cents.

Equipment characteristics and their relation to system performance for tropospheric communication circuits, A. F. Barghausen, F. O. Guiraud, R. E. McGavin, S. Murahata, and R. W. Wilber, NBS Tech. Note 103 (Jan. 15, 1963), $1.00.

A tabulation of the thermodynamic properties of normal hydrogen from low temperature to 300 °K and from 1 to 100 atmospheres, J. W. Dean, NBS Tech. Note 120 (Nov. 1961), 45 cents.

The thermodynamic properties of nitrogen from 114 to 540 °R between 1.0 and 3000 psia, Supplement A (British units), T. R. Strobridge, NBS Tech. Note 129A (Feb. 1963), 50 cents.

Coordinated color identifications for industry, K. L. Kelly, NBS Tech. Note 152 (Nov. 1962), 15 cents.

Thermal balance in the F region of the atmosphere, D. C. Hunt, NBS Tech. Note 162 (Sept. 1962), 50 cents.

Fading correlation bandwidth and short-term frequency stability measurements on a high-frequency transauroral path, J. L. Auterman, NBS Tech. Note 165 (Oct. 1962), 40 cents.

Ranking laboratories by round-robin tests, W. J. Youden, Mater. Res. Std. **3,** No. 1, 9–13 (Jan. 1963).

The error rate in a multiple-frequency-shift system and the output signal/noise ratio in a frequency modulation and a pulse-code-modulation/frequency-shift system, H. Akima, Intern. Conf. Satellite Communication p. 305–310 (Nov. 22–28, 1962).

Technical training in the weights and measures program, M. W. Jensen, Scale J. 49, No. 4, 4–5 (Jan. 1963); Southern Weights and Measures Program **14,** No. 12, 2–5 (Dec. 1962).

Corrosion rates of ferrous alloys (Fe, Cr, and Fe-Cr-Si) measursd by polarization techniques, W. J. Schwerdtfeger, Corrosion **19,** No. 1, 17t–25t (Jan. 1963).

A differential thermocouple voltmeter, J. E. Griffin and F. L. Hermach, AIEE Trans., Pt. I. Communications and Electronics No. 63, Article No. 62–819, 338–344 (Nov. 1962).

Color tests for antioxidants, E. J. Parks, L. T. Milliken, and F. J. Linnig, Rubber Age **92,** No. 2, 257–261 (Nov. 1962).

Cavitation problems in cyrogenics, R. B. Jacobs and K. B. Martin, J. Basic Eng. **82,** 756–757 (Sept. 1960).

Airglow research in the United States, F. E. Roach, (Triennium Report of U.S. Natl. Comm. IUGG) Trans. Am. Geophys. Union **41,** No. 2, 242–243 (1960).

The text revision of the international temperature scale of 1948, H. F. Stimson, Book, Temperature, Its Measurement and Control in Science and Industry **3,** Pt. 1, 59–66 (Reinhold Publ. Corp., New York, N.Y., 1962).

Analysis of rotation errors of a waveguide theory vane antennuator, W. Larson, IRE Intern. Conv. Record, Pt 3, 213–219 (1962).

Survey of U.S.A. ionospheric research 1957–1959, T. N. Gautier (Triennium Report of U.S. Natl. Comm. IUGG), Trans. Am. Geophys. Union **41,** No. 2, 232–236 (June 1960).

On the analysis of polarization rotation recordings of satellite radio signals, R. S. Lawrence and C. G. Little, Intern. Sci. Radio Union, IGY Comm. Some Ionospheric Results Obtained During th IGY; Proc. Symp. Organized by URSI/AGI Comm. Brussels, Belgium, p. 392–399 (Elsvier Publ. Co., Amsterdam, The Netherlands, 1960).

Widely separated clocks with microsecond synchronization and independent distribution system, T. L. Davis and R. H. Doherty, IRE WESCON Conv. Pt. 5, p. 3–17 (1960).

Memorial to Sir Ronald Aylmer Fisher: 1890–1962, W. J. Youden, J. Am. Stat. Assoc. **57,** No. 300, 727–728 (Dec. 1962).

A low impedance Maxwell bridge for measuring toroidally-shaped magnetic materials from 1 Kc to 100 Kc, A. L. Rasmussen and R. C. Powell, Proc. IRE **50,** 2505–2506 (Dec. 1962).

Radio properties of aurorae, C. G. Little, U.S.A. Natl. Comm. Intern. Sci. Radio Union Report to Natl. Acad. Sci.-Natl. Res. Council on 13th Gen. Assembly, Sept. 5–15, 1960, London, England, p. 216–270 (Natl. Acad. Sci.-Natl. Res. Council, Washington, D.C., 1961).

Electrophoretic deposits of barium titanate, V. A. Lamb and V. A. Lamb and H. I. Salmon, Am. Ceram. Soc. **41,** No. 11, 781–782 (Nov. 1962).

A rapid method of estimating the order of chemical reactions, J. H. Flynn, Chem. Eng. **69,** 137–140 (Aug. 1962).

Tests for contingency tables and Markov chains, S. Kullback, M. Kupperman and H. H. Ku, Technometrics **4,** No. 4, 573–608 (Nov. 1962).

Comments on the limits to the refractive index at ground level as a radio-meteorological parameter, B. R. Bean and G. D. Thayer, Proc. IRE **48,** No. 8, 1498–1501 (Aug. 1960).

Energy exchange in the biosphere, D. M. Gates, Book, Harper & Row Publ., New York, N.Y., 1962.

On the propagation of ELF pulses in the earth-ionosphere waveguide, J. R. Wait, Can. J. Phys. **40,** 1360–1369 (Oct. 1962).

Interpretation of *p*H measurements in alcohol-water solvents, R. G. Bates and R. A. Robinson, Proc. 7th Intern. Conf. Coordination Chemistry, Stockholm, Sweden, p. 342–344 (1962).

Polymorphism in fibrous polypeptides: $\alpha \rightleftarrows \beta$ transformation in naturally occurring keratin, A. F. Diorio, L. Mandelkern, and E. R. Lippincott, J. Phys. Chem. **66,** No. 11, 2096–2100 (Nov. 1962).

Recent radar observations of new forms of ionosphere scatter, K. L. Bowles, U.S.A. Natl. Comm. Intern. Sci. Radio Union Report to Natl. Acad. Sci.-Natl. Res. Council on 13th Gen. Assembly, Sept. 5–15, 1960, London, England, p. 288–295 (Natl. Acad. Sci.-Natl. Res. Council, Washington., D.C., 1961).

The significance of transients and steady-state behavior in nonlinear systems, W. J. Hartman, Proc. IRE Correspondence Section **49,** No. 3, 637 (Mar. 1961).

Photoionization from outer atomic subshells. A model study, J. W. Cooper, Phys. Rev. **128,** No. 2, 681–693 (Oct. 15, 1962).

Solar flare effects in the *F*-region of the ionosphere, R. W. Knecht and R. E. McDuffie (Proc. Intern. Conf. Cosmic Rays and the Earth Storm), J. Phys. Soc. Japan **17,** Suppl. A, Pt. I, 280–285 (1962).

Recent experiments on liquid helium vapor pressure measurements from 2° to 4° K, G. Cataland, M. H. Edlow, and H. H. Plumb, Book, Temperature, Its Measurement and Control in Science and Industry 3, Pt. 1, 413–417 (Reinhold Publ. Corp., New York, N.Y., 1962).

Low-level low-frequency detection system, N. T. Larsen, Rev. Sci. Instr. **33,** 1200–1208 (Nov. 1962).

On the extension of the low-chromosphere model to the region of origin of the UV solar spectrum, R. N. Thomas, (Proc. 10th Astrophysical Symp. Liege, Belgium), Mem. Roy. Soc. Belgium **20,** 305 (1961).

Very-low-frequency phase observations on the ionospheric effects of the solar flare of September 28, 1961, A. G. Jean and J. H. Crary, J. Geophys. Reas. **67,** No. 12, 4903–4905 (Nov. 1962).

The radiant energy from sources in the far infrared, E. K. Plyer, D. Yates, and H. A. Gebbie, J. Opt. Soc. Am. **52,** No. 8, 859–861 (Aug. 1962).

Obtaining the internal junction characteristics of a transistor for use in analog simulation, S. B. Geller, IRE Trans. Electron. Computers EC–**11**, No. 5, 709–710 (Oct. 1962).

Graphical evaluation of analytical results, W. J. Youden, Proc. Conf. Chemical Control Problems, p. 1–15 (Spon. Natl. Plant Food Inst., Washington, D.C., 1959).

The measurement of ionospheric drifts by means of a Doppler technique, K. Davies, J. Geophys. Res. **67,** No. 12, 4909–4913 (Nov. 1962).

Laboratory astrophysics, L. M. Branscomb and R. N. Thomas Phys. Today **15,** 42–44, 46 (Nov. 1962).

Standards—The key to success in engineering, A. T. McPherson, Rev. Centro Estud. Ing. **130,** No. 656, 352–355 (1961).

Precision phase meter, D. M. Waters, D. Smith, and M. C. Thompson, Jr., IRE Trans. Instr. I–II, 64–66 (Sept. 1962).

The effect of temperature and humidity on the oxidation of air-blown asphalts, P. G. Campbell, J. R. Wright, and P. B. Bowman, Mater. Res. Std. **2,** No. 12, 988–995 (Dec. 1962).

Standards for the future, R. D. Huntoon, Proc. Annual Spring Conf. Standards Engineers Society, Boston Section and Company Member Conf. of American Standards Association, May 24–25, 1962 (Boston, Mass., 1962).

Intramolecular rearrangements in the solid phase photolysis of 4-methyl-2-hexanone and sec-butyl acetate, R. E. Rebbert and P. Ausloos, J. Chem. Phys. **37,** No. 5, 1158–1159 (Sept. 1, 1962).

The vapor phase fluorescence and its relationship to the photolysis of propionaldehyde and the butyraldehydes, R. P. Borkowsik and P. Ausloos, J. Am. Chem. Soc. **84,** No. 21, 4044–4048 (Nov. 1962).

Crosslinking of polymers induced by excited species, L. A. Wall and R. B. Ingalls, J. Polymer Sci. Letter to Editor **62,** No. 173, S5–S6 (1962)

Standard electromotive force of the cell H_2; HBr(m); AgBr; Ag from 0 to 50°, H. B. Hetzer, R. A. Robinson, and R. G. Bates, J. Phys. Chem. **66,** No. 8, 1423–1426 (1962).

Vacuum ultraviolet photochemistry. IV. Photolysis of propane, H. Okabe and J. R. McNesby, J. Chem. Phys. **37,** No. 6, 1340–1346 (Sept 1962).

Conformation and frictional properties of polystyrene in dilute solutions, D. McIntyre, A. Wims, L. C. Williams, and L Mandelkern, J. Phys. Chem. **66,** 1932–1940 (Oct. 1962).

Use of a "peek-a-boo" information retrieval technique for a personal reference file, J. A. Bennett, J. Wash. Acad. Sci. **52,** No. 9, 216–219 (Dec. 1962).

Photographic strain measuring technique for use above 3,000 F, L. Mordfin and T. Rubusto, Jr., Proc. Instr. Soc. Am. **17,** Pt. 1, 3.4.62–1 (1962).

The speed of processes involved in electroplating: movement of solute, attainment of the steady state and formation of metal, A. Brenner, 49th Annual Tech. Proc. Am. Electroplaters Soc. p. 9–13 (1962).

**Publications for which a price is indicated may be obtained from the Superintendent of Documents, U.S. Government Printing Office, Washington 25, D.C. (foreign postage one-fourth additional). Reprints from outside journals and the NBS Journal of Research may often be obtained from the authors.*

U.S. GOVERNMENT PRINTING OFFICE:1963

UNIVERSITY MICROFILMS
313 NORTH FIRST STREET
ANN ARBOR, MICHIGAN
SJR-A-OCT

GOVERNMENT PRINTING OFFICE
DIVISION OF PUBLIC DOCUMENTS
WASHINGTON 25, D.C.

OFFICIAL BUSINESS

PENALTY FOR PRIVATE USE TO AVOID PAYMENT OF POSTAGE, $300 (GPO)

JOURNAL OF RESEARCH of the National Bureau of Standards — Vol. 67A, No. 3 — May-June 1963
A. Physics and Chemistry

Contents

	Page
An absolute calibration of the National Bureau of Standards Thermal Neutron Flux. E. J. Axton.	215
Absorption bands of carbon dioxide from 513 to 4.6 microns. Arthur G. Maki, Earle K. Plyler, and Robert J. Thibault.	219
Infrared spectrum of the ν_2-ν_3 band of $C^{12}C^{13}H_2$. Walter J. Lafferty and Earle K. Plyler.	225
Self-broadening of carbon monoxide in the 2ν and 3ν bands. Earle K. Plyler and Robert J. Thibault.	229
Thermodynamic properties of polyethylene predicted from paraffin data. Martin G. Broadhurst.	233
Spectrophotometric determination of the thermodynamic pK value of picric acid in water at 25 °C. Marion Maclean Davis and Maya Paabo.	241
Purity analysis of highly purified materials by time-temperature cryometry. Gaylon S. Ross and Herbert D. Dixon.	247
Synthesis of isomers of eugenol. Gerhard M. Brauer, Richard Warren Morris, and Willard B. Howe.	253
Analysis of families of curves. John Mandel and Frank L. McCrackin.	259
A controlled atmosphere chamber. Charles L. Gordon and Rolf B. Johannesen.	269
Publications of the National Bureau of Standards.	273

For sale by the Superintendent of Documents, U.S. Government Printing Office, Washington 25, D.C. Price 70 cents (single copy)
Subscription price: $4.00 a year; 75 cents additional for foreign mailing.

UNITED STATES GOVERNMENT PRINTING OFFICE, WASHINGTON : 1963

6